The Monte Carlo method for the solution of charge transport in semiconductors with applications to covalent materials

Carlo Jacoboni and Lino Reggiani

Gruppo Nazionale di Struttura della Materia, Istituto di Fisica dell'Università di Modena, Via Campi 213/A, 41100 Modena Italy

This review presents in a comprehensive and tutorial form the basic principles of the Monte Carlo method, as applied to the solution of transport problems in semiconductors. Sufficient details of a typical Monte Carlo simulation have been given to allow the interested reader to create his own Monte Carlo program, and the method has been briefly compared with alternative theoretical techniques. Applications have been limited to the case of covalent semiconductors. Particular attention has been paid to the evaluation of the integrated scattering probabilities, for which final expressions are given in a form suitable for their direct use. A collection of results obtained with Monte Carlo simulations is presented, with the aim of showing the power of the method in obtaining physical insights into the processes under investigation. Special technical aspects of the method and updated microscopic models have been treated in some appendixes.

CONTENTS

LIST OF SYMBOLS

a_0	lattice parameter
$a_q, a_q^\dagger$	phonon annihilation and creation operators
A	inverse valence-band parameter
b	impact parameter for ionized impurity scattering
$\mathbf{B}$	magnetic field
B	inverse valence-band parameter
c	velocity of light
$\lvert c \rangle$	crystal states
C	inverse valence-band parameter
$C(t)$	autocorrelation function of velocity fluctuations
d_0	deformation potential constant for hole optical-phonon interaction
D	diffusion coefficient
D_l	diffusion coefficient longitudinal with respect to the field direction
D_t	diffusion coefficient transverse with respect to the field direction
$(D_t K)$	deformation potential constant for optical and intervalley-phonon scattering with electrons
e	unit charge with its sign
$\mathscr{E}$	deformation potential tensor
$\mathscr{E}_1$	electron acoustic-phonon deformation potential
$\mathscr{E}_1^0$	hole acoustic-phonon deformation potential
$\mathbf{E}$	electric field
E_a	component of the electric field parallel to the drift velocity
E_c	a critical field used in connection with quasielastic approximation
E_H	Hall component of the electric field
$f(\mathbf{k})$	carrier distribution function in momentum space
$f_{c,h}$	carrier distribution in energy space of cold and hot valleys
g_I	electron-hole pair generation rate per particle per unit time
$\mathscr{G}$	overlap factor
$\mathbf{G}$	reciprocal lattice vector
$\hbar$	Planck constant divided by 2π
$\mathscr{H}'$	Fourier transform of the perturbation Hamiltonian
H'	perturbation Hamiltonian for scattering of electrons
$\mathbf{j}$	current density
$\mathbf{k}$	wave vector of a carrier
$\mathbf{k}_{a,b}$	$\mathbf{k}$ state after and before scattering
$\mathbf{k}_d$	average wave vector of a drifted Maxwellian distribution function
$k_{l,t}$	longitudinal and transverse electron wave-vector component for an ellipsoidal equienergetic surface
$\mathbf{k}_0$	initial value of $\mathbf{k}$
K_B	Boltzmann constant
K_2	modified Bessel function of order 2
$\mathbf{l}$	carrier mean free path
l_{op}	a mean free path for optical-phonon interaction
m	effective mass
m_c	conductivity effective mass
m_d	density-of-states effective mass
m_h	density-of-states effective mass of heavy holes
$m_{l,t}$	electron longitudinal and transverse effective masses for an ellipsoidal equienergetic surface
m_0	free-electron mass
m_Γ	electron effective mass at the Γ minimum of the conduction band
M_m	mth space moment of the carrier distribution
$n(\mathbf{k})$	carrier density in momentum space
$n(\mathbf{r})$	carrier density in real space
$n_{a,b}(\mathbf{k})$	after and before scattering distribution in $\mathbf{k}$ space
$n_{c,h}$	relative fraction of carriers in cold and hot valleys
n_I	impurity concentration
n_q	Fourier transform of $n(x)$
n_v	relative concentration of carriers in valley v
n_0	average carrier density in real space
N	number of simulated particles number of electron free flights number of fixed-time intervals
N_{op}	thermal equilibrium number of optical phonons
$N_{\mathbf{q}}$	thermal equilibrium number of phonons with wave vector $\mathbf{q}$
$\mathbf{p}$	crystal momentum of the electron
$\mathscr{P}(\mathbf{k},t)dt$	probability that an electron in $\mathbf{k}$ at a given time will be scattered between t and $t+dt$ later
$\mathscr{P}(x,t)$	probability that in absence of trapping a particle covers a distance x in a time t
$P(\mathbf{k})$	total collision probability per unit time
$P(\mathbf{k},\mathbf{k}')$	transition probability per unit time of scattering from $\mathbf{k}$ to $\mathbf{k}'$
$P_i(\mathbf{k})$	collisions probability per unit time due to the ith scattering mechanism
$P_n(\cos\theta)$	Legendre polynomials
$P_{e,\text{ac}}(\epsilon)$	acoustic scattering rate for electrons
$P_{e,I}(\epsilon)$	ionized impurity scattering rate for scattering of electrons
$P_{e,\text{op}}(\epsilon)$	optical-phonon scattering rate for electrons
$P_{h,\text{ac}}(\epsilon)$	acoustic scattering rate for holes
$P_{h,I}(\epsilon)$	ionized impurity scattering rate for scattering of holes
$P_{h,\text{op}}(\epsilon)$	optical-phonon scattering rate for holes
$P_{c,h;h,c}$	transition rate from cold to hot valleys and from hot to cold valleys
$\mathbf{q}$	phonon wave vector
r	random number evenly distributed in the

	interval (0,1)
$\mathbf{r}$	position in space
r_H	Hall factor
$\mathbf{R}$	vector of the direct lattice
$S_v(\omega)$	power spectrum of the velocity fluctuations
t	time
t_r	stochastic free-flight duration
T	period
	duration of a single history
T_e	electron temperature
T_n	white-noise temperature
T_0	lattice temperature
T_{ij}	Herring and Vogt transformation matrix
u	average sound velocity
$u_{\mathbf{k}}(\mathbf{r})$	periodic part of the Bloch wave function
$u_{l,t}$	longitudinal and transverse sound velocity
$\mathbf{v}(t)$	instantaneous electron velocity
$\mathbf{v}_d$	drift velocity
$v_{l,t}$	drift velocity component longitudinal and transverse with respect to the electric field direction
$\mathbf{v}_0$	drift velocity associated with a dc field $\mathbf{E}_0$
$\mathbf{v}_{1,2}$	sine and cosine Fourier transforms of the velocity response to a small ac field
$\mathbf{v}_{\mathrm{dv}}$	drift velocity in valley v
$\mathscr{V}(\mathbf{r})$	ionized impurity potential
V	crystal volume
x,y,z	space coordinates
$\mathbf{y}$	ion displacement
$\mathscr{Z}$	small signal impedance of a two-terminal device
Z	number of charge units of the impurity center
Z_f	number of final equivalent valleys for a given scattering
α	nonparabolicity parameter
α_I	impact ionization rate
β_s^{-1}	impurity screening length
Γ	total scattering rate including self-scattering
	center of the Brillouin zone
$\Gamma_{0,1,2}$	values of Γ in given ranges of energy
ϵ	carrier energy
ϵ_g	energy gap
ϵ_Γ	energy gap at Γ
ϵ_{ph}	phonon energy
ϵ_{so}	split-off energy of the lowest valence band
$\theta_{\mathrm{op,int}}$	equivalent temperature of the optical and intervalley phonons
κ	dielectric constant
$\lambda(\mathbf{k})$	total scattering rate
μ	mobility
μ'	differential mobility
μ_d	drift mobility obtained from a simulation in presence of a magnetic field
μ_E	longitudinal mobility in the direction of the electric field
μ_H	Hall mobility
ξ	phonon polarization
$\Xi_d \Xi_u$	deformation potential constants for ellipsoidal energy surfaces
ρ	crystal density
σ	cross section
$\tau^{-1}(\mathbf{k})$	scattering rate
τ_d^{-1}	trapping rate
τ_ϵ	energy relaxation time
$\Phi(t)$	normalized autocorrelation function of velocity fluctuations
$\psi_{\mathbf{k}}(\mathbf{r})$	Bloch wave function
ω	angular frequency
ω_c	cyclotron angular frequency
ω_i	intervalley-phonon angular frequency
ω_{op}	optical-phonon angular frequency
$\omega_{\mathbf{q}}$	phonon angular frequency
$\langle\ \rangle$	ensemble average at a given time
$\langle\ \rangle_T$	time average over a time interval T

I. INTRODUCTION

The study of charge transport in semiconductors is of fundamental importance both from the point of view of basic physics and for its application to electronic devices. On the one hand, the analysis of transport phenomena throws light on electronic interactions in crystals, on band structure, lifetimes, impact ionization, etc. On the other hand, the applied aspect of the problem is even more important, since modern microelectronics, whose influence in all human activities seems to be ceaselessly growing, depends heavily on a sophisticated knowledge of many aspects of charge transport in semiconductors.

Starting in the early 1950s, soon after the invention of transistors, it was recognized that electric field strengths so high as to be outside of the linear-response region where Ohm's law holds were encountered in semiconductor samples (Shockley, 1951). The field of nonlinear transport (the hot-electron problem), which had been initiated long before by a few pioneer papers (Landau and Kompanejez, 1934; Davydov, 1936, 1937), then entered a period of rapid development, and increasing numbers of researchers devoted their efforts to improving the scientific knowledge of this subject. Furthermore, in the process of studying these high-field problems, new phenomena were discovered [for example, the Gunn effect (1963)] and, based on these discoveries, new devices were designed (such as transit-time devices) which, in turn, required new and closer investigation. Thus one of the most interesting cases of positive feedback between science and technology in this century emerged. The subsequent tendency to miniaturization of devices, which has led to modern very-large-scale integration (VLSI) technology, has further enhanced the importance of high-field transport, since reducing the dimensions of devices had led to high-field strengths well outside the Ohmic response region for any reasonable voltage signal.

Charge transport is in general a tough problem, from both the mathematical and the physical points of view. In fact, the integro-differential equation (the Boltzmann equation) that describes the problem does not offer simple (or even complicated) analytical solutions except for very few cases, and these cases usually are not applicable to real systems. Furthermore, since transport quantities are derived from the averages over many physical processes whose relative importance is not known *a priori,* the formulation of reliable microscopic models for the physical system under investigation is difficult. When one moves

from linear to nonlinear response conditions, the difficulties become even greater: the analytical solution of the Boltzmann transport equation without linearization with respect to the external force is a formidable mathematical problem, which has resisted many attacks in the last few decades. In order to get any result, it is necessary to perform such drastic approximations that it is no longer clear whether the features of interest in the results are due to the microscopic model or to mathematical approximations. [Paige (1964) and Conwell (1967) give a full account of the first stage of the investigations carried out in this area.]

From the foregoing it is understandable that, when two new numerical approaches to this problem, i.e., the Monte Carlo technique (Kurosawa, 1966) and the iterative technique (Budd, 1966), were presented at the Kyoto Semiconductor Conference in 1966, hot-electron physicists received the new proposals with great enthusiasm. It was in fact clear that, with the aid of modern large and fast computers, it would become possible to obtain exact numerical solutions of the Boltzmann equation for microscopic physical models of considerable complexity. These two techniques were soon developed to a high degree of refinement by Price (1968), Rees (1969), and Fawcett *et al.* (1970), and since then they have been widely used to obtain results for various situations in practically all materials of interest. The Monte Carlo method is by far the more popular of the two techniques mentioned above, because it is easier to use and more directly interpretable from the physical point of view. Among the most significant developments of the Monte Carlo technique let us cite the fundamental work of the Malvern group with the introduction of the self-scattering scheme (Rees, 1968, 1969); nonparabolicity effects (Fawcett *et al.*, 1969); distribution anisotropy (Fawcett and Rees, 1969); and diffusion (Fawcett, 1973). Other important areas of development include many-particle simulation (Lebwohl and Price, 1971); the calculation of transients in time and their space equivalent (Ruch, 1972; Baccarani *et al.*, 1977); harmonic time variation (Price, 1973); the treatment of alloy semiconductors (Hauser *et al.*, 1976); and quantum effects of strong electric fields (Barker and Ferry, 1979).

Monte Carlo is a statistical numerical method used for solving mathematical problems; as such, it was born well before its application to transport problems (see, for example, Buslenko *et al.*, 1966), and has been applied to a number of scientific fields (Meyer, 1956; Marchuk *et al.*, 1980). In the case of charge transport, however, the statistical numerical approach to the solution of the Boltzmann equation proves to be a direct simulation of the dynamics of charge carriers inside the crystal, so that, while the solution of the equations is being built up, any physical information required can be easily extracted. In this respect it should be noted that, once a numerical solution of a given problem is obtained, its subsequent physical interpretation is still very important, in gaining an understanding of the phenomenon under investigation. The Monte Carlo method shows itself to be a very useful tool toward this end, since it permits simulation of particular physical situations unattainable in experiments, or even investigation of nonexistent materials in order to emphasize special features of the phenomenon under study. This use of the Monte Carlo makes it similar to an experimental technique; the simulated experiment can in fact be compared with analytically formulated theory.

The purpose of this review is to present the Monte Carlo method as applied to semiconductor transport in a comprehensive form that will be of value to various kinds of readers. For those who want to enter this field of research the authors have presented in tutorial form the main ideas and the technical methods for setting up one's own Monte Carlo program. Scholars already working in this field may find it helpful to have collected and discussed in a single paper material that is now scattered among many specialized papers.

For the sake of clarity, the method has been discussed both in itself and in its application to specific materials, namely, covalent semiconductors of group-four diamond, silicon, and germanium. The scope of the review was not extended to all semiconductors, in an effort to keep it to a reasonable size. In particular, polar materials such as III-V and II-VI compounds have not been considered. For the same reason we limited ourselves to investigation of the physical properties of bulk materials. The application of the method to special structures was left aside, and device simulation was only briefly mentioned at the end of the paper, since this subject, very interesting in itself, would have led us to the huge field of solid-state electronics, well beyond the limits of the present review. Finally, our intention was not to provide an exhaustive list of references on this subject. Papers have been quoted when their contents were relevant to the development of the theme of the review. Some previous reviews of semiconductor transport and Monte Carlo applications have been particularly useful in the preparation of the present paper (e.g., Alberigi-Quaranta *et al.*, 1971; Fawcett, 1973). Among them, we should like to mention in particular Price's (1979) remarkable review.

The paper is organized simply in three main parts. Section II presents the Monte Carlo method as applied to transport calculations in semiconductors. After a brief survey of the band-structure properties relevant to transport, in Sec. III the carrier scattering mechanisms are discussed with special attention to the formulation of theory necessary for application in a Monte Carlo program. Section IV presents, as examples of application, a collection of results in covalent semiconductors, and is followed by a brief conclusion with some consideration of future perspectives of this subject. Special technical aspects have been treated in appendixes, in order not to interrupt the presentation in the body of the paper.

II. THE MONTE CARLO METHOD

A. Fundamentals

The Monte Carlo method, as applied to charge transport in semiconductors, consists of a simulation of the

motion of one or more electrons[1] inside the crystal, subject to the action of external forces due to applied electric and magnetic fields and of given scattering mechanisms. The duration of the carrier free flight (i.e., the time between two successive collisions) and the scattering events involved in the simulation are selected stochastically in accordance with some given probabilities describing the microscopic processes. As a consequence, any Monte Carlo method relies on the generation of a sequence of random numbers with given distribution probabilities. Such a technique takes advantage of the fact that nowadays any computer generates sequences of random numbers evenly distributed between 0 and 1 at a sufficiently fast rate. The problem of generation of random numbers is treated in Appendix A.

When the purpose of the analysis is the investigation of a steady-state, homogeneous phenomenon, it is sufficient in general to simulate the motion of one single electron; from ergodicity we may assume that a sufficiently long path of this sample electron will give information on the behavior of the entire electron gas. When, on the contrary, the transport process under investigation is not homogeneous or is not stationary, then it is necessary to simulate a large number of electrons and follow them in their dynamic histories in order to obtain the desired information on the process of interest.

B. A typical Monte Carlo program

Let us summarize here the structure of a typical Monte Carlo program suited to the simulation of a stationary, homogeneous, transport process. The details of each step of the procedure will be given in the following sections. For the sake of simplicity we shall refer to the case of electrons in a simple semiconductor subject to an external electric field $\mathbf{E}$. The simulation starts with one electron in given initial conditions with wave vector $\mathbf{k}_0$; then the duration of the first free flight is chosen with a probability distribution determined by the scattering probabilities. During the free flight the external forces are made to act according to the relation

$$\hbar\dot{\mathbf{k}} = e\mathbf{E} , \tag{2.1}$$

where $\mathbf{k}$ is the carrier wave vector, e its charge with its sign ($e<0$ for electrons and $e>0$ for holes), and $\hbar$ the Planck constant divided by 2π. In this part of the simulation all quantities of interest, velocity, energy, etc., are recorded. Then a scattering mechanism is chosen as responsible for the end of the free flight, according to the relative probabilities of all possible scattering mechanisms. From the differential cross section of this mechanism a new $\mathbf{k}$ state after scattering is randomly chosen as initial state of the new free flight, and the entire process is iteratively repeated. The results of the calculation become more and more precise as the simulation goes on, and the simulation ends when the quantities of interest are known with the desired precision.

A simple way to determine the precision, that is, the statistical uncertainty, of transport quantities consists of dividing the entire history into a number of successive subhistories of equal time duration, and making a determination of a quantity of interest for each of them. We then determine the average value of each quantity and take its standard deviation as an estimate of its statistical uncertainty (see Sec. II.B.6.*c*).

Figure 1 shows a flowchart of a simple Monte Carlo program suited for the simulation of a stationary, homogeneous transport process.

Figure 2 illustrates the principles of the method by showing the simulation in $\mathbf{k}$ space and real space and the effect of collecting statistics in the determination of the drift velocity.

1. Definition of the physical system

The starting point of the program is the definition of the physical system of interest, including the parameters of the material and the values of physical quantities, such as lattice temperature T_0 and electric field. It is worth noting that, among the parameters that characterize the material, the least known, usually taken as adjustable parameters, are the coupling strengths describing the interactions of the electron with the lattice and/or extrinsic defects inside the crystal.

At this level we also define the parameters that control the simulation, such as the duration of each subhistory, the desired precision of the results, and so on.

The next step in the program is a preliminary calculation of each scattering rate as a function of electron energy. This step will provide information on the maximum value of these functions, which will be useful for optimizing the efficiency of the simulation (see Sec. II.B.3). Finally, all cumulative quantities must be put at zero in this preliminary part of the program.

2. Initial conditions of motion

In the case under consideration, in which a steady-state situation is simulated, the time of simulation must be long enough that the initial conditions of the electron motion do not influence the final results. The choice of a "good" time of simulation is a compromise between the need for ergodicity ($t\rightarrow\infty$) and the request to save computer time. When a highly improbable initial value for the electron wave vector $\mathbf{k}$ is chosen, the first part of the simulation can be strongly influenced by this inappropriate choice.

In the particular case of a very high electric field, if an energy of the order of $K_B T_0$ (K_B being the Boltzmann constant) is initially given to the electron, this energy will be much lower than the average energy in steady-state conditions, and during the transient it will increase towards its steady-state value. As a consequence, the electron response to the field, in terms of mobility, may be in-

[1] In the present review, for brevity we shall often write "electrons" meaning in fact "charge carriers," that is, electrons or holes indifferently.

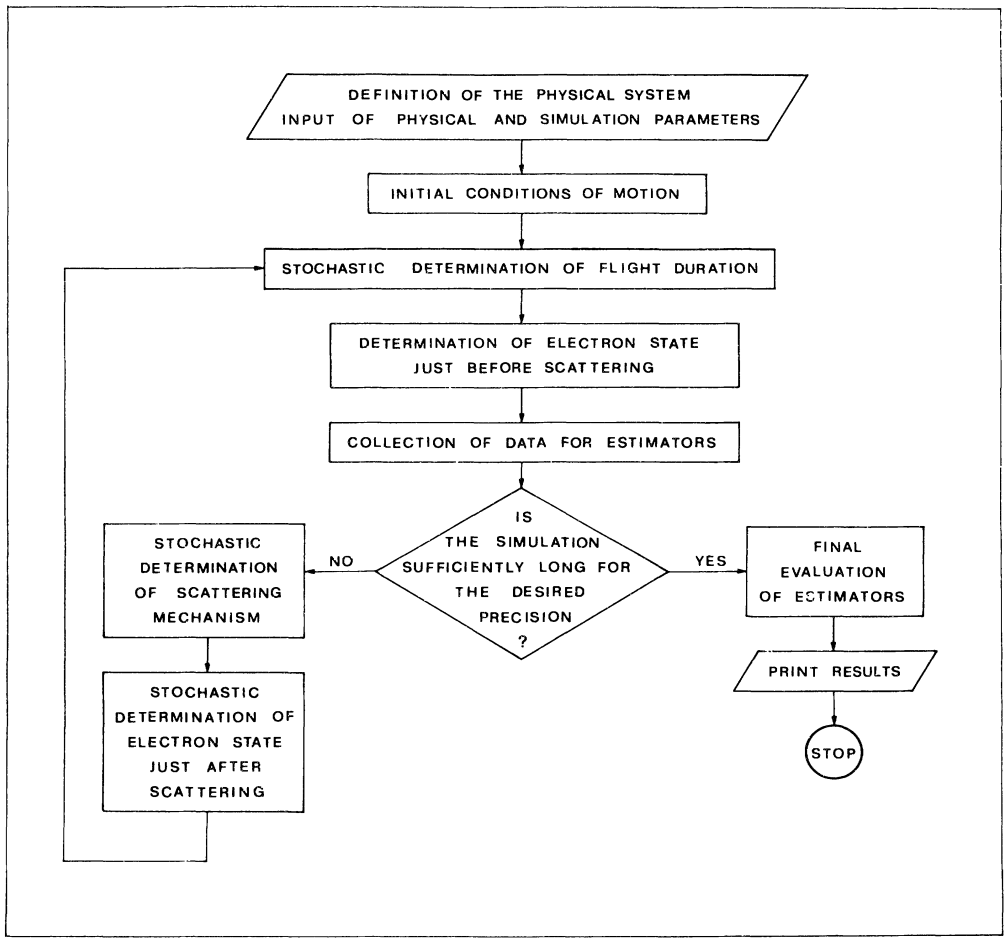

FIG. 1. Flowchart of a typical Monte Carlo program.

itially much higher than that of stationary conditions (see Secs. II.C.1 and IV.B.13). This is reflected in real space by initial free flights which are much longer than in stationary conditions because of an abnormally large momentum relaxation time initially (see Fig. 3).

The longer the simulation time, the less influence the initial conditions will have on the average results; however, in order to avoid the undesirable effects of an inappropriate initial choice and to obtain a better convergence, the elimination of the first part of the simulation from the statistics may be advantageous. When the simulation is divided into many subhistories, better convergence to steady state can be achieved by taking the initial state of each new subhistory as equal to the final state of the previous one. In this way, only the initial condition of the first subhistory will influence the final results in a biased way.

On the other hand, when a simulation is made to study a transient phenomenon and/or a transport process in a nonhomogeneous system (for example, when the electron transport in a small device is analyzed), then it is necessary to simulate many electrons separately; in this case the distribution of the initial electron states for the particular physical situation under investigation must be taken into account (see Sec. II.C.1), and the initial transient becomes an essential part of the results aimed at.

3. Flight duration—self-scattering

The electron wave vector $\mathbf{k}$ changes continuously during a free flight because of the applied field according to Eq. (2.1). Thus if $P[\mathbf{k}(t)]dt$ is the probability that an electron in the state $\mathbf{k}$ suffers a collision during the time dt, the probability that an electron which suffered a collision at time $t=0$ has not yet suffered another collision after a time t is

$$\exp\left[-\int_0^t P[\mathbf{k}(t')]dt'\right],$$

which, generally, gives the probability that the interval $(0,t)$ does not contain a scattering. Consequently, the probability $\mathscr{P}(t)$ that the electron will suffer its next collision during dt around t is given by

$$\mathscr{P}(t)dt = P[\mathbf{k}(t)]\exp\left[-\int_0^t P[\mathbf{k}(t')]dt'\right]dt \ . \tag{2.2}$$

Because of the complexity of the integral at the exponent, it is impractical to generate stochastic free flights

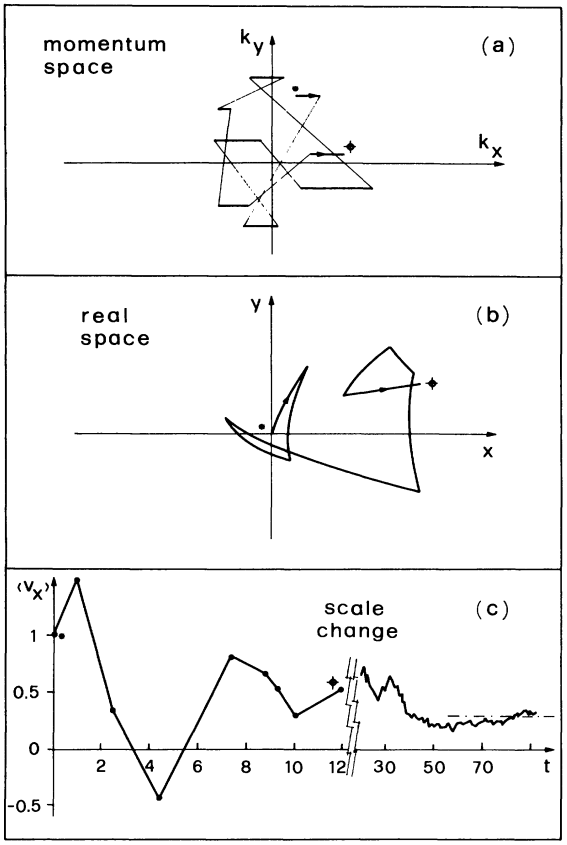

FIG. 2. The principles of the Monte Carlo method. For simplicity a two-dimensional model is considered here. (a) The simulation of the sampling particle, in the wave-vector space, subject to an accelerating force (field) oriented along the positive x direction. The heavy segments are due to the effect of the field during free flights; curves represent discontinuous variations of $\mathbf{k}$ due to scattering processes. (b) The path of the particle in real space. It is composed of eight fragments of parabolas corresponding to the eight free flights in part (a) of the figure. (c) The average velocity of the particle obtained as a function of simulation time. The left section of the curve ($t < 12$) is obtained by the simulation illustrated in the parts (a) and (b) of the figure. The horizontal dot-dashed curve represents the "exact" drift velocity obtained with a very long simulation time. Special symbols indicate corresponding points in the three parts of the figure (* is the starting point). All units are arbitrary.

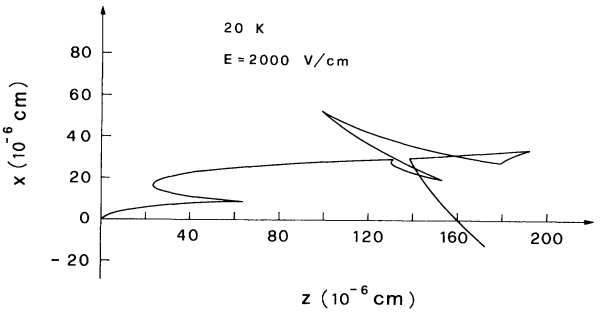

FIG. 3. Projection in the xz plane of real space of the trajectory of a carrier starting with thermal equilibrium mean energy, under the influence of a high electric field. The well-oriented initial free trajectories reflect values of the momentum relaxation times longer than under steady-state conditions as a consequence of the lower energy.

with the distribution of Eq. (2.2), starting from evenly distributed random numbers r and applying the techniques discussed in Appendix A: with this approach an integral equation would need to be solved for each scattering event (Kurosawa, 1966). Rees (1968, 1969) has devised a very simple method to overcome this difficulty. If $\Gamma \equiv 1/\tau_0$ is the maximum value of $P(\mathbf{k})$ in the region of $\mathbf{k}$ space of interest, a new fictitious "self-scattering" is introduced such that the total scattering probability, including this self-scattering, is constant and equal to Γ. If the carrier undergoes such a self-scattering, its state $\mathbf{k}'$ after the collision is taken to be equal to its state $\mathbf{k}$ before the collision, so that in practice the electron path continues unperturbed as if no scattering at all had occurred. Generally it is sufficient that Γ be not less than the maximum value of $P(\mathbf{k})$; furthermore, as we shall see below, Γ can be a convenient function of energy.

Now, with a constant $P(\mathbf{k}) = \tau_0^{-1}$, Eq. (2.2) reduces to

$$\mathcal{P}(t) = \frac{1}{\tau_0} \exp(-t/\tau_0) , \tag{2.3}$$

and random numbers r can be used very simply to generate stochastic free flights t_r with the direct technique described in Appendix A Sec. 2.a. They will be given by

$$t_r = -\tau_0 \ln(1-r) . \tag{2.4}$$

However, since r is evenly distributed between 0 and 1, so also is $(1-r)$, and in practice in place of Eq. (2.4) we generally use

$$t_r = -\tau_0 \ln(r) . \tag{2.5}$$

The computer time "wasted" in taking care of self-scattering events is more than compensated for by the simplification of the calculation of the free-flight duration.

As regards the choice of the constant Γ, we note that in general $P(\mathbf{k})$ is simply a function of the electron energy $P(\epsilon)$; a suitable choice for Γ is then the maximum value of $P(\epsilon)$ in the region of energies which are expected to be sampled during the simulation. When $P(\epsilon)$ is not a monotonic function of ϵ, its maximum value must be estimated in some way, for example, with a tabulation at the beginning of the computer program. When $P(\epsilon)$ is an increasing function of ϵ, as is often the case, one can take $\Gamma = P(\epsilon_M)$, where ϵ_M is a maximum electron energy with negligible probability of being achieved by the carrier during the simulation. It must be observed, however, that the range of energy "visited" by the electron during the simulation is not known at the beginning, when Γ is to be chosen. Therefore, an estimate must be made for ϵ_M, keeping in mind that ϵ_M cannot be taken as too large, if one is to prevent an unnecessarily large value of Γ that would result in a waste of computer time for self-

scattering events. One must also decide what action to take when, during the simulation, the electron energy ϵ happens to exceed the maximum value ϵ_M set up at the beginning of the computer run. Some authors in such circumstances arbitrarily reduce the electron energy ϵ to a value lower than ϵ_M and simply check at the end of the computer run that such a situation occurred a limited number of times. This procedure may be dangerous, since it may obscure the occurrence of an indefinite increase of electron energy (electron runaway) when this happens at energies above a critical value close to ϵ_M. A safer method is to increase the value of ϵ_M and correspondingly of Γ, if required, for the simulation to continue, without intervening in the electron energy. Since Γ must be independent of the simulated flight, it is always necessary to check that Γ has not been changed too many times. This is guaranteed when ϵ_M has been underestimated at the set-up of the program run, because it will quickly increase to a value above which the electron energy will rarely go.

For a semiconductor model that contains several valleys, a different value of E_M may be appropriately taken in each type of valley.

Sometimes the total scattering probability $P(\epsilon)$ has a large variation around some threshold value due to a strong scattering mechanism with a given activation energy (a typical case is intervalley scattering from central to upper valleys in polar semiconductors). In this case, a single value of Γ may result in a very large number of self-scattering events at low electron energies (see Fig. 4). It is then possible to introduce a step-shaped scattering rate $\Gamma(\epsilon)$ given by

$$\Gamma(\epsilon)=\begin{cases}\Gamma_1=\tau_1^{-1}, & \epsilon\le\epsilon_1\\ \Gamma_2=\tau_2^{-1}, & \epsilon>\epsilon_1\end{cases} \tag{2.6}$$

where ϵ_1 is a suitable threshold energy, and Γ_1 and Γ_2 are the maximum values of $P(\epsilon)$ in the two corresponding energy ranges.

In using $\Gamma(\epsilon)$ as given by Eq. (2.6), we should remember that, during a free flight, the electron energy may exceed the value ϵ_1. The following two cases may occur according to the initial state of the free flight.

(i) An electron begins a free flight with an energy below ϵ_1. A random number r is then used to generate with Γ_1 a free flight with duration t_r given by

$$t_r=-\tau_1\ln(r)\ . \tag{2.7}$$

If at the end of this free flight the electron energy is still less than ϵ_1, t_r is retained, and the simulation proceeds as usual. If, on the contrary, at the end of this free flight the electron energy is above ϵ_1, t_r as given by Eq. (2.7) cannot be retained. The same random number r is then used to generate a new duration of the free flight as follows. From Eq. (2.6) we have, instead of Eq. (2.3),

$$\mathcal{P}(t)=\begin{cases}\dfrac{1}{\tau_1}\exp(-t/\tau_1), & t<\tilde{t}\\ \dfrac{1}{\tau_2}\exp\{-[\tilde{t}/\tau_1+(t-\tilde{t})/\tau_2]\}, & t\ge\tilde{t}\end{cases} \tag{2.8}$$

where $\tilde{t}$ is the time necessary for the electron to reach the energy ϵ_1 and can be easily evaluated from the electron dynamics. By application of the direct technique (see Appendix A Sec. 2.a) t_r is then given by

$$t_r=-\tau_2\ln(r)+\tilde{t}(1-\tau_2/\tau_1)\ . \tag{2.9}$$

(ii) An electron begins a free flight with an energy above ϵ_1. The duration of this free flight can always be determined by Eq. (2.6) with $\tau=\tau_2$. In fact, even if the final enery is below ϵ_1, one is justified in considering the upper value Γ_2 of $\Gamma(\epsilon)$ extended to lower energies, as long as this is done independently of the particular value of r. Of course, Γ_2 must then be consistently considered in the determination of the scattering mechanism (in particular for self-scattering) which caused the end of the free flight (see next section).

The only situation not accounted for in the above discussion is when, during a single free flight, the electron energy starting from values below ϵ_1 first increases to above ϵ_1 and then decreases to below ϵ_1; but this situation cannot occur with static fields and normal band structures.

The above idea can be extended to piecewise functions $\Gamma(\epsilon)$ with more than one step. However, such a procedure must be compared, from the point of view of saving computer time, with the so called fast self-scattering technique (see next section).

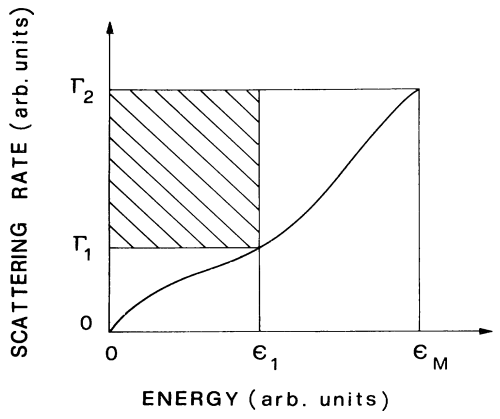

FIG. 4. Sketch of a two-level step-shaped total scattering rate, including self-scattering $\Gamma(\epsilon)$, appropriate for reducing the number of self-scattering events with respect to a single-level choice (the Γ_2). Γ_1 is used for energies between 0 and ϵ_1, as explained in the text. The shaded region illustrates the increased efficiency resulting from the two-level choice.

4. Choice of the scattering mechanism

During free flight, electron dynamics is governed by Eq. (2.1) so that at its end the electron wave vector and energy are known, and all scattering probabilities $P_i(\epsilon)$ can be evaluated, where i indicates the ith scattering mechanism. The probability of self-scattering will be the complement to Γ of the sum of the P_i's. A mechanism must then be chosen among all those possible: given a

random number r, the product $r\Gamma$ is compared with the successive sums of the P_i's, and a mechanism is selected as described in Appendix A Sec. 2.d.

Since each scattering probability $P_i(\epsilon)$ must be evaluated until a mechanism is chosen by the random number, in the computer program it is convenient to rank the P_i's in order of probability before beginning. It must be noted, however, that the occurrence of the various scatterings depends also on temperature and field strength, so that it may sometimes be difficult to predict their relative frequency.

If all scatterings have been tried and none of them has been selected, it means that $r\Gamma > P(\epsilon)$, and a self-scattering occurs. Ascertaining by this procedure that a self-scattering occurs is therefore most time consuming, since all P_i's must be explicitly calculated. However, the process may be shortened by use of an expedient that might be called fast self-scattering. It consists of setting up a mesh of the energy range under consideration at the beginning of the simulation and then recording in a vector the maximum total scattering probability $P^{(l)}$ in each energy interval $\Delta\epsilon^{(l)}$ (energy intervals equally distributed on a logarithmic scale may be useful). At the end of the flight if the electron energy falls in the nth interval, before trying all P_i's separately, one compares $r\Gamma$ with $P^{(n)}$. At this stage if $r\Gamma > P^{(n)}$ then a self-scattering certainly occurs; otherwise all P_i's will be successively evaluated. Thus only when $P(\epsilon) < r\Gamma < P^{(n)}$ does a self-scattering occur which requires the evaluation of all P_i's.

As regards the scattering probabilities of various mechanisms and their use in the Monte Carlo program, we shall consider in Sec. III the cases useful for covalent semiconductors. For other cases we refer the reader to the original literature.

5. Choice of the state after scattering

Once the scattering mechanism that caused the end of the electron free flight has been determined, the new state after scattering of the electron, $\mathbf{k}_a$ must be chosen as the final state of the scattering event. If the free flight ended with a self-scattering, $\mathbf{k}_a$ must be taken as equal to $\mathbf{k}_b$, the state before scattering. When, in contrast, a true scattering occurred, then $\mathbf{k}_a$ must be generated, stochastically, according to the differential cross section of that particular mechanism. The techniques used to select the state after each particular type of scattering are discussed in Sec. III.D.

6. Collection of results for steady-state phenomena

The data collected at each free flight will form the base for the determination of the quantity of interest.

a. Time averages

Generally speaking, we may obtain the average value of a quantity $\mathscr{A}[\mathbf{k}(t)]$ (e.g., the drift velocity, the mean energy, etc.) during a single history of duration T as

$$\langle \mathscr{A} \rangle_T = \frac{1}{T}\int_0^T \mathscr{A}[\mathbf{k}(t)]dt = \frac{1}{T}\sum_i \int_0^{t_i} \mathscr{A}[\mathbf{k}(t')]dt' , \tag{2.10}$$

where the integral over the whole simulation time T has been separated into the sum of integrals over all free flights of duration t_i. When a steady state is investigated, T should be taken as sufficiently long that $\langle \mathscr{A} \rangle_T$ in Eq. (2.10) represents an unbiased estimator of the average of the quantity $\mathscr{A}$ over the electron gas.

In a similar way we may obtain the electron distribution function: a mesh of $\mathbf{k}$ space (or of energy) is set up at the beginning of the computer run; during the simulation the time spent by the sample electron in each cell of the mesh is recorded and, for large T, this time conveniently normalized will represent the electron distribution function, that is, the solution of the Boltzmann equation (Fawcett *et al.*, 1970). This evaluation of the distribution function can be considered a special case of Eq. (2.10) in which we choose for $\mathscr{A}$ the functions $n_j(\mathbf{k})$ with value 1 if $\mathbf{k}$ lies inside the jth cell of the mesh and zero otherwise.

This method is the one most generally used to obtain transport quantities from Monte Carlo simulations. We shall see specific applications of it in Sec. IV.

b. Synchronous ensemble

Another method of obtaining an average quantity $\langle \mathscr{A} \rangle$ from the simulation of a steady-state phenomenon has been introduced by Price (1968, 1970); this is the synchronous-ensemble method. Let us consider Fig. 5, in which a time axis is specified for each of the N electrons of the physical system. Circles in these axes indicate scattering events. In principle, each of the axes can represent a simulated electron, and self-scattering can be included if wanted. In general the averge value of a quan-

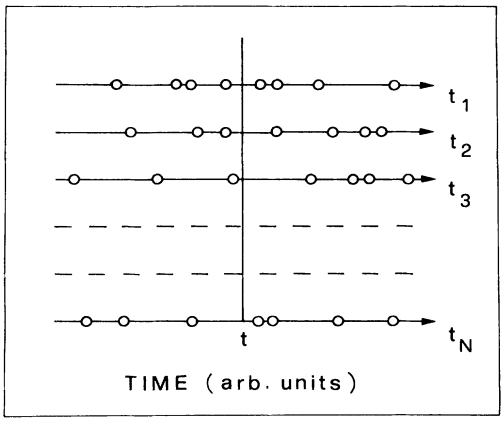

FIG. 5. Sketch illustrating the synchronous-ensemble method. Subscripts (1,2,3 . . . ,N) label the time axis of the ith particle; open circles indicate scattering events; t is the generic time of a steady-state condition.

tity $\mathscr{A}$ is defined as the ensemble average at time t over the N electrons of the system,

$$\langle \mathscr{A} \rangle = \frac{1}{N} \sum_i \mathscr{A}_i(t_i = t) \ . \tag{2.11}$$

In particular, the steady-state distribution function is proportional to the number of electrons $n(\mathbf{k})\Delta\mathbf{k}$ that at time t are found to be in a cell of fixed volume $\Delta\mathbf{k}$ around $\mathbf{k}$. Then Eq. (2.11) can also be evaluated as

$$\langle \mathscr{A} \rangle = \mathscr{C} \sum_{\mathbf{k}} n(\mathbf{k}) \mathscr{A}(\mathbf{k}) \ , \tag{2.12}$$

where $\mathscr{C}$ is an appropriate normalization constant, and $n(\mathbf{k})$ can be considered as proportional to the probability of finding any given electron in state $\mathbf{k}$.

Now, in the spirit of Chambers's path-integral method (Chambers, 1952), an electron will be found in $\mathbf{k}$ at time t if it has been scattered in the suitable $\mathbf{k}'$ an appropriate time interval t' before t and has not been scattered again between $(t - t')$ and t (see Fig. 6).

Let $n_a(\mathbf{k})$ be the so-called after-scattering distribution function, proportional to the probability that an electron is found in $\mathbf{k}$ immediately after a scattering event. Then $n(\mathbf{k})$ is proportional to

$$n(\mathbf{k}) \propto \int_0^\infty n_a[\mathbf{k}'(t')] \mathscr{P}[\mathbf{k}'(t'), t'] dt' \ ,$$

where $\mathscr{P}(\mathbf{k}', t')$ is the probability that an electron in $\mathbf{k}'$ at a given time will not be scattered before an interval of time t'.

If we now consider the before-scattering distribution function $n_b(\mathbf{k})$, proportional to the probability that an electron is found in $\mathbf{k}$ immediately before a scattering event, we shall find by an argument similar to that given above that

$$n_b(\mathbf{k}) \propto \frac{1}{\tau(\mathbf{k})} \int_0^\infty n_a[\mathbf{k}'(t')] \mathscr{P}[\mathbf{k}'(t'), t'] dt' \ ,$$

where $\tau^{-1}(\mathbf{k})$ is the scattering rate for an electron in $\mathbf{k}$. Thus the steady-state distribution function is given by

$$n(\mathbf{k}) = \frac{1}{\tau_0} n_b(\mathbf{k}) \tau(\mathbf{k}) \ , \tag{2.13}$$

where τ_0 is an appropriate normalization constant. If, by including self-scattering, we use a constant $\tau(\mathbf{k})$, then the steady-state distribution function becomes proportional to the before-scattering distribution[2]

$$n(\mathbf{k}) \propto n_b(\mathbf{k}) \ ,$$

and Eq. (2.12) can be used in a Monte Carlo simulation in the following form:

$$\langle \mathscr{A} \rangle = \frac{1}{N} \sum_i \mathscr{A}_{bi} \ , \tag{2.14}$$

where the sum covers all N electron free flights, and $\mathscr{A}_{bi}$ indicates the value of the quantity $\mathscr{A}$ evaluated at the end of the free flight immediately before the ith scattering event.

If self-scattering with a step-shaped total scattering probability, as described in Sec. II.B.3, is used, then the various terms in the sum of Eq. (2.14) must be weighted with a factor $\Gamma^{-1}(\mathbf{k})$; but in this case particular care must be taken when, during a flight, $\mathbf{k}(t)$ crosses the border from one value of Γ_i to another value, since $\tau(\mathbf{k})$ must be a unique, well-defined function of $\mathbf{k}$.

c. Statistical uncertainty

In order to estimate the statistical uncertainty of a time-average result $\langle \mathscr{A} \rangle_T$ due to the finite value of the simulation time T, as mentioned in Sec. II.B, we can divide[3] the whole history in N subhistories of duration T/N; for each of them a value $\langle \mathscr{A} \rangle_l$ is obtained. We may then take as the most probable value of $\langle \mathscr{A} \rangle$ the average of the $\langle \mathscr{A} \rangle_l$'s (which will be equal to $\langle \mathscr{A} \rangle_T$) and its standard deviation as the statistical uncertainty on $\langle \mathscr{A} \rangle_T$. The subhistories must be sufficiently long to be considered as independent of each other, but sufficiently short to allow us to perform a large number N of them.

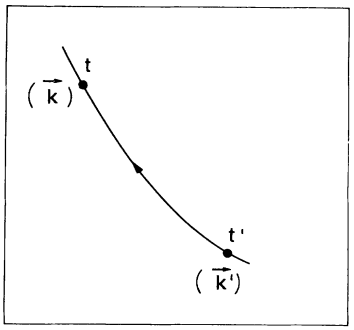

FIG. 6. Trajectory of an electron in $\mathbf{k}$ space. An electron that contributes to the distribution function $f(\mathbf{k}, t)$ must have scattered onto the trajectory at some previous time t' at the corresponding $\mathbf{k}'$ and have followed it without scattering until it arrived at point $\mathbf{k}$ at time t (Cohen *et al.*, 1960).

[2]It may seem strange that with a constant $\tau(\mathbf{k})$ the before-scattering distribution $n_b(\mathbf{k})$ is equal to the steady-state distribution, since the states just before the scattering events seem to be influenced "at the maximum" by the applied fields. However, one should consider that, while $n_b(\mathbf{k})$ weights equally all free flights (short and long ones) with average duration τ, when an instantaneous picture of the electron gas is taken at any time t, longer free flights are more likely to be caught. In other words, in the latter case the vertical line in Fig. 5 crosses free flights whose mean duration is longer than the average over all free flights; in fact, the distribution of the hemi-flights on the right and on the left of the line t reproduces the distribution of flight durations, so that the average length of the flights crossed by t is 2τ.

[3]This division requires the interruption of a free flight at the end of each subhistory simulation. The remaining part of the flight is thus used as the initial part of the successive subhistory simulation.

In this case the uncertainty decreases as $1/\sqrt{N}$. Furthermore, it is possible to carry out, on the series of partial results $\langle \mathscr{A} \rangle_l$, those tests (Hammersley and Handscomb, 1964) which verify the statistical nature of their fluctuations.

C. Time- and space-dependent phenomena

For time- and/or space-dependent problems the analytical solution of the Boltzmann equation is even more difficult than for homogeneous and stationary problems, while for Monte Carlo programs little work need be added to attack such problems. This confirms again the usefulness of the Monte Carlo method, in particular, for the analysis of small devices, where it is often necessary to consider both the transient dynamic response to the voltage changes and electronic behavior at different points of the device with different field or material properties (Baccarani *et al.*, 1977; Zimmermann and Constant, 1980).

As mentioned in Sec. II.A, for such problems we cannot rely on the ergodicity of the system; an ensemble of particles must be explicitly simulated (Lebwohl and Price, 1971a, 1971b).

One exception of this rule that will be discussed in Sec. II.C.3 is that of phenomena which are periodic in space and/or time. In this case the different situations experienced by the electron in equivalent positions or times will take into account the many possibilities of various particles, and again the simulation of a single electron may yield the necessary information about the entire electron gas.

1. Transients

We shall consider here the case of a homogeneous electron gas with time-dependent behavior. In particular, it is of interest to study the transient dynamic response to a sudden change in the value of an applied field. In this situation many particles must be independently simulated with appropriate distributions of initial conditions. Provided the number of simulated particles is sufficiently large, the average value of a quantity of interest, obtained on this sample ensemble as a function of time, will be representative of the average for the entire gas.

It must be stressed that the estimators given by Eqs. (2.10) and (2.14) are based on the hypothesis of steady-state conditions and cannot be used when a time-dependent phenomena is analyzed: the ensemble average of a quantity $\mathscr{A}$ must actually be estimated according to its definition, given by Eq. (2.11):

$$\langle \mathscr{A}(t) \rangle = \frac{1}{N} \sum_i \mathscr{A}_i(t) \ , \tag{2.15}$$

where i runs over all N simulated particles.

The duration of the transient response is not known *a priori* and will be of the order of the largest of the characteristic times of the electron system. This time may be called the "transient-transport time" and in general depends upon the values of the applied field and temperature; in our case of high-field transport in semiconductors, it may roughly correspond to the energy relaxation time or to the time for repopulation of different valleys.

To determine the precision of the results obtained, one separates the entire ensemble into a certain number of subensembles and estimates for each of them the quantity of interest $\mathscr{A}$. Then their average value and standard deviation can be taken, respectively, as the most probable value and the statistical uncertainty of $\mathscr{A}$.

The transient dynamic response obtained by means of the simulation will, of course, depend upon the initial conditions of the carriers, and these must be assumed according to the situation to be explored. Initial velocity distributions which may be of interest are, for example, a Maxwellian distribution at the lattice temperature and no drift, or a Maxwellian distribution with an electron temperature higher than that of the lattice, with or without drift.

2. Space-dependent phenomena

The simulation of a steady-state phenomenon in a physical system where electron transport depends upon the position in space is of particular interest for the analysis and modeling of devices. For this case, too, an ensemble of independent particles must be used, and averages must be taken over particles at given positions. The statistical uncertainties of the results can be obtained with subensembles, as indicated in the preceding section.

In a steady-state situation, particles enter the region of interest continuously, and in the simulation some initial wave vector must be assumed when a new particle is considered, according to the momentum distribution of the particles in the physical system under investigation. For example, a cold hemi-Maxwellian distribution, that is, one with only positive velocity components along a given direction, may be convenient in simulating the metallic contact of a device. If the simulated electron entering the device goes back to the contact, a new electron must be generated, but the "lost" electron must be accounted for in the final results in a way that depends on the particular analysis being carried out.

Space- and time-dependent phenomena may present similar characteristics, and they have sometimes been confused in simulation problems. For instance, if a field is suddenly switched on from zero to a large value, during the initial transient the drift velocity reaches values larger than those in steady-state conditions (overshoot effect), and this effect is sometimes useful in discussing the behavior of an electron stream, coming from a low-field region and entering a region with a high applied field.

If this mode of reasoning is correct from a qualitative point of view, in rigorous calculations the kind of average that must be taken is different depending on whether time- or space-dependent phenomena are considered. In a steady-state phenomenon with space-dependent applied fields it is, in general, necessary to consider the electron properties at given positions (Baccarani *et al.*, 1977; Zim-

mermann and Constant, 1980), so that the simulation must record average values for given points over time; when the object of the investigation is the evolution in time of a homogeneous sytem, average quantities must be evaluated at given times independent of the particle positions.

3. Periodic fields

Monte Carlo simulation can be extended to permit calculation of the response of charge carriers to periodic external fields of any strength (Lebwohl, 1973; Zimmerman *et al.*, 1978). If a field

$$\mathbf{E}=\mathbf{E}_0+\mathbf{E}_1\sin(\omega t) \tag{2.16}$$

is applied, and the ac term is small enough to be in the linear-response regime, the average electron velocity will be of the form

$$\langle \mathbf{v}(t)\rangle=\mathbf{v}_0+\mathbf{v}_1\sin(\omega t)+\mathbf{v}_2\cos(\omega t)\ . \tag{2.17}$$

The coefficients $\mathbf{v}_1$ and $\mathbf{v}_2$ of the fundamental response in Eq. (2.17) can be obtained as sine and cosine Fourier transforms, respectively, of the velocity of the simulated electron over its history. Since the equation of motion of the particle subject to a field given by Eq. (2.16) is known in explicit terms, the Fourier coefficients $\mathbf{v}_1$ and $\mathbf{v}_2$ can easily be obtained by the simulation (Lebwohl, 1973).

For large periodic fields, the periodic part of the current will contain higher harmonics, besides the fundamental frequency. These components can also be obtained by Fourier analysis of the simulated velocity, but in this case statistical-noise problems become severe.

It is also possible to obtain the total response of the electron gas without Fourier analysis, by sampling the electron velocity at fixed times, corresponding to definite phases in the period of the external force. To be more explicit, as illustrated in Fig. 7, let us suppose that we "read" from the simulation the electron velocity at times given by $0,\Delta t,2\Delta t,\ldots,l\Delta t,\ldots$, where Δt [with typical values within $(0.5-1)\times10^{-14}$ sec] is a fraction $1/N$ of the period $2\pi/\omega$ of the ac field:

$$\Delta t=\frac{1}{N}\frac{2\pi}{\omega}\ . \tag{2.18}$$

Then we average the values of $\mathbf{v}$ obtained at times $l\Delta t,(l+N)\Delta t,(l+2N)\Delta t,\ldots$. The result is an estimator of the average electron velocity $\langle\mathbf{v}\rangle$, which is a periodic function of t with the same period $2\pi/\omega$, at the times given above.

The synchronous-ensemble method described in Sec. II.B.6.*b* for static fields has been extended by Lebwohl (1973) to include the case of periodic fields. The result is a simple parametric dependence of Eq. (2.13) upon time:

$$n(\mathbf{k},t)=\frac{1}{\tau_0}n_b(\mathbf{k},t)\tau(\mathbf{k})\ , \tag{2.19}$$

and in the applications it is possible to operate as for static fields with the additional care of assigning each analyzed event to the proper phase (or time within the period).

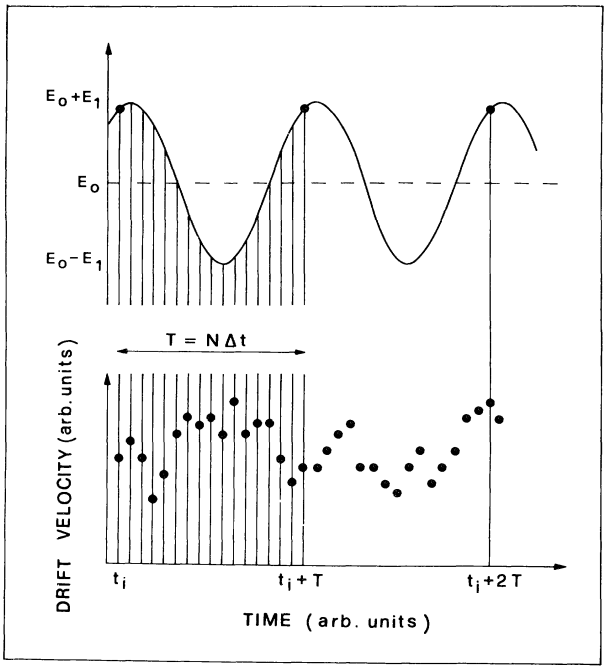

FIG. 7. Simulation of transport with periodic fields. A random variable (for example instantaneous velocity at time t_i) is recorded in response to the periodic input signal $E(t)$. Period T is divided into N intervals of equal duration Δt, and the average response is obtained by averaging the values at $t_i,t_i+T,t_i+2T,\ldots$ (Zimmermann *et al.*, 1978).

D. Diffusion

Diffusion may be considered a special, important case of a space-dependent phenomenon which is in general also time dependent, and a great deal of work has recently been done in this field with the Monte Carlo technique.

In the linear-response regime, diffusion D and mobility μ are related by the Einstein relation

$$D=(1/e)\mu K_B T_0\ . \tag{2.20}$$

Thus an independent determination of the diffusion coefficient does not add any particular information about the transport properties of a material that one could not obtain by determining the Ohmic mobility.

At high fields, however, the Einstein relation fails and the study of hot-electron diffusion becomes useful for two reasons: (i) from a basic point of view it provides an independent check, in addition to the drift velocity, of theoretical models of the material under investigation; (ii) from a more applied point of view, it provides useful information for the analysis of most solid-state devices.

It must be added that deviations of the diffusion coefficient from its equilibrium value can also occur at fields

lower than those at which hot-electron phenomena are usually present, because of the possibility of intervalley diffusion, which occurs in many-valley semiconductors (see Sec.IV.B.3).

1. Fick diffusion

Diffusion is described at a phenomenological level by the first Fick's equation,

$$j_i = -eD_{ij}\frac{\partial n(\mathbf{x})}{\partial x_j} \quad , \tag{2.21}$$

where $\mathbf{j}$ is the current density, D_{ij} is the diffusion tensor, $\mathbf{x}$ is the particle position in space, and $n(\mathbf{x})$ is the particle density; the sum over repeated indices is implied.

If an electric field is also present which would produce, in the absence of diffusion, a drift velocity v_d, and if diffusion and drift do not influence each other,[4] then for Eq. (2.21) we substitute

$$j_i = e\left[n(\mathbf{x})v_{d_i}(\mathbf{E}) - D_{ij}\frac{\partial n(\mathbf{x})}{\partial x_j}\right] \quad . \tag{2.22}$$

By combining this equation with the continuity equation,

$$e\frac{\partial n}{\partial t} = -\frac{\partial}{\partial x_i}j_i \quad , \tag{2.23}$$

we obtain the diffusion equation, sometimes called the second Fick's equation:

$$\frac{\partial n}{\partial t} = -v_{d_i}(\mathbf{E})\frac{\partial n}{\partial x_i} + D_{ij}\frac{\partial^2 n}{\partial x_i \partial x_j} \quad , \tag{2.24}$$

where v_d and D have been supposed to be space independent.

Under linear-response conditions, v_d depends linearly on field, and D is field independent, as can be obtained from the solution of the Boltzmann equation. The generalization at high fields of Eq. (2.24) is usually performed by assuming $D = D(\mathbf{E})$. As a matter of fact, a rigorous derivation from the Boltzmann equation of Eq. (2.24) with $D = D(\mathbf{E})$ can be performed only by assuming small concentration gradients and times longer than both the transient-transport time, defined in Sec. II.C.1, and the time necessary for setting up the correct space-velocity correlations (see Gantsevich *et al.*, 1974, 1979).

If, for simplicity, n is assumed to be a function of only one coordinate z parallel to the direction of v_d, and M_m is the mth moment of $n(z)$, defined by

$$M_m = \frac{1}{N}\int z^m n(z)dz \tag{2.25}$$

(N being the total number of particles), then from Eq. (2.24) we have, after successive integrations by parts (Jacoboni *et al.*, 1978; Price, 1979),

$$\begin{aligned} &\frac{dM_1}{dt} = v_d \quad , \\ &\frac{dM_2}{dt} = 2v_d M_1 + 2D_l \quad , \\ &\cdots \\ &\frac{dM_m}{dt} = mv_d M_{m-1} + m(m-1)D_l M_{m-2} \quad , \end{aligned} \tag{2.26}$$

where D_l is the diagonal component of D along v_d.

In particular, for the second central moment we have

$$D_l = \frac{1}{2}\frac{d}{dt}\langle (z - \langle z \rangle)^2 \rangle \quad . \tag{2.27}$$

This expression can be used to determine the diffusion coefficient by means of a Monte Carlo simulation: a number of particles is independently simulated and their positions are recorded at fixed times. For large enough simulation times, the second central moment shows the linearity predicted by Eq. (2.27), and from its slope D_l is obtained. For short simulation times Eq. (2.27) does not hold, for the reason discussed above.

Often, instead of Eq. (2.27), the following alternative equation is used (Fawcett, 1973; Fauquembergue *et al.*, 1980; Ferry, 1980):

$$D_l = \frac{\langle (z - \langle z \rangle)^2 \rangle}{2t} \quad . \tag{2.28}$$

Equation (2.28) may in fact be deduced from the solution of the diffusion equation (2.24) with $n(z,t=0) = N\delta(z)$ as initial condition:

$$n(z,t) = \frac{N}{\sqrt{4\pi D_l t}}\exp[-(z - v_d t)^2/(4D_l t)] \quad . \tag{2.29}$$

From Eq. (2.27) we may instead deduce

$$\langle (z - \langle z \rangle)^2 \rangle = 2D_l t + \mathscr{L} \quad . \tag{2.30}$$

D_l, as determined from Eq. (2.28), will coincide with the correct D_l obtained from Eq. (2.27) only for $t \to \infty$. Much longer simulation times are necessary for a good estimate of D_l by this method than by using Eq. (2.27), which yields the correct answer as soon as the diffusion equation holds. The whole point, clarified in Fig. 8, is that Eq. (2.29), which is the starting point for Eq. (2.28) for D_l, is never correct, since it is based on the validity of the diffusion equation (2.24) for all $t > 0$, while for short t it does not hold. The effect on the second central moment of the dynamics during this first initial transient is the term $\mathscr{L}$ in Eq. (2.30).

The above discussion also shows that during the transient, not described by Fick's law, diffusion will involve

[4]This is not a trivial point. For example, let us consider an open-circuit situation with a high applied electric field. Here diffusion and drift cancel each other out to produce a vanishing net current. They influence each other in that the electron energy distribution function is not the usual hot-electron distribution obtained for a homogeneous system, because power does not flow through the particle gas, and yet electrons experience a high field between successive collisions. A similar situation is realized within the space-charge region of a p-n junction in open-circuit conditions.

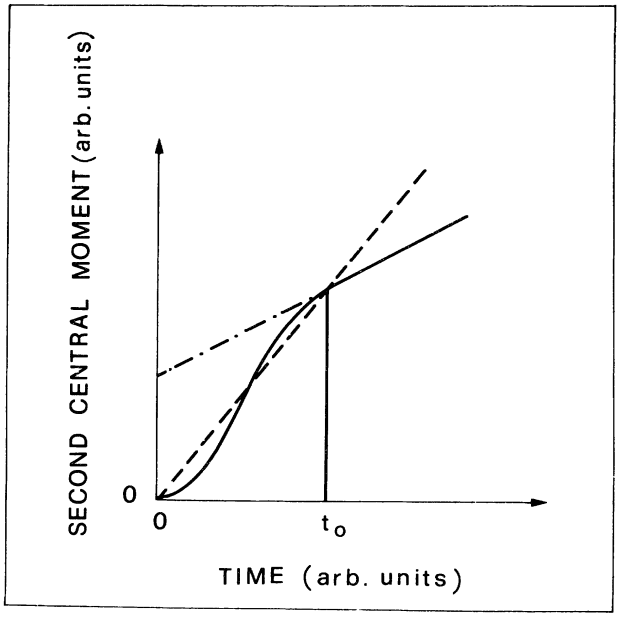

FIG. 8. Evaluation of the diffusion coefficient from the second central moment as a function of time (solid curve). At time t_0 a correct determination of D can be obtained, according to Eq. (2.27), by taking the time derivative (dot-dashed curve) of the second central moment, while the incorrect Eq. (2.28) discussed in the text still gives a wrong answer (dashed curve).

distances of the order of $\mathscr{L}^{1/2}$ (Alberigi-Quaranta *et al.*, 1973).

Other components of D can be obtained in a similar way, since in general we have, with analogous calculations,

$$D_{xy}=\frac{1}{2}\frac{d}{dt}\langle(x-\langle x\rangle)(y-\langle y\rangle)\rangle \ . \tag{2.31}$$

Furthermore, the consistency of the simulation can be checked by an analysis of the time derivatives of the third and higher central moments.

2. Velocity autocorrelation function

The diffusion coefficient D can also be determined from a Monte Carlo simulation through the evaluation of the autocorrelation function of velocity fluctuations (Gherardi *et al.*, 1975; Fauquembergue *et al.*, 1980; Ferry and Barker, 1981),

$$C_{ij}(t)=\langle\overline{\delta v_i(t')\delta v_j(t'+t)}\rangle \ , \tag{2.32}$$

where the bar indicates a time average. In fact the following relation holds (see the textbook of Reif, 1965):

$$D=\int_0^\infty C(t)dt \ . \tag{2.33}$$

The calculation of $C(t)$ may be of interest in itself and can be performed as follows. Let T be the time interval in which the autocorrelation function is to be sampled. In general T must be taken as much longer than the autocorrelation time, i.e., such that $C(t)\simeq 0$ for $t>T$. Then T is divided into a number N of intervals, of duration $\Delta T=T/N$, in order to determine $C(t)$ at times $0,\Delta T$, $2\Delta T,\ldots,N\Delta T=T$. During the simulation, the velocity of the sample particle is recorded at the time values $i\Delta T$, $i=0,1,2,\ldots$. When i becomes greater than or equal to N, the products,

$$v(i\Delta T)v[(i-j)\Delta T], \quad j=0,1,2,\ldots,N$$

are evaluated for each i. Products corresponding to the same value of i are averaged over the simulation, thus obtaining

$$\overline{v(t)v(t+j\Delta T)}=C(j\Delta T)+v_d^2 \ , \tag{2.34}$$

since in a steady-state situation the ensemble average is included in the time average.

3. Diffusion at small distances and short times; q- and ω-dependent diffusion

In Sec. II.D.1 we have seen that at small distances and short times transient diffusion is not correctly described by the classical Fick's law. It must be noted, however, that some conditions are required for the validity of Fick's law, independently of transient transport: the distances at which the gradient varies appreciably must be small compared with the electron mean free path, and the time during which the gradient varies appreciably must be long compared with any electron relaxation time. In recent years theoretical attempts to construct a generalized diffusion theory without these limits (Schlup 1971; Gantsevich *et al.*, 1974; Jacoboni, 1974; Jacoboni *et al.*, 1981b) have been made.

One way to do this, is to use Fourier analysis, and to assume the presence of a sinusoidal source of particles accompanied by a trapping mechanism with constant rate τ_d^{-1} which preserves their total number. For such a system the diffusion equation (in one dimension, for the sake of simplicity) becomes

$$\frac{\partial n}{\partial t}=D\frac{\partial^2 n}{\partial x^2}-v_d\frac{\partial n}{\partial x}+\frac{n_0}{\tau_d}\{1+\exp[i(qx-\omega t)]\}-\frac{n}{\tau_d} \ , \tag{2.35}$$

where n_0 is the average density of particles.

Here D is still a constant and Eq. (2.35) cannot describe diffusion outside the limits described above. However, taking advantage of its linearity, we may Fourier analyze Eq. (2.35); the Fourier transform of Eq. (2.35) is thus readily obtained as

$$n_q\left[-i\omega+q^2D+iqv_d+\frac{1}{\tau_d}\right]=\frac{n_0}{\tau_d}\exp(-i\varphi) \ , \tag{2.36}$$

where n_q and φ are the amplitude and phase shift of the harmonic disturbance, respectively.

Now D in Eq. (2.36) can be assumed to be a function of q, ω, and τ_d. Thus Eq. (2.36) can be used to describe diffusion with fast variation of the gradient in space and/or in time.

By using Chamber's methods, we can write a formal solution of Eq. (2.36) (Jacoboni *et al.*, 1981b), that yields an expression for $D(q,\omega,\tau_d)$ which can be used in Monte Carlo calculations:

$$D(q,\omega,\tau_d)=\frac{1}{q^2\tau_d R}[1-R+i\tau_d R(\omega-qv_d)] \ , \tag{2.37}$$

with

$$R=\int_0^\infty \frac{dt'}{\tau_d}\int_{-\infty}^{\infty} dx' \exp\left[-i(qx'-\omega t')-\frac{t'}{\tau_d}\right] \times \mathscr{P}(x',t') \ , \tag{2.38}$$

where $\mathscr{P}(x',t')$ is the probability density that, in the absence of trapping, a particle covers a distance x' in a time t'. $D(q,\omega)$ can be obtained as a special case of the above result in the limit $t_d \to \infty$.

For $\omega=0$, an expression of $D(q)$ is easily obtained for use on steady-state phenomena with strong spatial variation.

For vanishing q it is possible to obtain an extension of Eq. (2.33) valid for an arbitrary frequency,

$$D(\omega)=\int_0^\infty C(t)\exp(i\omega t)dt \ . \tag{2.39}$$

In order to obtain $D(q,\omega,\tau_d)$ from a Monte Carlo simulation, it is sufficient to include among the scatterings a trapping mechanism with a constant inverse rate τ_d. If the particle is trapped after it has covered a distance x' in a time t' the quantity $\exp[-i(qx'-\omega t')]$ is recorded. Then $R(q,\omega,\tau_d)$ is obtained as the mean value of this quantity, since the simulation automatically accounts for the weighting factor.

After a trapping process the particle starts again with a velocity chosen according to the desired initial conditions. If the particle starts with the velocity it had when decayed, the initial conditions are taken according to the steady-state distribution of velocities. In any case, for τ_d sufficiently long, the results will be independent of the initial conditions assumed. For short τ_d, results for the diffusivity are obtained for the transient transport regime according to the initial conditions assumed. Finally, we observe that Eq. (2.39) can be used to determine $D(\omega)$ in a Monte Carlo procedure, by determining the autocorrelation function $C(t)$, as described in the preceding section.

4. Noise and diffusion

Recently much interest has been shown (Hill *et al.*, 1979; Fauquembergue *et al.*, 1980) in the use of Monte Carlo techniques to determine the noise spectrum of velocity fluctuations in connection with diffusion.

If we consider, again for simplicity, a one-dimensional situation, the power spectrum of the velocity fluctuations is defined as

$$S_v(\omega)=\lim_{T\to\infty}\frac{1}{T}\left\langle\left|\int_0^T \delta v(t)\exp(i\omega t)dt\right|^2\right\rangle \ . \tag{2.40}$$

Now the Wiener-Khintchine theorem connects the autocorrelation function $C(t)$ and $S_v(\omega)$ through

$$S_v(\omega)=2\int_0^\infty C(t)\exp(i\omega t)dt \ . \tag{2.41a}$$

By taking into account Eq. (2.39), we obtain

$$S_v(\omega)=2D(\omega) \ . \tag{2.41b}$$

This result shows that a determination of the noise spectrum of the velocity fluctuations is equivalent to the determination of the frequency-dependent diffusivity. Thus the noise spectrum can be obtained as the Fourier transform of $C(t)$, as indicated for $D(\omega)$ in Sec. II.D.3. On the other hand, Eq. (2.40) can be used directly, not only for the determination of $S_v(\omega)$, but also for the determination of $D(\omega)$ in a Monte Carlo simulation. An average, over a particle ensemble, of the absolute squared Fourier transform of the electron velocity must be taken.

E. Ohmic mobility

When the Monte Carlo method is used to obtain the drift velocity of charge carriers at low applied fields, the statistical uncertainty originating from thermal motion may become particularly large. Of course, in principle, apart from the round-off errors of the computer, any desired precision can be obtained, but the computer time necessary for a high degree of precision often makes such a run impractical and expensive.

The uncertainty due to thermal motion is particularly bothersome when the Ohmic mobility is sought. For this case, however, it is possible to evaluate the diffusion coefficient at zero field with one of the methods discussed in Sec. II.D and then to obtain the Ohmic mobility by means of the Einstein relation [see Eq. (2.20)]. It is worth noting that when no external field is applied, the energy—and therefore the scattering probability of the particle—is constant during a free flight, so that no self-scattering need be introduced.

At low fields, another difficulty may arise when we deal with many-valley semiconductors. Intervalley scattering is due to phonons with a minimum equivalent temperature of the order of at least 100 K. If the lattice temperature is well below such a value, intervalley phonon absorption is almost absent because very few phonons are present in the crystal with that energy and, at low fields, the electron energy very rarely reaches values such as to make intervalley phonon emission possible. As a consequence, the Monte Carlo simulation may proceed for very long times without any valley change of the sampling electron. In this situation it is very difficult to obtain a correct estimate of the valley populations.

When Ohmic conditions are analyzed and no intervalley transition is present at all, this difficulty may be overcome by simulating one electron in each valley, since we know *a priori* that the populations of all valleys must be the same. On the other hand, when we enter the field re-

gion in which a repopulation occurs and intervalley transitions are very rare, the Monte Carlo method becomes inefficient. We shall return to this point in Sec. II.H when we consider several variance-reducing techniques.

F. Impact ionization

The impact ionization rate α_I can be obtained from the Monte Carlo method by introducing the probability of impact ionization as an independent scattering mechanism which is added to phonon and impurity scatterings (Lebwohl and Price, 1971a; Curby and Ferry, 1973; Shichijo *et al.*, 1981; Shichijo and Hess, 1981).

When an ensemble Monte Carlo method is used, the impact ionization process can be examined as follows (Lebwohl and Price, 1971a). The energy of the minority carrier (of the electron-hole pair created) relative to the band edge is neglected and the carrier itself is disregarded. Therefore the sum of the two majority-carrier final energies $(\epsilon_{f1}+\epsilon_{f2})$ equals $(\epsilon-\epsilon_g)$ where ε is the initial energy and ϵ_g the energy gap. After each ionization process, one of the resulting $(N+1)$ particles, chosen at random, is eliminated to maintain a fixed sample size. The pair generation rate per particle per unit time, g_I, is obtained by counting ionization events; it is converted to impact ionization rate by

$$\alpha_I = g_I / v_d \ . \tag{2.42}$$

In other papers (Curby and Ferry, 1973; Shichijo *et al.*, 1981; Shichijo and Hess, 1981) a single-particle Monte Carlo simulation is used, and when impact ionization occurs the created electron-hole pair is disregarded. The impact ionization rate has been obtained by averaging the distance to impact ionization over a sufficient number of ionizations, as in Eq. (2.42)

G. Magnetic fields

The scope of the Monte Carlo method can be extended to include the case where both magnetic and electric fields are present. In this case the equation of motion of a carrier during a free flight will be

$$\hbar\dot{\mathbf{k}} = e\left[\mathbf{E}+\frac{\mathbf{v}}{c}\times\mathbf{B}\right] \ , \tag{2.43}$$

where $\mathbf{B}$ is the magnetic field, c the light velocity in vacuum, and $\mathbf{v}$ the group velocity of the particle,

$$\mathbf{v}(\mathbf{k}) = \frac{1}{\hbar}\nabla_{\mathbf{k}}\epsilon(\mathbf{k}) \ . \tag{2.44}$$

Apart from this change in electron dynamics, the whole Monte Carlo simulation proceeds as usual (Boardman *et al.*, 1971; Chattopadhyay, 1974), but the drift velocity will not, in general, be parallel to the applied electric field. Loss of cylindrical symmetry requires in this case a full three-dimensional simulation, even with very simple models. With a spherical band and a magnetic field $\mathbf{B}$ orthogonal to $\mathbf{E}$, the drift velocity $\mathbf{v}_d$ is also in the plane perpendicular to $\mathbf{B}$, as shown in Fig. 9. A Monte Carlo simulation performed with such a geometry of fields for an infinite homogeneous sytem yields the drift velocity $\mathbf{v}_d$, and in particular the two components v_l and v_t parallel and perpendicular to $\mathbf{E}$, and the angle θ formed by $\mathbf{v}_d$ and $\mathbf{E}$.

At this point we may interpret the results of the simulation in two different physical ways (Boardman *et al.*, 1971), according to the particular system under consideration.

One interpretation corresponds to the case of a long sample. The electric field $\mathbf{E}$ is decomposed into two components $\mathbf{E}_a$, parallel to $\mathbf{v}_d$, which must be considered as the applied field, and $\mathbf{E}_H$, perpendicular to both $\mathbf{B}$ and $\mathbf{v}_d$, which must be considered as the Hall field [see parts (a) and (b) of Fig. 9]. In this case the drift mobility μ_d is determined by

$$\mu_d = \frac{v_d}{E_a} = \frac{v_d}{E\cos\theta} \ , \tag{2.45}$$

while the Hall mobility is

$$\mu_H = \frac{E_H}{BE_a} \ . \tag{2.46}$$

Therefore, from the Monte Carlo simulation it is possible to obtain a direct determination of the Hall scattering factor r_H given by

$$r_H = \frac{\mu_H}{\mu_d} = \frac{E_H}{Bv_d} \ . \tag{2.47}$$

This number is of particular interest, since it depends upon the particular type of scattering mechanism that controls the transport process.

The second interpretation corresponds to the case of

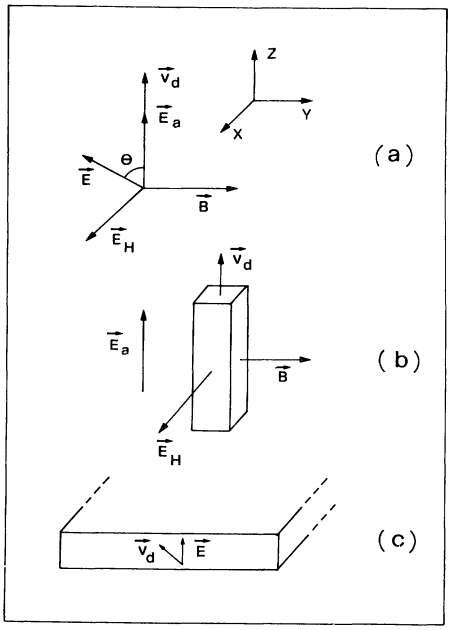

FIG. 9. Geometry for $\mathbf{B}$, $\mathbf{E}$, and $\mathbf{v}_d$ (see text).

very short flat samples in which the electrons can move from one contact to the other at the Hall angle θ with respect to the applied field, thus producing a transverse current and no Hall field [see part (c) of Fig. 9]. The longitudinal mobility in this case is obtained as

$$\mu_E = \frac{v_l}{E} = \frac{v_d}{E}\cos\theta = \mu_d \cos^2\theta \quad . \tag{2.48}$$

For complicated systems, such as nonspherical bands, multivalley bands, and bipolar conduction, the usual modifications of the Hall-effect analysis (Boardman *et al.*, 1971) must be applied to the interpretation of Monte Carlo results.

H. Electron-electron interaction

1. Electron-electron collisions

Interparticle collisions do not usually affect transport properties to a large extent in semiconductors. In fact, in such an interaction the total momentum and the total energy of the two colliding particles is conserved, and no dissipation occurs. Momentum and energy are, however, redistributed among the particles so that the shape of the electron distribution function $f(\mathbf{k})$ is influenced by an *e-e* interaction (a typical result is shown in Fig. 10). This fact has been used (Fröhlich and Paranjape, 1956; Conwell, 1967) as the basis for stating that, for high electron densities, $f(\mathbf{k})$ assumes a Maxwellian shape far from equilibrium, characterized by a mean drift velocity different from zero and an electron temperature T_e different from the crystal temperature T_0.

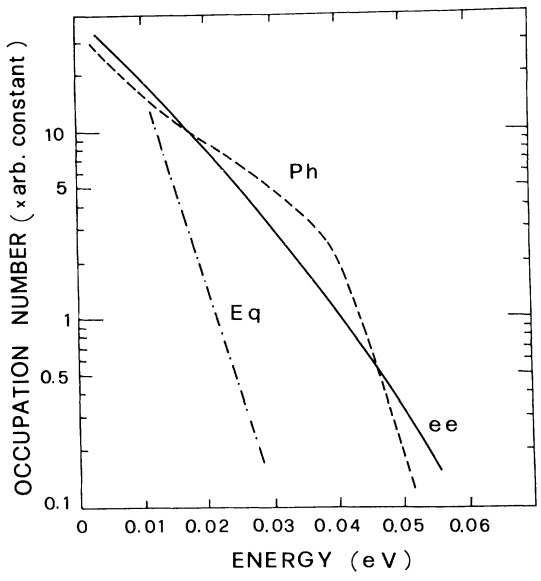

FIG. 10. Distribution function of electrons in a simple semiconductor modeled on Si obtained with Monte Carlo calculations at $T=45$ K and $E=300$ V/cm. The dashed curve (Ph) has been obtained by considering only phonon scattering; the solid curve (*e-e*) includes electron-electron interaction with a concentration of 10^{17} cm^{-3} electrons; the dot-dashed curve (Eq) indicates the equilibrium distribution (Jacoboni, 1976).

From the above considerations it is reasonable to expect that *e-e* interaction may affect to some extent the microscopic transport quantities which are more sensitive to the particular shape of the distribution function. It has been found both theoretically and in experimental measurements (Asche *et al.*, 1971; Nash and Holm-Kennedy, 1974; Jacoboni, 1976) that this is the case for energy relaxation time and valley repopulation (see Sec. IV.B).

The traditional Monte Carlo simulation does not include *e-e* collisions, since, on the basis of ergodicity, it substitutes time averages calculated over the simulation of a single particle history for ensemble averages.

Several attempts (Bacchelli and Jacoboni, 1972; Matulionis *et al.*, 1975; Jacoboni, 1976) have been made to include *e-e* interaction in Monte Carlo calculations. A fundamental difficulty must, however, be faced due to the nonlinear nature of such interaction. In fact, the scattering probability itself depends on the distribution function, both through the screening factor of the scattering potential and through the probability of the sampling electron's colliding with another electron of given wave vector $\mathbf{k}$. Some sort of self-consistent calculation must therefore be performed in which an assumed $f(\mathbf{k})$ is used to evaluate scattering probabilities and the same $f(\mathbf{k})$ results as solution.

Bacchelli and Jacoboni (1971) took an iterative approach consisting of the following procedure: in the first iteration, $f_1(\mathbf{k})$ is obtained from a Monte Carlo simulation without *e-e* interaction. Then in the successive iterations the Monte Carlo simulation is repeated, introducing *e-e* interaction with a constant scattering probability in which the final state of the collision is chosen randomly according to a drifted Maxwellian distribution, with the drift velocity and the mean energy obtained in the previous iterative step. The procedure ends when convergence to a stable result ensures self-consistency of the solution.

A somewhat different approach was proposed by Matulionis *et al.* (1975a, 1976), in which two electrons are simulated, each representing the whole system. For each of them, a record is kept of the most recent distribution function obtained from the simulation over a specified period. In the simulation of one electron, among the scattering mechanisms, an *e-e* interaction with a screened Coulomb potential is introduced, and evaluated by means of the memory of the other electron. At each collision, the memory of the simulated particle is updated by the new state, while the memory of the other electron is not changed. When the other electron is considered as a Monte Carlo electron, the memory of the former particle now represents the ambient electron gas. The procedure is recurrent, so that a sufficiently long simulation provides convergence of the final results.

A simultaneous simulation of many interacting particles has been tried (Jacoboni, 1976), but difficulties arose from the long-range nature of the Coulomb interaction.

From this brief review it appears that the introduction of an *e-e* interaction in Monte Carlo calculation is still an open problem.

2. Degenerate statistics

The Pauli exclusion principle, too, is a sort of electron-electron interaction which brings about nonlinear terms in the Boltzmann equation, and it requires some self-consistent procedure if it is to be included in a Monte Carlo calculation.

Bosi and Jacoboni (1976) suggested that the distribution function $f(\mathbf{k},t)$, as obtained from the simulation itself up to the simulation time t in which the scattering is attempted, be used to correct all the scattering probabilities by a factor $(1-f)$. Again, the simulation must continue until convergence of $f(\mathbf{k})$ is attained.

In order to include the factor $(1-f)$ in the scattering probabilities, the rejection technique is employed after the final state $\mathbf{k}_a$ has been selected: if a random number r in the interval (0,1) is greater than $f(\mathbf{k}_a)$, the scattering process is accepted, otherwise a self-scattering is assumed. In this way, under degenerate conditions, a very large number of self-scatterings is produced. However, with this procedure computer time is saved, as it is not necessary to use the whole distribution function to evaluate the scattering probabilities. Of course, in the evaluation of $f(\mathbf{k})$ the total density of carriers must be taken into account for normalization purposes.

Figure 11 shows an example of application to GaAs of the method described above.

I. Variance-reducing techniques

The Monte Carlo method is a statistical procedure for the solution of mathematical problems. Therefore, the results obtained by means of such a method are always affected by some statistical uncertainty. In Sec. II.B.6.*c* we discussed the standard algorithm used to evaluate this uncertainty for the solution of transport problems.

As a general rule, the statistical precision of the results increases as the square root of the number of trials and, therefore, the amount of computer time necessary to improve appreciably the quality of the results becomes quickly very long. It is thus of particular interest to find variance-reducing techniques, which can be defined in general as procedures which "change or at least distort the original problem in such a way that uncertainty in the answer is reduced" (Hammersley and Handscomb, 1964). It can easily be understood that the reduction of variance is of greatest importance in all Monte Carlo calculations, and in fact it has been widely studied. A dense and exhaustive review of variance-reducing techniques can be found in the textbook of Hammersley and Handscomb (1964). Among these techniques, some are specifically oriented to electron-transport problems, so we think it useful to review them here briefly.

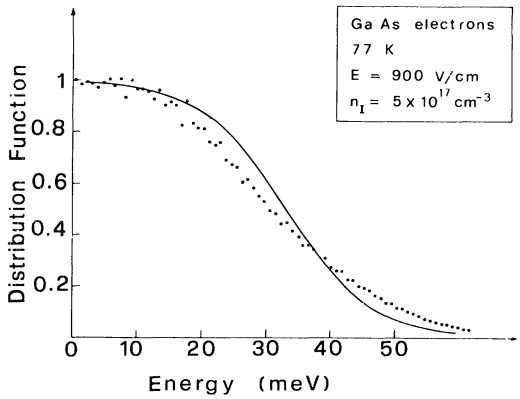

FIG. 11. Electron occupation number as a function of energy in GaAs at 77 K, obtained with the Monte Carlo simulation (dots) for a degenerate concentration. The solid curve indicates the equilibrium Fermi distribution for comparison.

1. Variance due to thermal fluctuations

In Monte Carlo simulation the drift velocity v_d of the sample electron is obtained as an average of its velocity during the simulation. If v_d is a small fraction of the thermal velocity $v_{\rm th}$, an estimate of v_d is, in general, heavily influenced by the variance due to $v_{\rm th}$ fluctuations. In many cases this contribution to the uncertainty on v_d can be strongly reduced by a modification of the Monte Carlo procedure (Hammar, 1971; Price, 1979), as described below.

When the transition probability per unit time is velocity randomizing, i.e., is such that

$$P(\mathbf{k},\mathbf{k}')=P(\mathbf{k},-\mathbf{k}') \ , \tag{2.49}$$

then a value $\mathbf{k}'$ for the state after scattering is as probable as its opposite $-\mathbf{k}'$. The random number used to generate $\mathbf{k}_a$, by selecting one of them, introduces a variance that, in turn, builds up the thermal fluctuation of the electron velocity.

It is possible to eliminate this fluctuation by splitting the simulation into two different histories, corresponding to the two equally probable initial conditions $\mathbf{k}_a$ and $-\mathbf{k}_a$ for the new free flight. If a constant Γ is used and the same random number is taken to generate the two flights, these latter have equal weights in the simulation. Thus both can be considered by taking into account the averages of the quantities evaluated in the two flights, thereby reducing the variance by eliminating the thermal contribution. One of the flights is finally chosen at random to continue the simulation.

This procedure can be extended to more than two states after scattering (Hammar, 1971; Price, 1979) and, with appropriate weights, to the case of non-velocity-randomizing processes.

For the carrier drift velocity, an estimator quite different from those generally used has been given by Price (1979):

$$\mathbf{v}_d = e\mathbf{E}\langle \nabla_{\mathbf{p}} \mathbf{l} \rangle \ , \tag{2.50}$$

where $\nabla_{\mathbf{p}}\mathbf{l}$ is the gradient in momentum space of the mean free path $\mathbf{l}$, i.e., a tensor whose ij component is $\partial l_i/\partial p_j$. A relatively small variance is associated with such an estimator; however, in practice it is useful only for simple

cases, when an analytical expression can be given for the quantity to be averaged in Eq. (2.50).

2. Variance due to valley repopulation

As is well known (Conwell, 1967), in a many-valley semiconductor when the valleys are differently oriented with respect to the applied field, they contribute with different valley drift velocities $\mathbf{v}_{dv}$ to the total average electron drift velcoity $\mathbf{v}_d$:

$$\mathbf{v}_d = \sum_v n_v \mathbf{v}_{dv} \ , \tag{2.51}$$

where n_v is the relative concentration of carriers in the vth valley.

Under hot-electron conditions, this situation corresponds to different carrier heating, and a redistribution of the electron among the different valleys occurs, called "valley repopulation."

At low fields and temperatures, intervalley transitions are very rare, and the variance of the concentration n_v and, in turn, of the drift velocity v_d may be very large. The situation may be improved (Hammar, 1971; Canali *et al.*, 1975) by using the distribution function, as obtained in each type of valley with the Monte Carlo calculation, and the transition probabilities from the valleys of different types, to evaluate the valley repopulation, as follows.

In a situation where two types of valleys, "hot" and "cold," exist, steady-state conditions require that the number of electrons passing per unit time from hot to cold valleys be equal to the number of electrons which perform the opposite transition. The above condition yields

$$n_h \int_0^\infty f_h(\epsilon) P_{hc}(\epsilon) d\epsilon = n_c \int_0^\infty f_c(\epsilon) P_{ch}(\epsilon) d\epsilon \ , \tag{2.52}$$

where n_h and n_c are the relative fractions of hot and cold carriers to be evaluated; f_h and f_c are the energy distribution function, which includes the density of states, normalized to one, in hot and cold valleys; P_{hc} and P_{ch} are the transition rates from hot to cold valleys and from cold to hot valleys, respectively. f_h and f_c are obtained from the Monte Carlo simulation, while P_{hc} and P_{ch} are known from the theory of scattering mechanisms (see Sec. III.D.1.*c*).

By dividing the energy axis into equal intervals, one obtains the repopulation ratio n_c/n_h from a numerical evaluation of Eq. (2.52). Such an estimate of n_c/n_h exploits all the information obtained during the simulation (i.e., information acquired when the electron "visits" the region of energy where intervalley scattering is possible), not only the information obtained from transitions that have actually happened. In this way the variance associated with the repopulation ratio is reduced. However, it must be noted that, in order to get correct results with the above procedure, one must know the tails of the distribution functions in hot and cold valleys with sufficient accuracy at energies above threshold for intervalley phonon emission. This again can become a severe problem, which can be approached with the variance-reducing technique described next.

3. Variance related to improbable electron states

When a physical phenomenon of interest is due to the occurrence of improbable electron states, the standard Monte Carlo simulation may lead to a large variance of the desired quantity. Situations of this kind are usually related to the tails of the energy distribution function, as, for example, in the case of valley repopulation seen above, impact ionization, or escapes of electrons into the gate insulator in a field-effect transistor (FET).

In such cases the variance can be reduced by the following procedure (Phillips and Price, 1977). Within a simulation, when an electron enters a fixed "rare region" of energy, its entering state is recorded and used for generating a fixed number N of different "parallel" simulations; each of these uses different random numbers and ends when the electron exits from the rare region. Then, starting from one of the N exit states chosen at random, the simulation proceeds in the usual way until the rare region is reached again. In the averaging procedures a weight $1/N$ must be given to each parallel simulation.

The variance-reducing techniques above may be very useful in some cases. It must be noted, however, that they are realized somehow by means of a distortion of the original problem, which causes the program to deviate from the strict simulation of possible electron histories.

A strict simulation, in general, has the advantage of yielding a simple and straightforward means of physical interpretation of the phenomenon under investigation. Consequently, as a general rule, a correct balance between computing time, transparency of the simulative procedure, and complexity of the computed program must be found in connection with the particular needs of each single case.

J. Survey of other techniques

The introduction of the Monte Carlo method in high-field transport studies has amply extended the range of problems that can be successfully approached. Other techniques exist, however, and are sometimes still used, which deserve consideration since they may be particularly useful under special conditions. In what follows, we shall review briefly these alternative techniques and compare them with the Monte Carlo method.

1. Analytical techniques

Analytical techniques for the solution of the nonlinearized Boltzmann equation were developed mainly during the two decades from the beginning of the study of the hot-electron problem [which can be dated from the works of Froehlich (1947) and Shockley (1951)] to the introduction of the numerical techniques, which were suggested at the Kyoto Conference in 1966 (Kurosawa, 1966; Budd,

1966). These techniques soon developed to a high degree of refinement (Rees, 1969; Fawcett *et al.*, 1970; Ruch and Fawcett, 1970; Price, 1973). A standard reference for the research performed in that period is Conwell's book (1967), and we refer the reader interested in details to this comprehensive review.

Even though analytical techniques require severe approximations in the calculations and can be applied only to extremely simple semiconductor models, they have the merit of having provided a first physical insight into the problem of nonlinear transport. Some important concepts, for example, the electron temperature, the energy and momentum relaxation times, are still valuable heuristic methods, although it is now known that a rigorous application of these concepts is possible only in a very limited number of actual cases.

Among the analytical techniques developed for the analysis of high-field transport, two main procedures can be recognized (for a review on the determination of the hot-electron distribution function see Bauer, 1974). In the first one an *a priori* analytical form of the distribution function is assumed, with some parameters to be determined by using the Boltzmann equation or, less frequently, through a variational principle (Adawi, 1959, 1960; Tauber, 1959). A heated and drifted Maxwellian distribution has been widely used:

$$f(\mathbf{k})=\mathscr{D}\exp[-\hbar^2(\mathbf{k}-\mathbf{k}_d)^2/(2mK_BT_e)] \ , \tag{2.53}$$

where $\mathscr{D}$ is a normalization constant, m the carrier effective mass, $\hbar\mathbf{k}_d$ the average momentum of the distribution, and T_e the electron temperature, which, under hot-electron conditions, is in general higher than the lattice temperature. The two parameters $\mathbf{k}_d$ and T_e are usually determined by satisfying the first two moments of the Boltzmann equation (Conwell, 1967); this procedure is equivalent to the requirements of momentum and energy conservation. A distribution function of the type given by Eq. (2.53) should be a good approximation when the electron concentration is sufficiently high (Conwell, 1967). Although it is applicable in a limited number of simple cases, it contains most of the essential features of hot-electron physics.

A second technique makes use of an expansion of the distribution function in spherical harmonics. For problems with cylindrical symmetry around the direction of the field, the expansion can be made in Legendre polynomials $P_n(\cos\theta)$:

$$f(\mathbf{k})=f_0(\epsilon)+f_1(\epsilon)P_1(\cos\theta)+\cdots \ , \tag{2.54}$$

where θ is the angle between the field direction and $\mathbf{k}$. When the expansion is substituted into the Boltzmann equation, by using the orthogonality property of Legendre polynomials one obtains a system of infinite coupled equations for $f_0, f_1, \ldots$. However, the scattering mechanisms that involve a finite amount of energy $\hbar\omega_0$ mix the values of those functions calculated at ϵ and at $\epsilon\pm\hbar\omega_0$, so that the equations prove to be both differential and finite-difference equations. Further approximations are then required at this stage, and the overall accuracy of the method becomes very questionable (Yamashita and Watanabe, 1954; Stratton, 1958a, 1958b; Yamashita and Inoue, 1959; Reik and Risken, 1962).

2. Other numerical techniques—the iterative technique

Other numerical techniques (Budd, 1966; Price, 1968; Rees, 1969; Hammar, 1972, 1973; Nougier and Rolland, 1973; Vinter, 1973) for the solution of the Boltzmann equation were developed more or less at the same time as the Monte Carlo method. The most important of them is closely related to the Monte Carlo technique and yields a solution of the Boltzmann equation by means of an iterative procedure. Since this method is still often used, and a comparison with the Monte Carlo method may be instructive, we shall outline it briefly in the following.

Let us consider the integro-differential Boltzmann equation for a spatially uniform system:

$$\frac{\partial f(\mathbf{k},t)}{\partial t}+\frac{e\mathbf{E}}{\hbar}\nabla_{\mathbf{k}}f(\mathbf{k},t)=\left.\frac{\partial f(\mathbf{k},t)}{\partial t}\right|_{\text{coll}} \ . \tag{2.55}$$

The collision term for the case of nondegenerate statistics can be written as

$$\left.\frac{\partial f(\mathbf{k},t)}{\partial t}\right|_{\text{coll}}=-f(\mathbf{k},t)\lambda(\mathbf{k})+\frac{V}{(2\pi)^3}\int d\mathbf{k}'f(\mathbf{k}',t)P(\mathbf{k},\mathbf{k}') \ , \tag{2.56}$$

where $P(\mathbf{k},\mathbf{k}')$ is the transition probability per unit time from $\mathbf{k}$ to $\mathbf{k}'$ due to all scattering mechanisms, and

$$\lambda(\mathbf{k})=\frac{V}{(2\pi)^3}\int P(\mathbf{k},\mathbf{k}')d\mathbf{k}' \ . \tag{2.57}$$

By introducing the path variables

$$\begin{aligned}\tilde{\mathbf{k}}&=\mathbf{k}-\frac{e\mathbf{E}}{\hbar}t \ ,\\ \tilde{t}&=t \ ,\end{aligned} \tag{2.58}$$

which represent the collisionless trajectory in $\mathbf{k}$ space of the electrons, we obtain from Eqs. (2.55) and (2.56)

$$\frac{df}{d\tilde{t}}\left[\tilde{\mathbf{k}}+\frac{e\mathbf{E}}{\hbar}\tilde{t},\tilde{t}\right]+\lambda\left[\mathbf{k}+\frac{e\mathbf{E}}{\hbar}\tilde{t}\right]f\left[\tilde{\mathbf{k}}+\frac{e\mathbf{E}}{\hbar}\tilde{t},\tilde{t}\right]=\frac{V}{(2\pi)^3}\int d\mathbf{k}'f(\mathbf{k}',\tilde{E})P\left[\tilde{\mathbf{k}}+\frac{e\mathbf{E}}{\hbar}\tilde{t},\mathbf{k}'\right] \ . \tag{2.59}$$

Multiplying through by the factor

$$\exp\left[\int_0^{\tilde{t}}\lambda\left[\tilde{\mathbf{k}}+\frac{e\mathbf{E}}{\hbar}\theta\right]d\theta\right] \ ,$$

and integrating between $\tilde{t}_1$ and $\tilde{t}_2$, we obtain

$$f\left[\tilde{\mathbf{k}}+\frac{e\mathbf{E}}{\hbar}\tilde{t}_2,\tilde{t}_2\right]\exp\left[\int_0^{\tilde{t}_2}\lambda\left[\tilde{\mathbf{k}}+\frac{e\mathbf{E}}{\hbar}\theta\right]d\theta\right]=f\left[\tilde{\mathbf{k}}+\frac{e\mathbf{E}}{\hbar}\tilde{t}_1,\tilde{t}_1\right]\exp\left[\int_0^{\tilde{t}_1}\lambda\left[\tilde{\mathbf{k}}+\frac{e\mathbf{E}}{\hbar}\theta\right]d\theta\right]$$

$$+\frac{V}{(2\pi)^3}\int_{\tilde{t}_1}^{\tilde{t}_2}d\tilde{t}\exp\left[\int_0^{\tilde{t}}\lambda\left[\tilde{\mathbf{k}}+\frac{e\mathbf{E}}{\hbar}\theta\right]d\theta\right]\int d\mathbf{k}'f(\mathbf{k}',\tilde{t})P\left[\tilde{\mathbf{k}}+\frac{e\mathbf{E}\tilde{t}}{\hbar},\mathbf{k}'\right]. \tag{2.60}$$

Coming back to the variables $(\mathbf{k},t)$ by putting

$$\mathbf{k}=\tilde{\mathbf{k}}+\frac{e\mathbf{E}}{\hbar}\tilde{t}_2\,,\qquad t=\tilde{t}_2\,, \tag{2.61}$$

and writing t' instead of $\tilde{t}_1$, for simplicity, we have from Eq. (2.60)

$$f(\mathbf{k},t)=f\left[\mathbf{k}-\frac{e\mathbf{E}}{\hbar}(t-t'),t'\right]\exp\left[-\int_{t'}^{t}\lambda\left[\mathbf{k}-\frac{e\mathbf{E}}{\hbar}(t-\theta)\right]d\theta\right]$$

$$+\frac{V}{(2\pi)^3}\int_{t'}^{t}d\tilde{t}\exp\left[-\int_{\tilde{t}}^{t}\lambda\left[\mathbf{k}-\frac{e\mathbf{E}}{\hbar}(t-\theta)\right]d\theta\right]\int d\mathbf{k}'f(\mathbf{k}',\tilde{t})P\left[\mathbf{k}-\frac{e\mathbf{E}}{\hbar}(t-\tilde{t}),\mathbf{k}'\right]. \tag{2.62}$$

Equation (2.62), which is an integral form of the Boltzmann equation, can be interpreted in simple physical terms as follows. Two different contributions combine to determine the carrier distribution function $f(\mathbf{k},t)$:

(a) the contribution of the electrons that were in the state $\mathbf{k}-e\mathbf{E}(t-t')/\hbar$ at the time t', and have drifted to the state $\mathbf{k}$ in the interval $(t-t')$ under the influence of the field $\mathbf{E}$, without being scattered [first term on the right-hand side of Eq. (2.62)];

(b) the contribution of the electrons that were scattered from any state $\mathbf{k}'$ to the new state $\mathbf{k}-e\mathbf{E}/\hbar(t-\tilde{t})$ at any time $\tilde{t}$ between t' and t, and that arrive at the state $\mathbf{k}$ at the time t without being scattered again [second term on the right-hand side of Eq. (2.62)].

Since, provided that $t'<t$, the time t' is arbitrary, we can consider the limiting form of the Eq. (2.62) when $t'\to-\infty$

$$f(\mathbf{k},t)=\frac{V}{(2\pi)^3}\int_0^{\infty}dt''\exp\left[-\int_0^{t''}\lambda\left[\mathbf{k}-\frac{e\mathbf{E}}{\hbar}t'''\right]dt'''\right]\int d\mathbf{k}'f(\mathbf{k}',t-t'')P\left[\mathbf{k}-\frac{e\mathbf{E}}{\hbar}t'',\mathbf{k}'\right], \tag{2.63}$$

where we have used the slight rearrangement of variables

$$t''=t-\tilde{t}\,,\qquad t'''=t-\theta\,. \tag{2.64}$$

The iterative technique for the solution of Eq. (2.63) consists in substituting an arbitrary function $f_0(\mathbf{k},t)$ on the right-hand side of Eq. (2.63), and calculating $f(\mathbf{k},t)$ as the right-hand side of Eq. (2.63) itself. This function is then resubstituted on the right-hand side, and the procedure is repeated until convergence is achieved.

Numerical iterative solutions of Eq. (2.63) have been discussed for stationary conditions, in which the dependence of f upon t vanishes (Budd, 1966; Rees, 1969; Price, 1970). The stability of the iterative procedure and refinements for quicker computations have been discussed by Rees (1969) and Vassel (1970). In particular, it has been shown that the introduction of a self-scattering such as that introduced for the Monte Carlo method, which yields a constant scattering rate Γ, greatly simplifies the evaluation of the integral in Eq. (2.63).

Another important result can be obtained when Γ is made large with respect to the scattering rate λ. Under this condition it has been shown (Fawcett, 1973) that the following relation holds:

$$f_{n+1}(\mathbf{k})\cong f_n(\mathbf{k})+\frac{1}{\Gamma}\frac{\partial f_n(\mathbf{k};t)}{\partial t}\,, \tag{2.65}$$

where $f_{n+1}(\mathbf{k})$ and $f_n(\mathbf{k})$ are the distribution functions obtained from the $(n+1)$th and the nth iteration, respectively.

Each step in the iterative process corresponds, then, to a time increment of $1/\Gamma$ for the evaluation of the physical system. This result enables us to use the iterative method to study the evolution of the distribution function during the transient from a given initial condition $f_0(\mathbf{k})$ to the stationary state. The accuracy of the analysis can be improved by increasing Γ and therefore by performing a larger number of iterations.

3. A critical comparison of the different techniques

The techniques discussed in the previous sections are compared in Table I, in terms of their generality, complexity, difficulty of implementation, and reliability of results.

When compared with the Monte Carlo method or other exact techniques, the two analytical procedures sketched in Sec. II.J.1 differ markedly in their degree of usefulness. The drifted-Maxwellian technique aims at giving a simple physical insight into a hot-electron problem, and, as such, is still a very valuable method when we are not looking for particular details. The Legendre-polynomial expansion, on the other hand, was intended to be the most refined analytical method for as exact as possible a solution of the Boltzmann equation, and, as such, it has been superseded by the more recent numerical techniques.

Consequently, approximate analytical solutions of the Boltzmann equation to include time- and space-dependent phenomena as well as details of the microscopic model (both for band structure and for scattering mechanisms) have been scarce, and the reliability of the results obtained with analytical techniques is limited to simple physical situations, to simple microscopic models, and to narrow ranges of temperature and fields.

If we now move to a comparison between iterative and Monte Carlo techniques, we may first comment that both of them give the exact numerical solution for a homogeneous, steady-state, hot-electron phenomenon with noninteracting particles. Both of them can include details of the microscopic model without difficulties and can be extended to time-dependent phenomena.

The iterative technique processes the whole distribution function at each step of the procedure, while with the Monte Carlo method the distribution function is sampled at each electron flight, so that it is available only at the end of the simulation. For this reason the iterative technique can be more convenient when we deal with physical phenomena that depend on details of the distribution function, as for example in the case of valley repopulation at low temperatures (see Sec. IV.B.6). Knowing the distribution function at each step of iteration can also be useful for the inclusion of particle-particle interactions.

On the other hand, some difficulties may arise in the evaluation of the integral in Eq. (2.63), and the effect on

TABLE I. Comparison of different techniques for the solution of the Boltzmann equation.

Analytical technique	Iterative technique	Monte Carlo technique
From simple parametrized distribution function to complex series expansion.	Numerical procedure at medium level of difficulty.	Stochastic calculation at minimum level of difficulty.
	To fully exploit the potentiality of the technique, very fast computers are necessary.	
Approximate solutions of the Boltzmann equation are obtained.	An exact solution of the Boltzmann equation is obtained.	
Extension to time- and space-dependent phenomena is not easily available.	Extension to time-dependent phenomena can be easily achieved. Extension to space-dependent phenomena is not easy.	Extension to time- and space-dependent phenomena can be easily achieved.
The microscopic interpretation of phenomena in terms of band structure and scattering processes is somewhat hidden.		The microscopic interpretation of phenomena is quite transparent.
High level of difficulty in including realistic band structure and scattering models.	Realistic band structure and scattering models can be easily included.	
No direct evaluation of fluctuation phenomena can be obtained.		The analysis can be immediately extended to fluctuation phenomena.
Electron-electron interaction is difficult to include, since it makes the Boltzmann equation nonlinear. It can suggest particular forms for the distribution function.	Electron-electron interaction can be easily included in the method.	Electron-electron interaction can be included with difficulty through an extension of the technique using self-consistent calculations.

final results of any numerical approximation may not be easy to control.

The major advantage of the Monte Carlo technique (besides its easy implementation) arises from its being a direct dynamical simulative procedure, so that any complicated phenomenon can be analyzed in terms of its elementary processes in a quite simple way. Furthermore, fluctuations can be studied with a very straightforward analysis. However, interparticle collisions can be introduced in the calculations only with difficulty. Finally, through an ensemble simulation, space- and time-dependent phenomena (as for devices) can be easily studied.

These arguments are at the basis of the popularity of the Monte Carlo method, which is at present much more widely used in hot-electron studies than any other technique.

III. APPLICATION TO COVALENT SEMICONDUCTORS—MICROSCOPIC MODEL

A. Band structure

The energy region of the band structure of a semiconductor which is of interest in transport problems is centered on the energy gap and extends some ϵ_g (the width of the energy gap) above the minimum of the conduction band and below the maximum of the valence band.

Since only covalent semiconductors of group four will be considered in this paper, we shall present a general model for the band structure which enables us to interpret the macroscopic properties of these materials. It should be noted that such a model will more generally provide a correct description of the band structure for the whole class of cubic semiconductors belonging to both diamond and zinc-blende structures.

The model consists of one conduction band, with three sets of minima, and three valence bands. The minima of the conduction band are located at the Γ point ($k=0$), at the L points [$\mathbf{k}=(\pi/a_0,\pi/a_0,\pi/a_0)$, a_0 being the lattice parameter], and along the Δ lines ($\mathbf{k}=k,0,0$). The tops of the valence bands are located at Γ. Two of these bands are degenerate at this point, while the third one is split off by spin-orbit interaction.

The main features of the band structure in cubic semiconductors are summarized in Fig. 12.

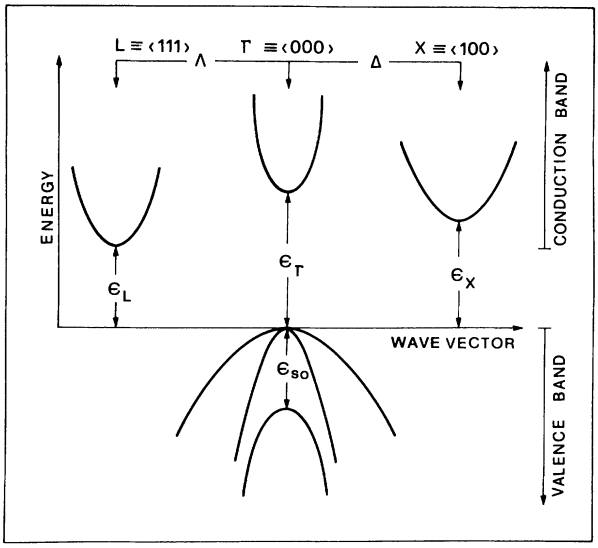

FIG. 12. Band structure of the cubic-model semiconductor.

1. Relationship of energy to wave vector

The particular form of the energy-wave-vector relationship $\epsilon=\epsilon(\mathbf{k})$ of charge carriers determines their dynamical properties under the influence of an external force. In the following we shall explicitly refer to electrons or holes when we consider $\mathbf{k}$ states belonging to the conduction or valence band, respectively.

In the region around the minima of the conduction band, usually called valleys, or around the maximum of the valence band, the function $\epsilon(\mathbf{k})$ is given by a quadratic function of $\mathbf{k}$ (parabolic bands), which may assume one of the following forms:

$$\epsilon(\mathbf{k})=\frac{\hbar^2k^2}{2m}, \tag{3.1}$$

$$\epsilon(\mathbf{k})=\frac{\hbar^2}{2}\left[\frac{k_l^2}{m_l}+\frac{k_t^2}{m_t}\right], \tag{3.2}$$

$$\epsilon(\mathbf{k})=ak^2[1\mp g(\vartheta,\psi)]. \tag{3.3}$$

When Eqs. (3.1) and (3.2) are used for electrons, $\mathbf{k}$ is measured from the centers of the valleys.

Equation (3.1) (spherical case) represents a band with spherical equienergetic surfaces with a single scalar effective mass m, and it is appropriate for the minimum of the conduction band located at Γ and for the maximum of the split-off valence band. This case is the simplest one, and it is generally adopted as a simple model for any material when rough estimates of transport properties are sought.

Equation (3.2) (ellipsoidal case) represents a band with ellipsoidal equienergetic surfaces, with a tensor effective mass ($1/m_l$ and $1/m_t$ are the longitudinal and transverse components, respectively, of the inverse effective-mass tensor). The ellipsoids have rotational symmetry around the crystallographic directions which contain the center of the valleys. This case is appropriate for the minima of the conduction band located at L and along Δ; for symmetry reasons several equivalent valleys are present (many-valley model).[5]

[5]In this model it is assumed that electrons cannot move from one valley to another with continuous variation of their $\mathbf{k}$ values, because of the existence of intermediate regions of $\mathbf{k}$ space with too high energies.

Equation (3.3) (warped case) represents a band with warped equienergetic surfaces, and it is appropriate for the two degenerate maxima of the valence band (here $\mp$ refer to heavy and light holes, respectively). ϑ and ψ are the polar and azimuthal angles of $\mathbf{k}$ with respect to crystallographic axes so that $g(\vartheta,\psi)$ contains the angular dependence of the effective mass, which is given by (Ottaviani *et al.*, 1975) as

$$g(\vartheta,\psi)=[b^2+c^2(\sin^4\vartheta\cos^2\psi\sin^2\psi+\sin^2\vartheta\cos^2\vartheta)]^{1/2} \tag{3.4}$$

with

$$a=\frac{\hbar^2|A|}{2m_0},\quad b=\frac{|B|}{|A|},\quad c=\frac{|C|}{|A|},$$

where A, B, and C are the inverse valence-band parameters (Dresselhaus *et al.*, 1955) and m_0 the free-electron mass.

The different shapes of the surfaces of constant energy for the three cases considered above are shown in Fig. 13.

2. Nonparabolicity

For values of $\mathbf{k}$ far from the minima of the conduction band and/or from the maxima of the valence band, the energy deviates from the simple quadratic expressions seen above, and nonparabolicity occurs.

For the conduction band, a simple analytical way of introducing nonparabolicity is to consider an energy-wavevector relation of the type (Conwell and Vassel, 1968)

$$\epsilon(1+\alpha\epsilon)=\gamma(\mathbf{k})\equiv\frac{\hbar^2k^2}{2m} \tag{3.5}$$

or

$$\epsilon(\mathbf{k})=\frac{-1+\sqrt{1+4\alpha\gamma}}{2\alpha},$$

where the right-hand side of Eq. (3.5) can be replaced by one of the right-hand sides of Eqs. (3.1) and (3.2); α is a nonparabolicity parameter, which can be related to other band quantities. In particular, the following approximate expressions have been given for minima at Γ (Fawcett *et al.*, 1970), L (Paige, 1964), and Δ (see Appendix B):

$$\alpha(\Gamma)=\frac{1}{\epsilon_\Gamma}\left[1-\frac{m_\Gamma}{m_0}\right]^2, \tag{3.6}$$

$$\alpha(L)=\frac{1}{\epsilon_{L'_{3v}}-\epsilon_{L_{1c}}}, \tag{3.7}$$

$$\alpha(\Delta)=\frac{1}{2(\epsilon_{\Delta'_{2c}}-\epsilon_{\Delta_{1c}})}\left[1-\frac{m_l}{m_0}\right]^2, \tag{3.8}$$

where M_Γ is the value of the effective mass at the bottom of Γ valley, ϵ_Γ is the direct energy gap at Γ, L'_{3v} and L_{1c} are the states of the valence and conduction bands with the given symmetry, and Δ'_{2c} and Δ_{1c} are states of the conduction band with the given symmetry for minima along Δ.

For the valence band, nonparabolicity cannot be parameterized in a form like that of Eq. (3.5). In this case nonparabolicity has two main features (Kane, 1956): (i) it

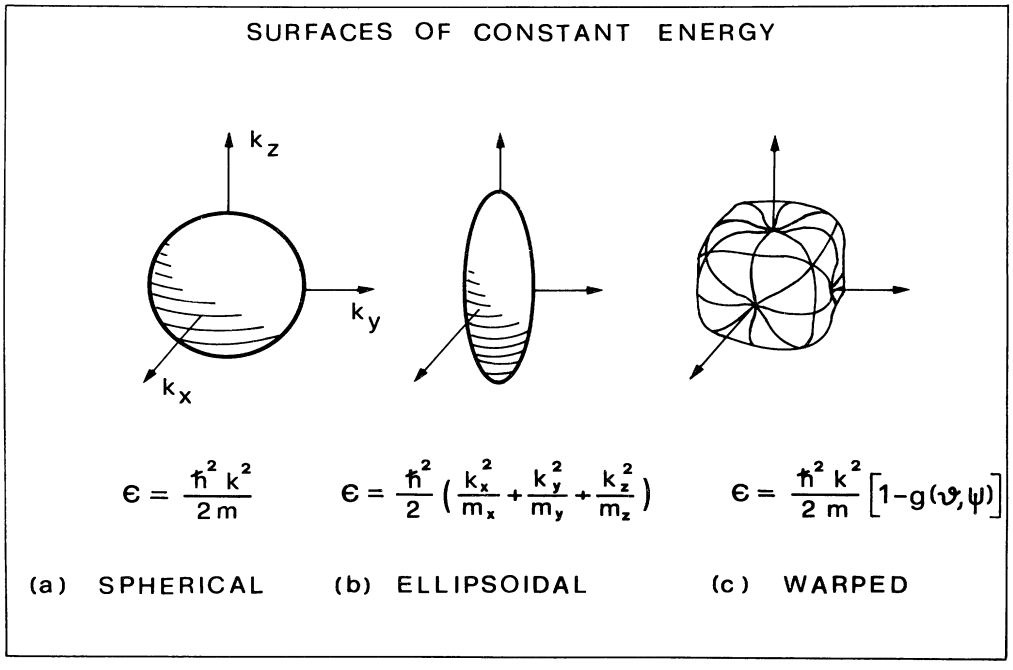

FIG. 13. Different shapes of surfaces of constant energy for electrons and holes in cubic semiconductors.

is more pronounced along ⟨110⟩ and ⟨111⟩ directions for heavy and light holes, respectively; (ii) if ϵ_{so} is the split-off energy of the lowest valence band, nonparabolicity is mostly effective at energies near $\frac{1}{3}\epsilon_{so}$; in the limits of $\epsilon/\epsilon_{so} \ll 1$ and $\epsilon/\epsilon_{so} \gg 1$ the bands are parabolic.

For a nonparabolic band of the type in Eq. (3.5), the velocity associated with a state $\mathbf{k}$ proves to be

$$v(\mathbf{k}) = \frac{1}{\hbar}\frac{\partial \epsilon}{\partial \mathbf{k}} = \frac{\hbar \mathbf{k}}{m(1+2\alpha\epsilon)} \tag{3.9}$$

so that the conductivity effective mass m_c defined by

$$\mathbf{v} = \frac{\hbar \mathbf{k}}{m_c} \tag{3.10}$$

is given by

$$m_c = m(1+2\alpha\epsilon) . \tag{3.11}$$

The effect of nonparabolicity on the density-of-states effective mass m_d can be calculated following Gagliani and Reggiani (1975) as

$$m_{de}^{3/2} = (m_t^2 m_l)^{1/2}(2\beta/\pi)^{1/2}\exp(\beta)K_2(\beta) , \tag{3.12}$$

$$m_{di}^{3/2} = \pi^{-3/2}\int \exp[\epsilon_i^v(\mathbf{x})/(K_B T_0)]d\mathbf{x}, i = h,l,\text{so} \tag{3.13}$$

where subscripts e and i refer to conduction and valence bands, respectively; $\beta = (2\alpha K_B T_0)^{-1}$; K_2 is the modified Bessel function of order 2; $\mathbf{x} = \hbar\mathbf{k}/(2m_0 K_B T_0)^{1/2}$; ϵ_i^v taken with its sign is the energy-wave-vector relationship of the heavy ($i=h$), light ($i=l$), and spin-orbit ($i=$so) valence bands, respectively [to a good approximation ϵ_i^v can be evaluated, according to Kane (1956), from $\mathbf{k}\cdot\mathbf{p}$ calculations: see also Humphreys (1981)]. The integration is carried out over the whole $\mathbf{k}$ space.

The temperature dependence of the density-of-states effective mass is sketched in Fig. 14 for the case of electrons and holes. From this figure it can be seen how nonparabolicity effects lead to an unlimited increase of the effective mass for the case of electrons, while for the case of all three types of holes the increase (or decrease for the split-off band) of the effective mass is confined within a well-defined region of energy.

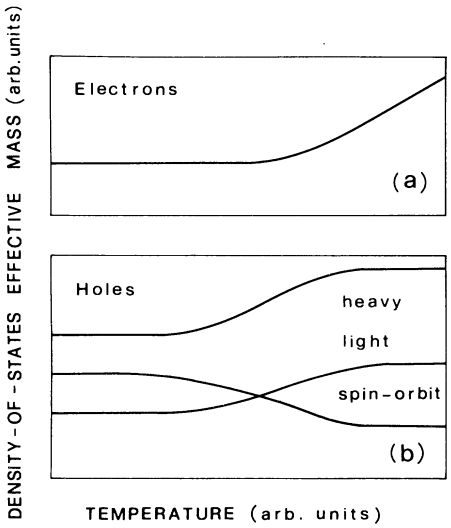

FIG. 14. Schematic representation of the dependence upon temperature of the carrier density-of-states effective mass: (a) electrons, (b) holes.

3. Herring and Vogt transformation

When considering the ellipsoidal case of Eq. (3.2), in order to simplify analytical calculations, it is useful to introduce the Herring-Vogt (1956) transformation, which reduces the ellipsoidal equienergetic surfaces to spheres and is defined by

$$k_i^{*(m)} = T_{ij} k_j^{(m)} \tag{3.14}$$

where $\mathbf{k}^{*(m)}$ is the transformed wave vector. For an electron in the mth valley the transformation matrix T_{ij} takes the form

$$T^{(m)} = \begin{vmatrix} \left(\frac{m_0}{m_t}\right)^{1/2} & 0 & 0 \\ 0 & \left(\frac{m_0}{m_t}\right)^{1/2} & 0 \\ 0 & 0 & \left(\frac{m_0}{m_l}\right)^{1/2} \end{vmatrix} \tag{3.15}$$

in the valley frame of reference, i.e., in the frame centered at the center of the valley, with the z axis along its symmetry axis. Consequently, the energy-wave-vector relationship in the starred space becomes of spherical type:

$$\epsilon(\mathbf{k}) = \frac{\hbar^2}{2m_0} T_{ij} T_{il} k_j k_l = \frac{h^2 k^{*2}}{2m_0} \tag{3.16}$$

and the volume element $d\mathbf{k}$ is modified to $d\mathbf{k}^* = (m_0/m_d)^{3/2} d\mathbf{k}$, where $m_d = (m_l m_t^2)^{1/3}$ is the density-of-states effective mass.

To preserve vector equations, the transformation in Eq. (3.14) must be applied to other vector quantities, such as driving forces and phonon wave vectors. Thus the equation of motion for an electron under the influence of an external force $\mathcal{F}$ becomes

$$\frac{d}{dt}(\hbar\mathbf{k}^*) = \mathcal{F}^* . \tag{3.17}$$

The electron velocity as a function of $\mathbf{k}^*$ is given by

$$v_i = \frac{\hbar}{m_0} T_{ij} k_j^* , \tag{3.18}$$

which is again generalized to the nonparabolic case by simply replacing m_0 with the expression $m_0(1+2\alpha\epsilon)$.

B. Actual bands of covalent semiconductors

In this section the main features of the band structure of the three covalent semiconductors of group four, silicon, germanium, and diamond, will be briefly described

with regard to their use in charge transport calculations. The values of the parameters that describe conduction and valence bands for these materials are reported in Appendix C, together with other parameters of interest.

1. Conduction band

a. Silicon

The band structure of silicon is such that the electrons which contribute to charge transport, even at high electric fields, are those in the six equivalent ellipsoidal valleys along the ⟨100⟩ directions at about 0.85 (Ivey and Mieher, 1972) from the center of the Brillouin zone. In fact, owing to their small density-of-states effective mass and distance in energy, the other secondary minima can be neglected.

The effect of band nonparabolicity is particularly important at high electric fields, when the electrons can reach energies far from the bottom of the conduction band (Jacoboni *et al.*, 1975) (see Sec. IV.B.4).

b. Germanium

The absolute minima of the conduction band in germanium lie along the ⟨111⟩ directions at the L points. There are, therefore, four equivalent ellipsoidal valleys. Owing to their proximity in energy, the spherical upper valley at the center of the Brillouin zone and the six ellipsoidal upper valleys along the ⟨100⟩ directions can be populated by electrons at high electric fields, so that it is necessary to include them in high-field transport calculations.

As for the case of Si, nonparabolicity may influence the dynamical behavior of the electrons that populate the lowest bands, while for the bands associated with the upper minima this effect is expected to be much lower, due to the lower kinetic energies of the electrons that populate them. For this reason upper valleys are usually assumed to be parabolic in electron transport calculations.

c. Diamond

Experimental information on the band structure of diamond is still scarce. This fact reflects the near impossibility, to date, of growing crystals with controlled properties. Nonetheless, from theoretical considerations it is well established that the conduction band of diamond is Si-like (Herman, 1952; Zunger and Freeman, 1977; Nava *et al.*, 1980), with six lower minima along the ⟨100⟩ directions, located at about 0.76 (Dean *et al.*, 1965) from the center of the Brillouin zone. By analogy with the case of Si, the upper minima can be neglected.

2. Valence band

The valence bands of all covalent semiconductors of group four are very similar to each other, and a pioneer $\mathbf{k}\cdot\mathbf{p}$ calculation of Kane (1956) well approximates (the larger the direct energy gap, the better the approximation) the energy-wave-vector relationship of the three bands around the center of the Brillouin zone, in terms of four band parameters characteristic of each material:

$$\epsilon_i = \epsilon_i(\mathbf{k}, A, B, C, \epsilon_{so}) \ . \tag{3.19}$$

Here the subscript i stands for heavy, light, and spin-orbit bands. Equations (3.3) and (3.4) are approximate versions of Kane's expression which well describe heavy and light bands under the condition $\epsilon_i \ll \epsilon_{so}$.

The difficulties one encounters in dealing with three bands that include the full details of Eq. (3.19) are usually overcome by neglecting the third band, because of its separation in energy and small density of states, and by introducing further simplifications in treating the remaining two bands (heavy and light holes). Among these simplified models we mention the following:

(i) A single parabolic band (heavy holes) for rough calculations.

(ii) A single warped, parabolic band.

(iii) Two spherical and parabolic bands, with effective masses related to some plausible average in $\mathbf{k}$ space of Eq. (3.19) (Costato *et al.*, 1974; Bosi *et al.*, 1979).

Nonparabolicity can be approximately accounted for by means of an iterative procedure which verifies that the values of the effective mass and of the mean energy, measured in equivalent temperature, fit a curve of heavy mass versus temperature like that reported in Fig. 14, calculated for the material of interest (Reggiani *et al.*, 1977; Reggiani, 1980).

C. Scattering mechanisms in covalent semiconductors

We now turn our attention to analyzing the scattering mechanisms that act on charge carriers in the host crystal. As usual, the dynamics of the electronic interactions is assumed to be independent of the applied field, and the collisions are assumed to occur instantaneously (for interesting exceptions, see Barker and Ferry, 1979).

All scattering calculations presented here will be carried out with a first-order perturbative approach; consequently only two-body interactions will be analyzed.

1. Classification

The transitions of interest for electron transport in semiconductors can be classified as intravalley, if both initial and final states of the electron lie in the same valley, or intervalley, if the final state lies in a valley different from that of the initial state. For the case of holes, the same classification holds in terms of intraband and interband transitions.

The carrier transitions are induced by different scattering sources present in the crystal of which the most important are phonons, impurities, and other electrons.

The carrier-phonon interaction is due to the deformation, associated with phonons, of the otherwise perfect

crystal, and in covalent semiconductors it is described in the framework of the deformation-potential method (for a review of this method see the textbook of Bir and Pikus, 1974) for both acoustic and optical phonons.

As regards impurities, they can be ionized or neutral. In the former case the interaction is of the long-range Coulomb type; in the latter, the interaction is of much shorter range, and the overall effect of neutral impurities is, in general, much weaker. At normal concentrations neutral impurities can influence electron transport in semiconductors only very little and only at very low temperatures (Jacoboni and Reggiani, 1979). The concomitance of other mechanisms, such as ionized impurities and acoustic phonons, makes the analysis of this type of scattering from experimental data very difficult. So far, to the best of the authors' knowledge, neutral impurities have not been included in Monte Carlo calculations, and they will not be treated in the present review.

The effect of the electron-electron collisions is in general very limited. As discussed in Sec. II.G, this interaction is very difficult to include in transport theory.

Since the Coulomb cross section decreases rapidly with increasing momentum transfer, scattering from ionized impurities must in general be considered only for intravalley or intraband transitions, owing to the large $\Delta\mathbf{k}$ involved in intervalley and, to a minor extent (Costato and Reggiani, 1973), interband transitions. Intervalley transitions can be induced by impurities with a mechanism that has been studied by Price and Hartman (1964) and Asche and Sarbei (1969). This effect may be competitive with intervalley phonon scattering at low temperatures and fields but, to the best of the authors' knowledge, it has never been included in Monte Carlo calculations.

In the following, after a brief review of the fundamentals of scattering theory, the most important carrier interactions will be studied (see Table II below), and for each scattering mechanism differential and integrated scattering probabilities will be calculated from a knowledge of the matrix element of the perturbation between two Bloch states. In particular, the simple spherical and parabolic model, together with the more refined ellipsoidal, nonparabolic, and warped models, will be considered in the calculations. Results for intermediate models will be obtained as particular cases.

Special attention will be devoted to the application of the results to the determination of the final state of the interacting particle in the Monte Carlo procedure.

2. Fundamentals of scattering

a. General theory

In order to study the transitions of an electron between different Bloch states in a crystal, one starts with the assumption that the system can be separated into the electron of interest and the rest of the crystal. The vector state for such a combined system can be written as the direct product

$$|\mathbf{k},c\rangle = |\mathbf{k}\rangle\,|c\rangle \tag{3.20}$$

where $|\mathbf{k}\rangle$ and $|c\rangle$ represent the unperturbed states of the electron and of the crystal, respectively.

The expression for the transition probability per unit time from a state $|\mathbf{k},c\rangle$ to a state $|\mathbf{k}',c'\rangle$ induced by a perturbation Hamiltonian H' is given to first order by the golden rule:

$$P(\mathbf{k},c;\mathbf{k}',c') = \frac{2\pi}{\hbar}\,|\langle \mathbf{k}',c'|H'|\mathbf{k},c\rangle|^2 \times \delta[\epsilon(\mathbf{k}',c')-\epsilon(\mathbf{k},c)] \,. \tag{3.21}$$

H' acts, in general, on the coordinate $\mathbf{r}$ of the electron and on the variables which describe the state $|c\rangle$ of the crystal, e.g., on the ion displacement $\mathbf{y}$ with respect to their equilibrium position and on the coordinates $\mathbf{r}'$ of the other electrons.

It is now convenient to expand H' in a Fourier series,[6]

$$H'(\mathbf{r},\mathbf{y},\mathbf{r}') = \frac{(2\pi)^{3/2}}{V}\sum_{\mathbf{q}} \mathscr{H}'(\mathbf{q},\mathbf{y},\mathbf{r}')\exp(i\mathbf{q}\cdot\mathbf{r}) \,, \tag{3.22}$$

which gives to the matrix element in Eq. (3.21) the following form:

$$\langle \mathbf{k}',c'|H'|\mathbf{k},c\rangle = \frac{(2\pi)^{3/2}}{V}\sum_{\mathbf{q}}\langle c'|\mathscr{H}'(\mathbf{q},\mathbf{y},\mathbf{r}')|c\rangle \int d\mathbf{r}\,\psi_{\mathbf{k}}^*(\mathbf{r})\exp(i\mathbf{q}\cdot\mathbf{r})\psi_{\mathbf{k}}(\mathbf{r}) \,, \tag{3.23}$$

where

$$\psi_{\mathbf{k}}(\mathbf{r}) = N^{-1/2}u_{\mathbf{k}}(\mathbf{r})\exp(i\mathbf{k}\cdot\mathbf{r}) \tag{3.24}$$

is the standard form for a Bloch state; N is the number of unit cells in the crystal, and the factor $N^{-1/2}$ is introduced in order to have $\psi_{\mathbf{k}}$ normalized to one in the crystal with $u_{\mathbf{k}}(\mathbf{r})$ normalized to one in the unit cell.

Let us now focus attention on the integral I on the right-hand side of Eq. (3.23). It can be calculated as a sum over the cells labeled by the vectors $\mathbf{R}$ of the direct lattice, and if we put

[6]According to the periodic boundary conditions, H' also has the periodicity of the crystal, no matter whether it comes from phonons or impurities, so that its Fourier series contains only the $\mathbf{q}$ vectors of reciprocal space.

$$\mathbf{r}''=\mathbf{r}-\mathbf{R}\ , \tag{3.25}$$

$$I=\sum_{\mathbf{R}}\exp[i(\mathbf{k}-\mathbf{k}'+\mathbf{q})\cdot\mathbf{R}]\frac{1}{N}\int_{\text{cell}}d\mathbf{r}''u^*_{\mathbf{k}'}(\mathbf{r}'')u_{\mathbf{k}}(\mathbf{r}'')\exp[i(\mathbf{k}-\mathbf{k}'+\mathbf{q})\cdot\mathbf{r}'']\ . \tag{3.26}$$

By taking into account that $\mathbf{k}=\mathbf{k}'+\mathbf{q}$ is a vector of the reciprocal space and $\mathbf{R}$ a vector of the direct lattice, we have (see, for example, the textbook of Ziman, 1972)

$$\sum_{\mathbf{R}}\exp[i(\mathbf{k}-\mathbf{k}'+\mathbf{q})\cdot\mathbf{R}]=\begin{cases}N & \text{if } \mathbf{k}-\mathbf{k}'+\mathbf{q}=\mathbf{G}\\ 0 & \text{otherwise}\end{cases} \tag{3.27}$$

where $\mathbf{G}$ is a vector of the reciprocal lattice. The terms of the sum in Eq. (3.23) which correspond to $\mathbf{G}=0$ are called "Normal" (or "N") terms, while when $\mathbf{G}$ is different from zero we speak of "umklapp" (or "U") terms.

In dealing with perturbations due to phonons, the sum contains only $\mathbf{q}$-vectors in the Brillouin zone, so that $\mathbf{k}$ and $\mathbf{k}'$ in Eq. (3.23) determine whether the transition is "N" or "U."

In the case of impurities, the sum in Eq. (3.23) may in principle contain infinite "U" terms, although the "N" term will be dominant.[7]

By collecting the above results, we have

$$P(\mathbf{k},c;\mathbf{k}',c')=\frac{(2\pi)^4}{\hbar V^2}\left|\sum_{\mathbf{q}}\langle c'|\mathscr{H}'(\mathbf{q},\mathbf{y})|c\rangle\right|^2 \times\mathscr{G}\delta[\epsilon(\mathbf{k}',c')-\epsilon(\mathbf{k},c)] \tag{3.28}$$

where $\mathscr{G}$ is the overlap integral

$$\mathscr{G}=\left|\int_{\text{cell}}d\mathbf{r}\,u^*_{\mathbf{k}'}(\mathbf{r})u_{\mathbf{k}}(\mathbf{r})\exp(i\mathbf{G}\cdot\mathbf{r})\right|^2 . \tag{3.29}$$

To proceed further, we must give explicit forms to $\mathscr{H}'$, which depend on the particular scattering mechanism considered.

b. Overlap factor

Expressions for the overlap factor $\mathscr{G}$ in Eq. (3.29) as a function of $\mathbf{k}$ and $\mathbf{k}'$ have been given in the literature for various cases. For electrons, an intravalley transition process is, in general, of "N" type, because the distance between $\mathbf{k}$ and $\mathbf{k}'$ is small compared to the dimensions of the Brillouin zone. For "N" processes, $\mathscr{G}$ is equal to unity for exact plane waves or for wave functions formed with pure s states. When lower symmetries are involved in the Bloch wave functions (as, for example, p states in the case of cubic semiconductors), an overlap factor less than unity is obtained, which depends mainly upon the angle θ between initial and final states $\mathbf{k}$ and $\mathbf{k}'$, measured from the center of the Brillouin zone.

In the case of a minimum located at Γ, $\mathscr{G}$ is strictly related to nonparabolicity, since both of them come from the presence of p terms in the electron wave functions. Fawcett *et al.* (1970) gave for $\mathscr{G}$ the expression

$$\mathscr{G}(\mathbf{k},\mathbf{k}')=\frac{[(1+\alpha\epsilon)^{1/2}(1+\alpha\epsilon')^{1/2}+\alpha(\epsilon\epsilon')^{1/2}\cos\theta]^2}{(1+2\alpha\epsilon)(1+2\alpha\epsilon')}\ . \tag{3.30}$$

In the many-valley model, for intervalley transitions the process can be of "U" type, because of the large values associated with $\mathbf{k}$ and $\mathbf{k}'$. For both intravalley and intervalley transitions, the angle θ between initial and final states depends mostly on the valleys involved in the transition, and $\mathscr{G}$ is thus almost constant within each type of intravalley or intervalley scattering process (Reggiani and Calandra, 1973). The values for $\mathscr{G}$ in these cases may be included in the coupling constants.

For transitions of holes within heavy or light bands, Wiley (1971) found the simple expression

$$\mathscr{G}(\mathbf{k},\mathbf{k}')=\tfrac{1}{4}(1+3\cos^2\theta)\ , \tag{3.31}$$

while for interband transitions he used

$$\mathscr{G}(\mathbf{k},\mathbf{k}')=\tfrac{3}{4}\sin^2\theta\ . \tag{3.32}$$

D. Scattering probabilities

1. Phonon scattering

The general theory reviewed above for electron scattering in crystals will now be applied to the case of interaction with phonons. The subject will be confined to the case of deformation-potential interaction, which is the one of interest in covalent semiconductors. In this case the interaction Hamiltonian for a single band at Γ is written as (Kittel, 1963)

$$H'=\mathscr{E}\frac{\partial\mathbf{y}}{\partial\mathbf{r}} \tag{3.33}$$

where $\partial\mathbf{y}/\partial\mathbf{r}$ is the deformation of the crystal due to the phonons, and $\mathscr{E}$ is a tensor that describes the shift of the electron band per unit deformation. In the approximation of a continuous medium, the ion displacement field $\mathbf{y}$ can be written in terms of phonon creation $a_q^\dagger$ and annihilation a_q operators as (Kittel, 1963)

[7] In fact, the scattering cross section for ionized impurities decreases sharply with increasing momentum transfer, and in any case the overlap factor (see next section) will be smaller for $\mathbf{G}\neq 0$).

$$\mathbf{y}=\sum_{\mathbf{q}}\left[\frac{\hbar}{2\rho V\omega_q}\right]^{1/2}(a_{\mathbf{q}}+a^{\dagger}_{-\mathbf{q}})\exp(i\mathbf{q}\cdot\mathbf{r})\boldsymbol{\xi} \tag{3.34}$$

where ρ is the density of the crystal, ω_q the phonon angular frequency, and $\boldsymbol{\xi}$ its polarization. By using Eq. (3.34) we obtain for Eq. (3.33) the expression

$$H'=\sum_{\mathbf{q}}\left[\frac{\hbar}{2\rho V\omega_q}\right]^{1/2}(a_{\mathbf{q}}+a^{\dagger}_{-\mathbf{q}})\exp(i\mathbf{q}\cdot\mathbf{r})i\mathscr{E}_{lj}q_l\xi_j \tag{3.35}$$

where the sum is implied for the coordinate subscripts l and j. Equation (3.35) is an explicit form of the Fourier transform indicated in Eq. (3.32); a_q and $a^{\dagger}_{-q}$ appear in Eq. (3.35) in such a way that only two terms in the sum over $\mathbf{q}$ give a contribution to the matrix element; they correspond to states $|c'\rangle$ with the occupation number of one mode $\mathbf{q}$ changed by one unit with respect to $|c\rangle$. More precisely, they correspond to the emission and the absorption of a phonon with wave vector

$$\mathbf{q}=\mathbf{k}'-\mathbf{k}+\mathbf{G} \tag{3.36}$$

for absorption, or

$$\mathbf{q}=\mathbf{k}-\mathbf{k}'+\mathbf{G} \tag{3.37}$$

for emission. This fact states the conservation law of crystal momentum from the point of view of the crystal subsystem, as Eq. (3.27) states the same law from the point of view of the electrons.

For the two cases above we have

$$|\langle c'|a_q|c\rangle|^2=N_q \tag{3.38}$$

and

$$|\langle c'|a^{\dagger}_{-q}|c\rangle|^2=N_q+1 \tag{3.39}$$

for absorption and emission, respectively, where N_q is the phonon number.

By collecting the foregoing results we obtain the following expression for the transition probability per unit time of an electron from state $\mathbf{k}$ to state $\mathbf{k}'$:

$$P(\mathbf{k},\mathbf{k}')=\frac{\pi}{\rho V\omega_q}\begin{bmatrix} & N_q \\ N_q & +1\end{bmatrix}\mathscr{G}\,|\,\mathscr{E}_{ij}q_j\xi_i\,|^2 \times\delta[\varepsilon(\mathbf{k}')-\varepsilon(\mathbf{k})\mp\hbar\omega_q]\,, \tag{3.40}$$

where the upper and lower symbols refer to absorption and emission, respectively.

This equation will be used in the following sections for the analysis of the various carrier transitions due to phonons. In particular it will also be applied, in a slightly modified form (Harrison, 1956; Bir and Pikus, 1961), to the case of optical modes, for which the above theory is not directly applicable. In Secs. III.D.1.*b* and III.D.1.*e*, we shall briefly consider this problem, but for a more detailed discussion we refer the reader to the original literature. (For a review see Ziman, 1960, and Bir and Pikus, 1974. For a microscopic theory see Lawaetz, 1969; Vogl, 1976; Pötz and Vogl, 1981.)

In what follows, the phonon number N_q will be assumed to be equal to its equilibrium value at the temperature of the crystal. This assumption is not always correct, and the problem has received some attention (for a review see Kocevar, 1980), but at present no Monte Carlo application has been developed for it.

a. Electron intravalley scattering—acoustic phonons

For a nondegenerate band at the center of the Brillouin zone of a cubic semiconductor, the deformation potential $\mathscr{E}$ of Eq. (3.40) is a second-rank tensor with cubic symmetry, which, as a rule, has a diagonal form with equal diagonal elements and therefore can be treated as a scalar quantity $\mathscr{E}_1$. The squared factor that appears in Eq. (3.40) reduces to $\mathscr{E}_1^2q^2$ for longitudinal phonons, while it vanishes for transverse modes.

In this simple case, energy and momentum conservation imply

$$q=\mp 2\left[k\cos\theta-\frac{mu_l}{\hbar}\right], \tag{3.41}$$

where u_l is the longitudinal sound velocity; m the electron effective mass, θ the angle between $\mathbf{k}$ and $\mathbf{q}$, and upper and lower signs refer to absorption and emission, respectively. The maximum value of q is obtained for absorption with backward scattering, and is given by

$$q_{\max}=2k+\frac{2mu_l}{\hbar}\,. \tag{3.42}$$

If the scattering mechanism were elastic, a backward collision would involve $q_{\max}=2k$; thus the second term in Eq. (3.42) is the correction due to the energy of the phonon involved in the transition. The relative contribution of this term can be seen in Eq. (3.42) to be given by u_l/v, where v is velocity of the electron which, in general, is much larger than u_l. The maximum q involved in these transitions is therefore very close to $2k$; the corresponding maximum energy transfer is

$$\hbar q_{\max}u_l\approx 2\hbar ku_l=2mvu_l\,, \tag{3.43}$$

which, again, is in general much smaller than the electron kinetic energy $mv^2/2$. For these reasons acoustic scattering is very often considered an elastic process.

However, we have to make some important observations in this connection which may become essential when the transport problem is solved with a Monte Carlo simulative technique.

When Ohmic transport is investigated by analytic means, the energy distribution function is assumed to be the equilibrium Maxwellian distribution (for nondegenerate statistics), and no energy exchange of the electrons with the heat bath is explicitly required. On the other hand, when a simulation analysis is undertaken at low fields and temperatures, in order to obtain a correct

steady-state condition, we need a mechanism which can exchange an arbitrarily small amount of energy between electrons and the heat bath (the crystal): physically this role is played by the interaction with acoustic phonons. To consider this mechanism elastic is therefore, in general, illegitimate, because in itself acoustic-phonon interaction will never produce a steady-state condition; the Joule heating due to the field will increase the carrier mean energy indefinitely.

When, in contrast, high fields and/or high temperatures are considered, acoustic scattering can be treated as an elastic process, since the average electron energy is of the order of the optical-phonon energy, and optical phonons can assume the task of exchanging energy between the electrons and the crystal. In this case the presence of the external field is essential for smearing out, through the acceleration process, the energy of each single electron; in fact, in the absence of external fields, the electron energy would take only its initial value plus or minus a whole number of optical-phonon energy quanta.

In the paragraphs below acoustic scattering will be treated in an elastic approximation, then analogous calculations will be developed with correct energy exchange.

(1) Elastic, energy-equipartition approximation—spherical, parabolic bands. When we deal with acoustic scattering in an elastic approximation, the phonon population N_q is usually represented by the equipartition expression

$$N_q \simeq \frac{K_B T_0}{\hbar q u_l} - \frac{1}{2} . \tag{3.44}$$

This approximation is closely related to the elastic approximation discussed above. In fact, Eq. (3.44) is valid when $\hbar q u_l \ll K_B T_0$, i.e., when the thermal energy is much larger than the energy of the phonon involved in the transition. At very low temperatures and/or at very high fields, this condition may break down (Costato and Reggiani, 1970). Furthermore, when a precise energy balance is to be obtained, exchange of electron energy with the heat bath via acoustic phonons must be taken into account. The exact expression for N_q or a good approximation of it must be used (see Appendix D).

The expression for the scattering probabilities per unit time from a state $\mathbf{k}$ to a state $\mathbf{k}'$ given by Eq. (3.40), in elastic and energy-equipartition approximations, becomes

$$P(\mathbf{k},\mathbf{k}') = \frac{\pi q \mathscr{E}_1^2}{V u_l \rho} \left[\frac{K_B T_0}{\hbar q u_l} \mp \frac{1}{2} \right] \delta[\epsilon(\mathbf{k}') - \epsilon(\mathbf{k})] , \tag{3.45}$$

where upper and lower spins refer to absorption and emission, and the overlap factor $\mathscr{G}$ has been taken as equal to one, in accord with the comments in Sec. III.C.2.*b*. Since in the elastic approximation no distinction is made between final states attained by means of absorption or emission processes, we can consider the sum of the transition probabilities per unit time to be given by

$$P(\mathbf{k},\mathbf{k}') = \frac{2\pi K_B T_0}{\hbar V u_l^2 \rho} \mathscr{E}_1^2 \delta[\varepsilon(\mathbf{k}') - \varepsilon(\mathbf{k})] . \tag{3.46}$$

From this equation we conclude that, in the above approximations, acoustic scattering becomes isotropic.

In a frame of reference with the polar axis along the direction of $\mathbf{k}$, integration of Eq. (3.46) over all possible final states $\mathbf{k}'$ yields the integrated scattering probability per unit time which accounts for both absorption and emission processes:

$$P_{e,\mathrm{ac}}(\epsilon) = \frac{2^{1/2} m^{3/2} K_B T_0 \mathscr{E}_1^2}{\pi \hbar^4 u_l^2 \rho} \epsilon^{1/2} . \tag{3.47}$$

This expression, for acoustic phonons in elastic and energy-equipartition approximation, can be used in a Monte Carlo simulation. Its energy dependence, a simple proportionality $\epsilon^{1/2}$, is shown in Fig. 15.

As regards the choice of the electron state after scattering, owing to the isotropic character of the scattering, any state $\mathbf{k}'$ belonging to the energy-conserving sphere has the same probability of occurrence, independently of the angle formed with the initial state $\mathbf{k}$. The probability that the polar angles of $\mathbf{k}'$ with respect to any convenient directions will be contained in the intervals $d\theta$ and $d\varphi$ is proportional to $\sin\theta \, d\theta \, d\varphi$. By application of the direct technique (see Appendix A Sec.2.a) θ and φ can be chosen with two random numbers r_1 and r_2 as

$$\cos\theta = 1 - 2r_1 , \tag{3.48}$$

$$\varphi = 2\pi r_2 . \tag{3.49}$$

When this simple model is used, the polar axis is usually taken along the direction of the applied field.

(2) Elastic, energy-equipartition approximation—ellipsoidal, nonparabolic bands. If we move from the simple spherical and parabolic case to more realistic band structures, many complications arise.

For an ellipsoidal, nonparabolic model, the energy-

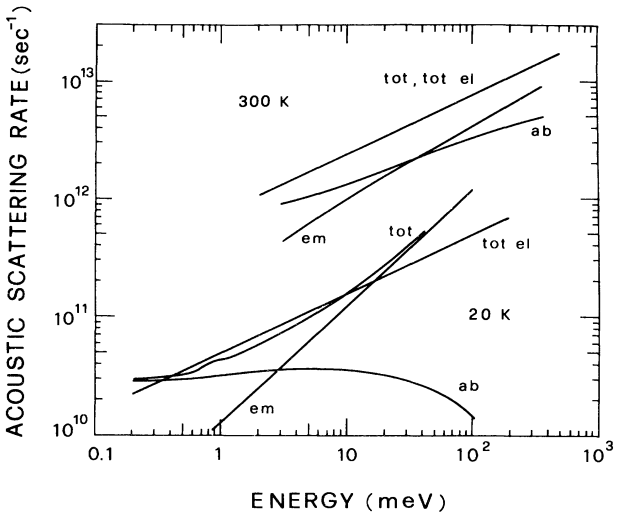

FIG. 15. Integrated acoustic-scattering probability per unit time as a function of energy at the temperatures reported. The model used refers to electrons in Si with a parabolic band structure: (ab) absorption; (em) emission; (tot el) total in elastic approximation; (tot) total when acoustic energy dissipation and exact phonon population are accounted for.

wave-vector relationship is

$$\gamma(\mathbf{k})=\epsilon(1+\alpha\epsilon)$$
$$=\frac{\hbar^2}{2}\left[\frac{1}{m}\right]_{ij}k_i k_j\ , \tag{3.50}$$

and it is usually treated by means of the Herring-Vogt transformation (see Sec. III.A.3).

In a model with valleys centered along ⟨100⟩ or ⟨111⟩ directions, for symmetry reasons we have two independent components Ξ_d and Ξ_u of the deformation-potential tensor (Herring and Vogt, 1956) and electron-acoustic-phonon interaction is allowed with transverse as well as longitudinal modes. In this case Eq. (3.46) becomes

$$P_l(\mathbf{k},\mathbf{k}')=\frac{2\pi K_B T_0}{\hbar V u_l^2\rho}(\Xi_d+\Xi_u\cos^2\theta)^2$$
$$\times\delta[\epsilon(\mathbf{k}')-\epsilon(\mathbf{k})] \tag{3.51}$$

for longitudinal modes, and

$$P_t(\mathbf{k},\mathbf{k}')=\frac{2\pi K_B T_0}{\hbar V u_t^2\rho}(\Xi_u\sin\theta\cos\theta)^2\delta[\epsilon(\mathbf{k}')-\epsilon(\mathbf{k})] \tag{3.52}$$

for transverse modes. Here u_t is the transverse sound velocity and θ is the angle between $\mathbf{q}$ and the longitudinal axis of the valley considered.

The effect of anisotropy is not large (Conwell, 1967), so that it is in general neglected by replacing u_l,u_t with an average value $u=\frac{1}{3}(2u_t+u_l)$ and the expressions in brackets with mean values $\mathscr{E}_i^2$ over the angle θ.[8] Thus a simple expression for the scattering probability per unit time is again used, of the type of Eq. (3.46):

$$P(\mathbf{k},\mathbf{k}')=\frac{2\pi K_B T_0}{\hbar V u^2\rho}\mathscr{E}_1^2\delta[\epsilon(\mathbf{k}^{*\prime})-\epsilon(\mathbf{k}^*)]\ . \tag{3.53}$$

Band effects are carried on by the energy forms in the argument of the δ function. The last expression is again independent of the direction of $\mathbf{k}^*$ and $\mathbf{k}^{*\prime}$, so that the scattering is still isotropic.

Integration over all possible final states $\mathbf{k}^{*\prime}$ yields the integrated scattering probability per unit time which accounts for both absorption and emission processes:

$$P_{e,\mathrm{ac}}(\epsilon)=\frac{2^{1/2}m_d^{3/2}K_B T_0\mathscr{E}_1^2}{\pi\hbar^4 u^2\rho}$$
$$\times\epsilon^{1/2}(1+2\alpha\epsilon)(1+\alpha\epsilon)^{1/2}\ . \tag{3.54}$$

From Eq. (3.54) it is also possible to determine the expressions of $P_{e,\mathrm{ac}}(\epsilon)$ for "intermediate" models, i.e., spherical nonparabolic [$m_d=m$ and $u=u_l$ in Eq. (3.54)] or ellipsoidal parabolic [$\alpha=0$ in Eq. (3.54)].

Concerning the choice of the electron state after scattering, Eqs. (3.48) and (3.49) of the preceding section can be used, because of the isotropy of the scattering.

(3) Inelastic acoustic scattering—spherical, parabolic bands. In order to treat correctly energy dissipation via acoustic phonons we must take into account, the energy of the phonon involved in the energy balance of the collision:

$$\epsilon(\mathbf{k}')=\epsilon(\mathbf{k})\pm\hbar q u_l\ . \tag{3.55}$$

Here again and in what follows, upper and lower signs refer to absorption and emission, respectively.

In a simple spherical and parabolic band, only longitudinal modes contribute to the scattering, and energy and momentum conservation imply [see Eq. (3.41)]

$$\cos\theta=\pm\frac{q}{2k}+\frac{mu_l}{\hbar k}\ . \tag{3.56}$$

The condition $-1\le\cos\le 1$ determines the range of phonon wave vectors that may be involved in a collision with an electron in state $\mathbf{k}$.

The results are reported in Table II where, instead of q, use has been made of the more convenient dimensionless variable $x=(\hbar q u_l)/(K_B T_0)$, and where $\epsilon_u=mu_l^2/2$ is the kinetic energy of an electron with velocity equal to the longitudinal sound velocity.

In order to be consistent with the correct treatment of energy exchange in acoustic-phonon scattering, the exact expression of the phonon number N_q must be included in

TABLE II. Scattering mechanisms in covalent semiconductors.

Phonons	electrons	intravalley	acoustic
			optical
		intervalley	
	holes	intraband	acoustic
			optical
		interband	
Ionized impurity	electrons (intravalley)		
	holes (intraband)		
Carrier-carrier			

[8]This approximation can be removed by replacing the angular quantities in the brackets of Eq. (3.51) and (3.52) with their maximum value $\{F_{\max}\}$ and, then, by using the rejection technique when the angle θ for the transition has been chosen: if a random number r is such that

$$r\{F_{\max}\}>\{F(\theta)\}\ ,$$

the event is to be considered a self-scattering, and the electron path continues unperturbed.

the calculations. Thus the transition probability of Eq. (3.40) for the case of interest becomes

$$P(\mathbf{k},\mathbf{k}')=\frac{\pi q\mathscr{E}_1^2}{V\rho u_l}\begin{bmatrix} N_q \\ N_q+1 \end{bmatrix}\delta[\epsilon(\mathbf{k}')-\epsilon(\mathbf{k})\mp\hbar q u_l] \ . \tag{3.57}$$

To perform the integration over all possible final states, it is convenient to consider integration over $\mathbf{q}$, and to use polar coordinates with the polar axis along $\mathbf{k}$. The δ function of energy conservation can be used to integrate over the polar angle θ between $\mathbf{q}$ and $\mathbf{k}$, which leads to

$$P(k,q)dq=\frac{m\mathscr{E}_1^2}{4\pi\rho u_l\hbar^2 k}\begin{bmatrix} N_q \\ N_q+1 \end{bmatrix}q^2dq \ . \tag{3.58}$$

This expression will be useful later for the determination of the state $\mathbf{k}'$ after scattering.

Final integration over q leads to the integrated scattering probability per unit time as a function of energy:

$$P_{e,\mathrm{ac}}(\epsilon)=\frac{m^{1/2}(K_BT_0)^3\mathscr{E}_1^2}{2^{5/2}\pi\hbar^4u_l^4\rho}\epsilon^{-1/2}\begin{Bmatrix} F_1(x_{2,a})-F_1(x_{1,a}) \\ G_1(x_{2,e})-G_1(x_{1,e}) \end{Bmatrix} , \tag{3.59}$$

where

$$F_1(x)=\int_0^x N_q(x')x'^2dx' \ , \tag{3.60}$$

$$G_1(x)=\int_0^x[N_q(x')+1]x'^2dx' \tag{3.61}$$

relate to absorption and emission processes, respectively, and $x_{1,a}$, $x_{2,a}$, $x_{1,e}$, and $x_{2,e}$ are those given in Table III. The numerical evaluation of the functions $F_1(x)$ and $G_1(x)$ is reported in Appendix D.

In Fig. 15, the integrated acoustic scattering probabilities, given by Eq. (3.59), are shown and compared with the results of the elastic approximation.

For determination of the final states after scattering, the following procedure can be used: first the value of q involved in the transition is chosen with the aid of the rejection technique (see Appendix A Sec.2.d), applied to the probability in Eq. (3.58). Then the magnitude of the electron wave vector $\mathbf{k}'$ after scattering is obtained by energy conservation, while the angle β between $\mathbf{k}'$ and $\mathbf{k}$ is obtained by momentum conservation. The angle φ of rotation around the direction of $\mathbf{k}$ is chosen at random according to Eq. (3.49).

If the components of $\mathbf{k}'$ are to be determined with respect to fixed directions $\hat{x}$, $\hat{y}$, and $\hat{z}$, as is necessary when full three-dimensional simulation is performed, the following formulas can be used (see Fig. 16):

$$k_x'=k'(\cos\beta\cos\gamma+\sin\beta\cos\varphi\sin\gamma) \ , \tag{3.62}$$

$$k_y'=k'(\cos\beta\cos\gamma'-\sin\beta\cos\varphi\cos\gamma\cos\eta -\sin\beta\sin\varphi\sin\eta) \ , \tag{3.63}$$

$$k_z'=k'(\cos\beta\cos\gamma''-\sin\beta\cos\varphi\sin\eta\cos\gamma +\sin\beta\sin\varphi\cos\eta) \ , \tag{3.64}$$

where $\gamma=\hat{kz}$, $\gamma'=\hat{ky}$, $\gamma''=\hat{kx}$, η is the angle between y and the component of $\mathbf{k}$ in the x-y plane; the origin of the angle φ is taken along the plane formed by $\mathbf{k}$ and $\hat{z}$.

(4) Inelastic acoustic scattering—ellipsoidal, nonparabolic bands. When all details of ellipsoidal many-valley electron bands and acoustic energy relaxation are considered, the transition probability $P(\mathbf{kk}')$ has the form given in Eqs. (3.51) and (3.52), where, in addition, the argument of the δ function contains the energy of the phonon, as in Eq. (3.55), and nonparabolicity is accounted for by assuming, for the energy-wave-vector relationship, the expression in Eq. (3.50).

We shall again keep the isotropic approximation for the deformation-potential coupling and, in applying the Herring-Vogt transformation for $\mathbf{k}$ and $\mathbf{q}$-vectors, approximate the magnitude of $\mathbf{q}$ as

$$q=q^*\left[\frac{m_l}{m_0}\cos^2\theta^*+\frac{m_t}{m_0}\sin^2\theta^*\right]^{1/2} \approx q^*\left[\frac{m_d}{m_0}\right]^{1/2} , \tag{3.65}$$

where θ^* is the angle between $\mathbf{k}^*$ and the principal axis of the valley. This last approximation is rather poor when the valley is strongly anisotropic, as for the case of Ge, and better approximations should be sought for exact numerical solutions of the Boltzmann equation.

TABLE III. Limits of the values of q for inelastic acoustic scattering determined through the condition $-1\le\cos\theta\le 1$. See text for discussion.

Absorption	Emission	
$x_{1,a}=\frac{4\epsilon_u^{1/2}}{K_BT_0}(\epsilon_u^{1/2}-\epsilon^{1/2})$	absent	$\epsilon<\epsilon_u$
$x_{2,a}=\frac{4\epsilon_u^{1/2}}{K_BT_0}(\epsilon_u^{1/2}-\epsilon^{1/2})$		
$x_{1,a}=0$	$x_{1,e}=0$	$\epsilon>\epsilon_u$
$x_{2,a}=\frac{4\epsilon_u^{1/2}}{K_BT_0}(\epsilon_u^{1/2}-\epsilon^{1/2})$	$x_{2,e}=\frac{4\epsilon_u^{1/2}}{K_BT_0}(\epsilon^{1/2}-\epsilon_u^{1/2})$	

The requirement that the argument of the δ vanish yields

$$\cos\theta = \mp\frac{q^*}{2k^*}(1-4\alpha\epsilon_u^*)+\left[\frac{\epsilon_u^*}{\gamma(\epsilon)}\right]^{1/2}(1+2\alpha\epsilon)\ , \tag{3.66}$$

where θ is the angle between $\mathbf{q}^*$ and $\mathbf{k}^*$, and $\epsilon_u^* = m_d u^2/2$.

As in the standard procedure the condition $-1 \le \cos\theta \le 1$ yields the limits of variability of q^*. These limits are conveniently expressed in terms of the dimensionless variable $x = (\hbar q^* u / K_B T_0)(m_d/m_0)^{1/2}$ and are given in Table III, under the condition, verified in our cases, that $4\alpha\epsilon_u^* < 1$. By using polar coordinates as for the previous case, we obtain by integration over the angle variables

$$P(\epsilon,x)dx = \frac{m_d^{1/2}(K_B T_0)^3 \mathscr{E}_1^2}{2^{5/2}\pi\hbar^4 u^4 \rho}\gamma^{-1/2}(\epsilon)\begin{bmatrix} N_q(x) \\ N_q(x)+1 \end{bmatrix}(1+2\alpha\epsilon \pm 2\alpha K_B T_0 x)x^2 dx\ . \tag{3.67}$$

Final integration over x leads to the integrated scattering probability per unit time as a function of energy,

$$P_{e,\mathrm{ac}}(\epsilon) = \frac{m_d^{1/2}(K_B T_0)^3 \mathscr{E}_1^2}{2^{5/2}\pi\hbar^4 u^4 \rho}\gamma^{-1/2}(\epsilon)\begin{Bmatrix} (1+2\alpha\epsilon)[F_1(x_{2a})-F_1(x_{1,a})]+2\alpha K_B T_0[F_2(x_{2,a})-F_2(x_{1,a})] \\ (1+2\alpha\epsilon)[G_1(x_{2,e})-G_1(x_{1,e})]-2\alpha K_B T_0[G_2(x_{2,e})-G_2(x_{1,e})] \end{Bmatrix}, \tag{3.68}$$

where

$$F_2(x) = \int_0^x N_q(x')x'^3 dx'\ , \tag{3.69}$$

$$G_2(x) = \int_0^x [N_q(x')+1]x'^3 dx'\ . \tag{3.70}$$

The numerical evaluation of the functions $F_2(x)$ and $G_2(x)$ is reported in Appendix D.

For the determination of the electron state after scattering, a procedure similar to that described in the preceding section can be followed.

The intermediate case of spherical nonparabolic bands can be dealt with by substituting m for m_d in Eq. (3.68).

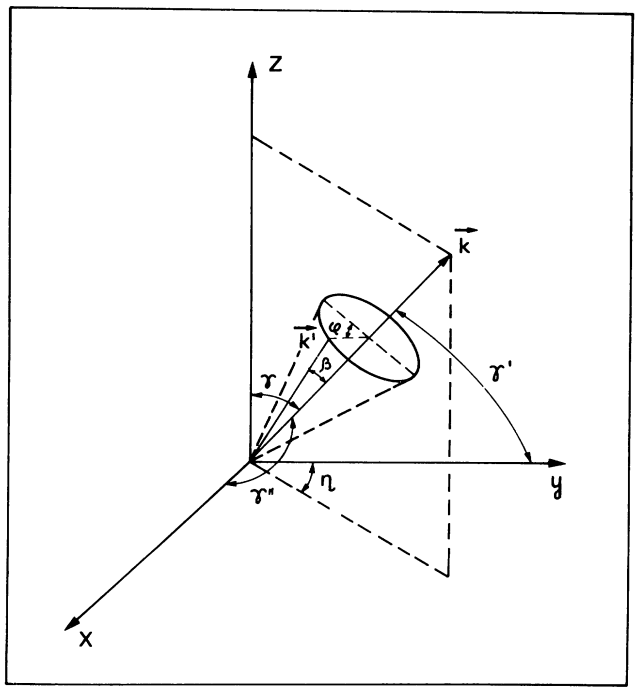

FIG. 16. Geometry for the determination of the state after scattering when full three-dimensional simulation is performed (see text).

The nonspherical parabolic result is recovered by putting $\alpha = 0$ in Eq. (3.68). In Fig. 17 the integrated acoustic probabilities given by Eq. (3.68) are shown and compared with the results of the parabolic case.

b. Electron intravalley scattering—optical phonons

For optical modes the perturbation Hamiltonian to the lowest value of approximation is assumed to be proportional to the atomic displacement (Harrison, 1956; Bir and Pikus, 1961; Lawaetz, 1969) and not to its derivative, as in the case of acoustic vibrations. The continuous-medium approximation adopted for long-wavelength acoustic modes would be inconsistent for optical phonons. Nevertheless, the final result of the correct theory is the same for the simplest case, which is obtained by assuming

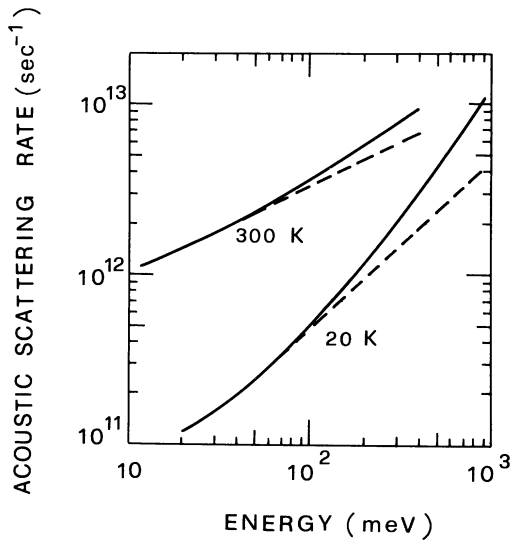

FIG. 17. The total integrated acoustic-scattering probability per unit time when acoustic dissipation and exact phonon population are accounted for: dashed curve, parabolic case; solid curve, nonparabolic case.

a wavelength equal to the lattice constant, to represent the fact that atoms belonging to the same unit cell vibrate in opposite directions. The scattering probability can then be written, starting from Eq. (3.40), by replacing $\mathscr{E}_1^2 q^2$ with a squared optical coupling constant $(D_t K)^2$ which can also include the $\mathscr{G}$ factor, as indicated in Sec. III.C.2.*b*. The energy associated with optical phonons in intravalley transitions can be assumed constant, given by $\hbar\omega_{op}=K_B\theta_{op}$, where θ_{op} is the equivalent temperature of the phonon, since the dispersion curve of such a phonon is quite flat for the q values involved in electronic intravalley transitions. For the same reason N_q becomes q independent ($N_q=N_{op}$). The resulting scattering probability per unit time is

$$P(\mathbf{k},\mathbf{k}')=\frac{\pi(D_tK)^2}{\rho V\omega_{op}}\begin{bmatrix}N_{op}\\N_{op}+1\end{bmatrix}\times\delta[\epsilon(\mathbf{k}')-\epsilon(\mathbf{k})\mp\hbar\omega_{op}]\ . \tag{3.71}$$

No angular dependence upon the direction of $\mathbf{k}'$ is present, and the scattering is therefore isotropic.

(1) Spherical, parabolic bands. For spherical and parabolic bands, integration of Eq. (3.71) over $\mathbf{k}'$ yields, with standard calculations, the integrated scattering probability per unit time

$$P_{e,op}(\epsilon)=\frac{(D_tK)^2m^{3/2}}{2^{1/2}\pi\hbar^3\rho\omega_{op}}\begin{bmatrix}N_{op}\\N_{op}+1\end{bmatrix}(\epsilon\pm\hbar\omega_{op})^{1/2}\ . \tag{3.72}$$

The probability of emission is obviously zero when $\epsilon<\hbar\omega_{op}$, since the carrier does not have enough energy to emit the phonon.

Figure 18 shows the optical-phonon scattering probability per unit time as a function of energy, given in Eq. (3.72). A simple proportionality to $\epsilon^{1/2}$, as for acoustic modes, is attained when the carrier energy is much larger than the phonon energy, so that the scattering becomes approximately elastic. As regards the choice of the final state, due to the isotropic character of the scattering, the same method as given by Eqs. (3.48) and (3.49) can be applied.

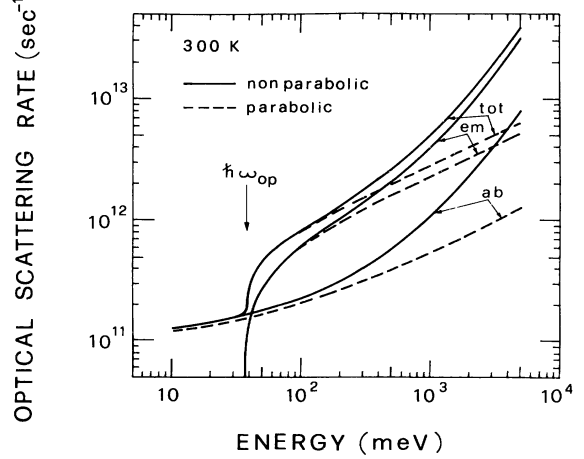

FIG. 18. Integrated optical-scattering probability per unit time as a function of energy. The model used refers to electrons in Ge with parabolic (dashed curves) and nonparabolic (solid curves) band structure: (ab) absorption; (em) emission; (tot) total.

(2) Ellipsoidal, nonparabolic bands. In dealing with ellipsoidal bands it is convenient to apply the Herring-Vogt transformation, as for acoustic phonons. The transition probability can be derived from the general expression in Eq. (3.40), as indicated above for simple bands. Since the transition probability is independent of $\mathbf{q}$, approximation in Eq. (3.65) is not necessary. The resulting transition probability is the same as in Eq. (3.71), with $\mathbf{k}^*$ and $\mathbf{k}^{*'}$ in place of $\mathbf{k}$ and $\mathbf{k}'$; and so the integrated scattering probability per unit time is the same as in Eq. (3.72), with m replaced by m_d.

When nonparabolicity is included, integration over $\mathbf{k}^{*'}$ yields an extra factor $[1+2\alpha(\epsilon\pm\hbar\omega_{op})]$, so that the integrated scattering probability per unit time for optical phonons is given by

$$P_{e,op}(\epsilon)=\frac{(D_tK)^2m_d^{3/2}}{2^{1/2}\pi\hbar^3\rho\omega_{op}}\begin{bmatrix}N_{op}\\N_{op}+1\end{bmatrix}\times\gamma^{1/2}(\epsilon\pm\hbar\omega_{op})[1+2\alpha(\epsilon\pm\hbar\omega_{op})] \tag{3.73}$$

where γ is defined in Eq. (3.5).

As regards the final state, it is still random, with constant probability over the energy-conserving sphere of $\mathbf{k}^{*'}$. In Fig. 18 the integrated optical intravalley scattering probabilities for the parabolic and nonparabolic cases are shown as a function of energy.

c. Electron intervalley scattering

Electron transitions between states in two different equivalent valleys can be induced by both acoustic- and optical-mode phonon scattering.

The phonon wave vector $\mathbf{q}$ involved in a transition remains very close to the distance between the minima of the initial and final valleys, even for high-energy electrons. Consequently, given these two valleys, $\Delta\mathbf{k}$ is almost constant, and, for a given branch of phonons, the energy $\hbar\omega_i$ involved in the transition is also about constant, as in the case of optical intravalley scattering. Thus intervalley scattering is usually treated, formally, in the same way as intravalley scattering by optical phonons with a deformation-potential interaction (Harrison, 1956; Conwell, 1967).

The squared coupling constant $(D_tK)_i^2$ depends upon the kinds of valleys (initial and final) and the branch of phonons involved in the transition, and it may include, as indicated in Sec. III.C.2.*b*, an overlap factor.

When the electron energy is sufficiently high, electrons can scatter into valleys higher in energy than the lowest-energy valleys. In this case the appropriate $\Delta\mathbf{k}$ in the

Brillouin zone must of course be considered together with the variation of the electron kinetic energy due to the energy difference between minima of the initial and final valleys.

The integrated scattering probability per unit time for intervalley transitions due to phonons, in spherical and parabolic valleys, is therefore given by

$$P_{e,i}(\epsilon)=\frac{(D_tK)_i^2 m^{3/2} Z_f}{2^{1/2}\pi\rho\hbar^3\omega_i}\begin{bmatrix} N_i \\ N_i+1 \end{bmatrix}(\epsilon\pm\hbar\omega_i-\Delta\epsilon_{fi})^{1/2}\,, \tag{3.74}$$

where Z_f is the number of possible final equivalent valleys for the type of intervalley scattering under consideration, N_i is the number of phonons involved in the transition, and $\Delta\epsilon_{fi}$ is the difference between the energies of the bottoms of the final and initial valleys.

When ellipsoidal and/or nonparabolic valleys are considered, the same corrections must be introduced relative to m_d and to the extra factor $[1+2\alpha(\epsilon\pm\hbar\omega_i-\Delta\epsilon_{fi})]$ as in the case of optical intravalley phonon scattering.

Figure 19 shows the integrated scattering probabilities per unit time for intervalley transitions to nonequivalent valleys. For equivalent valleys, when $\Delta\epsilon_{fi}=0$, the behavior of $P_{e,i}(\epsilon)$ is the same as that of $P_{e,\mathrm{op}}(\epsilon)$ (see Fig. 18).

When the final state has to be chosen in the simulation, all states in the energy-conserving sphere are equally probable. However, when several equivalent valleys are possible as final valleys of the transition, one of them must be selected at random. Sometimes it may be convenient not to distinguish between final valleys which are totally equivalent in the simulation, i.e., equivalent from the crystallographic point of view, and equally oriented

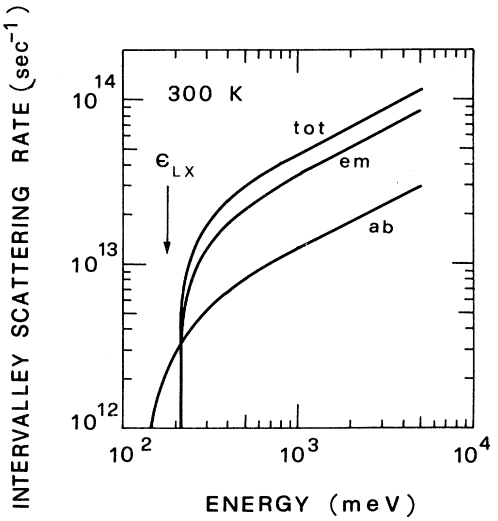

FIG. 19. Integrated scattering probability per unit time for intervalley transitions to nonequivalent valleys as a function of energy. The model used refers to electrons in Ge with parabolic upper bands. For symbol notation see Fig. 18.

with respect to the applied field. In this case appropriate weights must be given to the possible "representative" final valleys for each type of intervalley scattering.

d. Hole intraband scattering—acoustic phonons

Owing to the complexity of the valence-band structure, with its peculiarities of degeneracy and warping, the description of acoustic-phonon interaction requires three deformation-potential parameters (Bir and Pikus, 1961; Tiersten, 1961, 1964). Furthermore, the characteristic p-like symmetry of hole wave functions introduces an overlap factor which, in a good approximation, assumes the form given in Eqs. (3.31) and (3.32).

To overcome analytical difficulties, at the same time keeping the physics, a single coupling constant, which for convenience of notation will be called $\mathscr{E}_1^0$, is used in place of the original three parameters, and a single warped parabolic band, the heavy one, will be considered in the following, with the notation given by Eqs. (3.3) and (3.4).

When a warped, parabolic band is considered, the hole intraband scattering with acoustic phonons closely follows the electron—acoustic-phonon case reported in Sec. III.C.1.*a*. The transition probability of Eq. (3.40) for the case of interest becomes

$$P(\mathbf{k},\mathbf{k}')=\frac{\pi q\mathscr{E}_1^{0^2}}{V\rho u}\begin{bmatrix} N_q \\ N_q+1 \end{bmatrix}\tfrac{1}{4}(1+3\cos^2\theta)$$

$$\times\delta[\epsilon(\mathbf{k}')-\epsilon(\mathbf{k})\mp\hbar qu]\,, \tag{3.75}$$

where θ, the angle between $\mathbf{k}$ and $\mathbf{k}'$, is expressed in terms of initial ϑ,ψ and final ϑ',ψ' angles as

$$\cos\theta=\cos\vartheta\cos\vartheta'+\sin\vartheta\sin\vartheta'\cos(\psi-\psi')\,. \tag{3.76}$$

To perform integration in Eq. (3.75), we can replace q to a good approximation with $2^{1/2}k(1-\cos\theta)^{1/2}$, and by integrating over k' we find

$$P(\mathbf{k},\vartheta',\psi')=\frac{\mathscr{E}_1^{0^2}}{2^{1/2}\pi^2\rho u}\begin{bmatrix} N_q \\ N_{q+1} \end{bmatrix}(1+3\cos^2\theta)k$$

$$\times\frac{\{(1-\cos\theta)[\epsilon(\mathbf{k})\pm\epsilon_{\mathrm{ph}}]\}^{1/2}}{\{a[1-g(\vartheta',\psi')]\}^{3/2}}\,, \tag{3.77}$$

where $\epsilon_{\mathrm{ph}}=\hbar qu$ is the energy of the phonon. This expression will be useful later on for the determination of the state $\mathbf{k}'$ after scattering.

In order to obtain the integrated scattering probabilities, we carry out the integration over the solid angle Ω' in the "nearly elastic approximation" (i.e., $(\epsilon\pm\epsilon_{\mathrm{ph}})^{1/2}\simeq\epsilon^{1/2}[1\pm\epsilon_{\mathrm{ph}}/(2\epsilon)]$) and in the "small warping approximation" (i.e., $a[1-g(\vartheta',\psi')]=\hbar^2/(2m_h)$) by taking $\mathbf{k}$ as polar axis for the angular integration (Reggiani *et al.*, 1977). The former approximation is sufficiently accurate down to temperatures of the order of 10 K; the latter approximation is quite reasonable, since it substitutes the density-of-states effective mass for a warping-dependent effective mass (Reggiani *et al.*, 1977).

By introducing for convenience the dimensionless variable $x=(2m_h^{1/2}u\epsilon^{1/2})/(K_BT_0)$, we obtain the integrated scattering probability per unit time for acoustic absorption and emission processes

$$P_{h,\mathrm{ac}}(\epsilon)=\frac{\mathscr{E}_1^{02}m_h^{1/2}(K_BT_0)^3}{2^{9/2}\pi\rho u^4\hbar^4}\times\epsilon^{-1/2}\begin{Bmatrix}F_3(x)+(K_BT_0/\epsilon)F_4(x)\\ G_3(x)-(K_BT_0/\epsilon)G_4(x)\end{Bmatrix} \tag{3.78}$$

with

$$F_3(x)=\int_0^{\sqrt{2}x}\frac{z^2[1+3(1-z^2/x^2)^2]}{\exp(z)-1}dz\ , \tag{3.79}$$

$$F_4(x)=\int_0^{\sqrt{2}x}\frac{z^3[1+3(1-z^2/x^2)^2]}{\exp(z)-1}dz\ , \tag{3.80}$$

$$G_3(x)=\int_0^{\sqrt{2}x}\frac{z^2[1+3(1-z^2/x^2)^2]}{1-\exp(-z)}dz\ , \tag{3.81}$$

$$G_4(x)=\int_0^{\sqrt{2}x}\frac{z^3[1+3(1-z^2/x^2)^2]}{1-\exp(-z)}dz\ . \tag{3.82}$$

The numerical evaluation of the functions $F_3(x)$, $F_4(x)$, $G_3(x)$, and $G_4(x)$ is reported in Appendix D.

The energy dependence of $P_{h,\mathrm{ac}}(\epsilon)$ is analogous to that of Eq. (3.59) for electrons reported in Fig. 15.

For determination of the final state after scattering, the following procedure can be used. First the values of the final angles ϑ' and ψ' are generated according to Eqs. (3.48) and (3.49) and the phonon wave vector q is taken as $2^{1/2}k(1-\cos\theta)^{1/2}$, k being the absolute value of the wave vector before scattering. Then the above final angles are accepted with the aid of the rejection technique (Appendix A Sec. 2.b) applied to the probability in Eq. (3.77) and so the absolute value of the wave vector k' after scattering is obtained by energy conservation.

e. Hole intraband scattering—optical phonons

Optical scattering for the case of holes is described in terms of one deformation-potential parameter and has been found to be isotropic even when the symmetry of the hole wave function is taken into account (Bir and Pikus, 1961; Lawaetz, 1967). In analogy with the preceding section, a single warped band like that described by Eqs. (3.3) and (3.4) will be considered.

The transition probability of Eq. (3.40) for the case of interest becomes

$$P(\mathbf{k},\mathbf{k}')=\frac{3\pi d_0^2}{2\rho V\omega_{\mathrm{op}}a_0^2}\begin{bmatrix}N_{\mathrm{op}}\\ N_{\mathrm{op}}+1\end{bmatrix}\times\delta[\epsilon(\mathbf{k}')-\epsilon(\mathbf{k})\mp\hbar\omega_{\mathrm{op}}]\ , \tag{3.83}$$

where d_0 is the optical deformation potential. Again the probability of emission is obviously zero when $\epsilon<\hbar\omega_{\mathrm{op}}$.

By integrating Eq. (3.83) over k' we find

$$P(\mathbf{k},\vartheta',\psi')=\frac{3d_0^2}{2^5\pi^2\rho\omega_0a_0^2}\begin{bmatrix}N_{\mathrm{op}}\\ N_{\mathrm{op}}+1\end{bmatrix}\times\frac{(\epsilon\pm\hbar\omega_{\mathrm{op}})^{1/2}}{\{a[1-g(\vartheta',\psi')]\}^{3/2}}\ . \tag{3.84}$$

This expression will be useful later on for determination of the state $\mathbf{k}'$ after scattering.

Integration of Eq. (3.84) over the solid angle Ω' yields the integration scattering probability per unit time

$$P_{h,\mathrm{op}}(\epsilon)=\frac{3d_0^2m_h^{3/2}}{2^{3/2}\pi\hbar^3\rho\omega_{\mathrm{op}}}\begin{bmatrix}N_{\mathrm{op}}\\ N_{\mathrm{op}}+1\end{bmatrix}(\epsilon\pm\hbar\omega_{\mathrm{op}})^{1/2}\ , \tag{3.85}$$

with

$$m_h^{3/2}=\frac{m_0^{3/2}}{4\pi|A|^{3/2}}\times\int_0^{2\pi}d\psi'\int_0^{\pi}\sin\vartheta'[1-g(\vartheta',\psi')]^{-3/2}d\vartheta'\ . \tag{3.86}$$

The angular integral in Eq. (3.86) can be performed numerically.

The energy dependence of $P_{h,\mathrm{op}}(\epsilon)$ is analogous to that of Eq. (3.72) reported in Fig. 18.

For the determination of the final state after scattering, final angles, generated according to Eqs. (3.48) and (3.49), are accepted with the aid of the rejection technique applied to the probability in Eq. (3.84).

f. Hole interband scattering

When a two-band model, with heavy and light holes, is considered, interband scattering should be accounted for. For the case of two spherical and parabolic bands, the scattering probabilities for different microscopic mechanisms have been calculated by Costato and Reggiani (1973). For the case of acoustic-phonon scattering, inclusion of energy dissipation and exact phonon population has been considered by Bosi *et al.* (1979). Owing to the complexity of the calculations involved and to their rather limited interest in practical cases, we shall not treat this subject further, but refer the reader to the appropriate literature.

g. Selection rules

Intravalley optical and intervalley phonons are subject to selection rules when initial and final $\mathbf{k}$ states are along high-symmetry directions (see, for example, the textbook of Bir and Pikus, 1974). In dealing with cubic semiconductors, intravalley optical-phonon interaction is forbidden to zero order in the phonon wave vector for electrons at the Γ point and along $\langle 100\rangle$ directions (e.g., in Si and

diamond), while it is allowed along ⟨111⟩ directions (e.g., in Ge) (Harrison, 1956; Paige, 1964). Similarly, zero-order transitions are allowed for the valence band at Γ (Harrison, 1956; Bir and Pikus, 1961).

Concerning intervalley scattering, group-theoretical analysis including time-reversal symmetry (Streitwolf, 1970; Lax and Birman, 1972) shows that, in the case of Si and diamond, processes are allowed to zero order with phonons whose wave functions transform according to the representation Δ_2 and S_1 (for a review, see Asche and Sarbei, 1981). Accordingly, longitudinal-optical modes assist g scattering (between parallel valleys) and longitudinal-acoustic as well as transverse-optical modes assist f scattering (between perpendicular valleys). In the case of Ge, analogous arguments show that only phonons of symmtery X_1 can contribute (Paige, 1964). Accordingly, longitudinal-acoustic and longitudinal-optical modes assist intervalley scattering.

It is worth noting that, in practice, initial and final states do not exactly coincide with high-symmetry points, and consequently the selection rules need not be strictly fulfilled, as is confirmed in magnetophonon experiments (Eaves *et al.*, 1975). However, from continuity, it is reasonable to expect that the forbidden transitions will remain weak when compared with allowed processes.

Ferry (1976) has calculated the matrix element for optical and/or intervalley scattering to first order in the phonon wave vector; this may become significant when the zero-order transition is forbidden by symmetry.

2. Ionized impurity scattering

This type of collision is elastic in nature and, therefore, it cannot alone control the transport process in the presence of an external field; it must be accompanied by some dissipative scattering mechanism if the proper energy distribution of electrons is to be derived from theory.

For an ionized impurity, the scattering source is simply a screened Coulomb potential. The problem has been initially treated with two different formulations: the Conwell and Weisskopf (1950) approach (CW), and the Brooks and Herring (1951) approach (BH). Since then several authors have presented refinements of the theory of ionized impuity scattering. A review paper has recently appeared in this journal (Chattopadhyay and Queisser, 1981), and the interested reader is referrred to that work for details.

The BH and CW approaches differ in the model used to screen the potential of the ion, and both of them use the Born approximation, consistent with the scattering theory outlined in Sec. III.C.2.*a*.

In the BM approach, a simple exponential screening factor is introduced, so that the potential scattering is given by

$$\mathcal{V}(\mathbf{r})=\frac{Ze^2}{\kappa r}\exp(-\beta_s r)\ , \tag{3.87}$$

where β_s^{-1} is the screening length, κ the dielectric constant of the material, and Z the number of charge units of the impurity. In the Debye formulation, for nondegenerate statistics,

$$\beta_s=\left[\frac{4\pi e^2 n_0}{\kappa K_B T_0}\right]^{1/2}\ , \tag{3.88}$$

where n_0 is the free-carrier density.

In the CW approach, a bare potential is assumed, cut off at the mean distance b between impurities:

$$b=\left[\frac{3}{4\pi n_I}\right]^{1/3}\ , \tag{3.89}$$

where n_I is the impurity concentration.

In this brief review we shall unify the calculations by using the potential given in Eq. (3.87) also for the CW approach, taking for this case $\beta_s=0$ and a maximum impact parameter b, or a minimum scattering angle θ_m.

When a high degree of compensation is present, very few free carriers are available to screen the ionized impurities, which, however, effectively screen each other, so that the CW approach seems to be more convenient for this condition. When, in the opposite case, each ionized impurity contributes one free carrier, n_I can be used instead of n in Eq. (3.88). Figure 20 shows, for this case, the space dependence of the scattering potential in the two approaches. We should also note that the screening length given in Eq. (3.88) is evaluated with the assumption that the electrons have equilibrium energy distribution. When at high fields the energy distribution deviates from equilibrium Eq. (3.88) fails, and the screened potential depends on the carrier distribution, so that the screening problem makes the transport equation nonlinear in the distribution function.

As a general trend, when the average electron energy increases, the screening effect decreases, as can be seen from Eq. (3.88) in an electron temperature approximation,

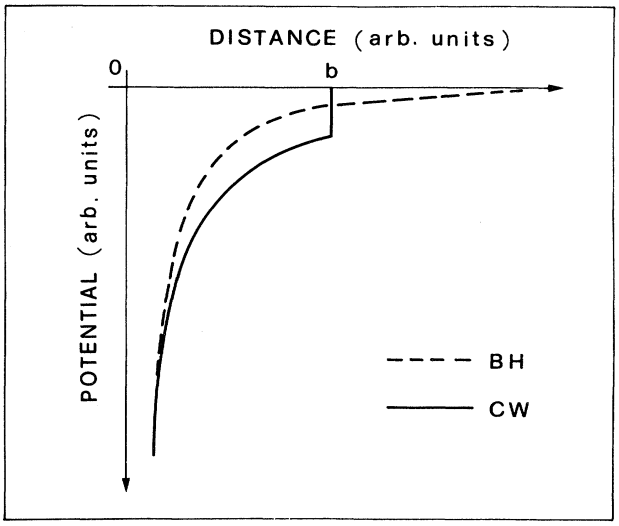

FIG. 20. Spatial dependence of the ionized impurity potential in the Brooks-Herring (BH) and Conwell-Weisskopf (CW) approaches.

or by simple physical considerations.

According to the general definition given by Eq. (3.22), the Fourier transform of a screened Coulomb potential is given by

$$\mathscr{H}'(q)=\frac{1}{(2\pi)^{3/2}}\int d\mathbf{r}\,\mathscr{V}(\mathbf{r})\exp(-i\mathbf{q}\cdot\mathbf{r}) =\frac{2^{1/2}Ze^2}{\pi^{1/2}\kappa}\frac{1}{\beta_s^2+q^2}\,. \tag{3.90}$$

This expression inserted in Eq. (3.28) and multiplied by the number of ionized impurities in the crystal yields the scattering probability per unit time:

$$P(\mathbf{k},\mathbf{k}')=\frac{2^5\pi^3Z^2n_Ie^4}{\hbar V\kappa^2}\mathscr{G}\frac{1}{(\beta_s^2+q^2)^2}\delta[\epsilon(\mathbf{k}')-\epsilon(\mathbf{k})]\,. \tag{3.91}$$

a. Electrons

(1) Spherical, parabolic bands. The integrated scattering probability is obtained from Eq. (3.91) by taking $\mathscr{G}=1$, multiplying by the density of states $V/(2\pi)^3$, and integrating over the possible states $\mathbf{k}'$. Polar coordinates are assumed with $\mathbf{k}$ as polar axis. In this simple band model we thus obtain

$$P(\mathbf{k})=\frac{2^3\pi Z^2n_Ie^4mk}{\hbar^3\kappa^2}\int_{-1}^{\cos\theta_m}\frac{d\xi}{[\beta_s^2+2k^2(1-\xi)]^2}\,. \tag{3.92}$$

Final integration over $\xi=\cos\theta$ gives the integrated scattering probability per unit time

$$P_{e,I}(\epsilon)=\frac{2^{3/2}\pi Z^2n_Ie^4m^{1/2}}{\hbar^2\kappa^2}\epsilon^{-1/2}\left[\frac{1}{\beta_s^2+\frac{4m\epsilon}{\hbar^2}(1-\cos\theta_m)}-\frac{1}{\beta_s^2+\frac{8m}{\hbar^2}\epsilon}\right]. \tag{3.93}$$

Expression (3.93) can be written in more physical terms by introducing the maximum impact parameter b and by using the following notation:

$$\epsilon_\beta=\frac{\hbar^2\beta_s^2}{2m}\,, \tag{3.94}$$

$$\epsilon_b=\frac{e^2}{2\kappa b}\,, \tag{3.95}$$

$$a_b=\frac{\epsilon_b^2}{\epsilon^2+\epsilon_b^2}\,. \tag{3.96}$$

Then if we remember the following classical relation between b and θ_m

$$\mathrm{tg}\left(\frac{\theta_m}{2}\right)=\frac{\epsilon_b}{\epsilon}\,, \tag{3.97}$$

Eq. (3.93) becomes

$$P_{e,I}(\epsilon)=n_I\sigma v\frac{Z^2}{\left(1+\frac{\epsilon\beta}{4\epsilon}\right)\left(1+\frac{\epsilon_\beta}{4a_b\epsilon}\right)} \tag{3.98}$$

where $\sigma=\pi b^2$ is the geometric cross section.

In the CW approach $\beta_s=0$, thus $\epsilon_\beta=0$, and Eq. (3.98) reduces to

$$P_{e,I}^{\mathrm{CW}}(\epsilon)=n_I\sigma vZ^2 =\pi n_IZ^2b^2(2/m)^{1/2}\epsilon^{1/2}\,. \tag{3.99}$$

In the BH approach $b^{-1}=0$, and we have, from Eq. (3.98),

$$P_{e,I}^{\mathrm{BH}}(\epsilon)=\frac{2^{5/2}\pi n_IZ^2e^4}{\kappa^2\epsilon_\beta^2m^{1/2}}\frac{\epsilon^{1/2}}{(1+4\epsilon/\epsilon_\beta)}\,. \tag{3.100}$$

Figure 21 shows the dependence upon energy of the integrated scattering probability per unit time for ionized impurities in the two different approaches.

For the determination of the state after scattering, the angle θ between $\mathbf{k}$ and $\mathbf{k}'$ can be determined by application of the direct technique (described in Appendix A) to the probability that the scattering angle is θ, which is the integrand in Eq. (3.92):

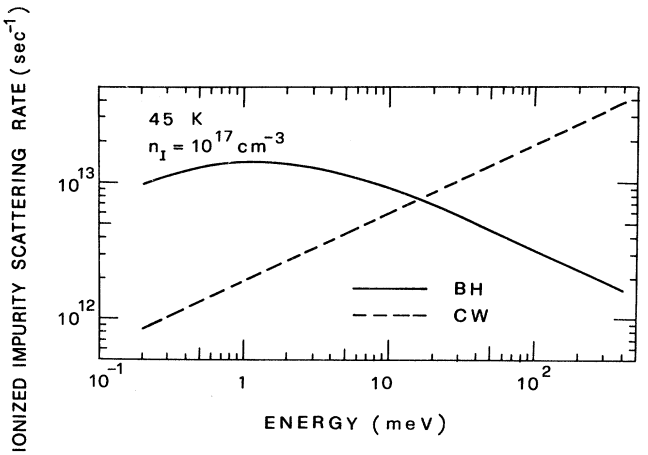

FIG. 21. Integrated scattering probability per unit time for ionized impurity scattering as a function of energy. The model used refers to electrons in Si with a parabolic band.

$$r=\frac{2^3\pi Z^2 n_I e^4 mk}{\hbar^3\kappa^2 P_{e,I}(\epsilon)}\int_{\cos\theta_r}^{\cos\theta_m} d\xi\frac{1}{[\beta_s^2+2k^2(1-\xi)]^2}\ . \tag{3.101}$$

Such an equation can be solved with straightforward calculations, and yields

$$\cos\theta_r=1-2\frac{(1+4\epsilon/\epsilon_\beta)\sin^2(\theta_m/2)+r\cos^2(\theta_m/2)}{1+4\frac{\epsilon}{\epsilon_\beta}[1-r\cos^2(\theta_m/2)]}\ . \tag{3.102}$$

Equation (3.102) in the CW approach becomes

$$\cos\theta_r^{\rm CW}=\frac{(\epsilon/\epsilon_b)^2 r-1}{(\epsilon/\epsilon_b)^2 r+1}\ , \tag{3.103}$$

and in the BH approach

$$\cos\theta_r^{\rm BH}=1-\frac{2(1-r)}{1+4\frac{\epsilon}{\epsilon_\beta}r}\ . \tag{3.104}$$

In both theories the azimuthal angle φ of $\mathbf{k}'$ around $\mathbf{k}$ is chosen at random. In evaluating the importance of impurity scattering, Eqs. (3.99) and (3.100) must be set against the fact that, at high energies, Coulomb scattering is strongly peaked along the forward direction, so that a large number of scattering events may result in a small effect on the electron path. In this respect the BH formula of Eq. (3.100) seems to be more appropriate, since the integrated scattering probability itself decreases at sufficiently high energies.

(2) Ellipsoidal, nonparabolic bands. As for the other scattering mechanisms, when ellipsoidal and/or nonparabolic valleys are taken into account, the Herring-Vogt transformation is applied, and nonparabolicity must be considered in the integration over the magnitude of $\mathbf{k}^{*'}$, which is performed by means of the δ function. The calculations are straightforward, and the results can be given in a form which shows the generalization of Eqs. (3.99), (3.100), (3.103), and (3.104):

$$P_{e,I}^{\rm CW}(\epsilon)=\pi n_I Z^2 b^2 (2/m_d)^{1/2}\frac{\epsilon^2(1+2\alpha\epsilon)}{\gamma^{3/2}(\epsilon)}\ , \tag{3.105}$$

$$P_{e,I}^{\rm BH}(\epsilon)=\frac{2^{5/2}\pi n_I Z^2 e^4}{\kappa^2\epsilon_\beta^{1/2}m_d^{1/2}}\gamma^{1/2}(\epsilon)\frac{1+2\alpha\epsilon}{1+4\frac{\gamma(\epsilon)}{\epsilon_\beta'}}\ , \tag{3.106}$$

for the CW and BH approaches, respectively, where

$$\epsilon_\beta'=\frac{\hbar^2\beta_s^2}{2md} \tag{3.107}$$

and

$$\cos\theta_r^{\rm CW}=\frac{\left[\frac{\gamma(\epsilon)}{\epsilon_b(1+2\alpha\epsilon)}\right]^2 r-1}{\left[\frac{\gamma(\epsilon)}{\epsilon_b(1+2\alpha\epsilon)}\right]^2 r+1}\ , \tag{3.108}$$

$$\cos\theta_r^{\rm BH}=1-\frac{2(1-r)}{1+4r\frac{\gamma(\epsilon)}{\epsilon_\beta'}}\ . \tag{3.109}$$

b. Holes

(1) Spherical, parabolic bands. The scattering probability given in Eq. (3.91) can be applied also to the case of holes for a single spherical and parabolic band by accounting for the overlap factor as given in Eq. (3.31) (Costato and Reggiani, 1973). By using the BH approach, we obtain the ionized-impurity-scattering probability per unit time for holes

$$P(\mathbf{k},\mathbf{k}')=\frac{2^5\pi^3 Z^2 n_I e^4}{\hbar V\kappa^2}\frac{\frac{1}{4}(1+3\cos^2\theta)}{(\beta_s^2+q^2)^2}\times\delta[\epsilon(\mathbf{k}')-\epsilon(\mathbf{k})]\ , \tag{3.110}$$

with $\epsilon(k)$ given by Eq. (3.1) and θ being the angle between $\mathbf{k}$ and $\mathbf{k}'$.

By assuming the $\mathbf{k}$ state before scattering to be the polar axis and integrating Eq. (3.110) over k', we find

$$P(\mathbf{k},\theta)=\frac{2^{1/2}Z^2 n_I e^4}{\kappa^2 m^{1/2}}\epsilon^{-3/2}\frac{1}{4}\frac{1+3\cos^2\theta}{[2(1-\cos\theta)+\epsilon_\beta/\epsilon]^2}\ . \tag{3.111}$$

Integration of Eq. (3.111) over the solid angle yields the integrated scattering probability per unit time

$$P_{h,I}^{\rm BH}(\epsilon)=\frac{2^{5/2}\pi Z^2 n_I e^4}{\kappa^2\epsilon_\beta^2 m^{1/2}}\frac{\epsilon^{1/2}}{(1+4\epsilon/\epsilon_\beta)}F_{\rm ov} \tag{3.112}$$

with

$$F_{\rm ov}=\frac{1}{4}\left[1+\frac{3(1+4\epsilon/\epsilon_\beta)(1+2\epsilon/\epsilon_\beta)^2}{4(\epsilon/\epsilon_\beta)^2}\left[\frac{1}{(1+4\epsilon/\epsilon_\beta)}+\frac{1}{(1+2\epsilon/\epsilon_\beta)^2}+\frac{\ln[1/(1+4\epsilon/\epsilon_\beta)]}{2(1+2\epsilon/\epsilon_\beta)\epsilon/\epsilon_\beta}\right]\right]\ . \tag{3.113}$$

For the determination of the final state after scattering, $\mathbf{k}'$, the following combined procedure is used (see Appendix A Sec. 2.c). The $\mathbf{k}$ state before scattering is assumed to be the polar axis, and the polar angle θ is generated according to Eq. (3.104). Then, this angle is accepted with the aid of the rejection technique applied to the overlap factor $\frac{1}{4}(1+3\cos^2\theta)$. The azimuthal angle φ is finally chosen at random.

Note that the inclusion of the overlap has the net effect of decreasing the efficiency of the impurity scattering mechanism.

(2) Warped band. Band warping can be included (Reggiani, 1978) by using in the Eq. (3.91) $\epsilon(\mathbf{k})$ as given by Eqs. (3.3) and (3.4). By integration over k' we obtain

$$P(\mathbf{k},\vartheta',\psi')=\frac{2Z^2 n_I e^4}{\hbar\kappa^2}[a(1-g)]^{1/2}\epsilon^{-3/2}\frac{\frac{1}{4}(1+3\cos^2\theta)(1-g)^{3/2}}{(1-g')^{3/2}\left[1+\frac{1-g}{1-g'}-2\frac{(1-g)^{1/2}}{(1-g')^{1/2}}\cos\theta+\beta_s^2 a(1-g)/\epsilon\right]^2}, \tag{3.114}$$

where g and g' refer to initial (ϑ,ψ) and final (ϑ',ψ') angles taken with respect to crystallographic axes. Integration of Eq. (3.114) over the solid angle Ω' yields the integrated scattering probability. As follows from Eq. (3.114), warping introduces a dependence of the integrated scattering probability on the initial orientation of $\mathbf{k}$. Provided the warping is not very pronounced, this effect can be neglected in Monte Carlo calculations when choosing the scattering mechanism, and Eq. (3.112) can still be used with an appropriate average value for the effective mass m_h [see Eq. (3.86)]; this is accomplished by setting $g=g'$ and $a(1-g)=\hbar^2/(2m_h)$ in Eq. (3.114). For the determination of the final state, warping can be easily accounted for by applying the combined technique (see Appendix A Sec. 2.c) to the angular probability given by Eq. (3.114), starting from a polar angle ϑ' generated according to Eq. (3.104), and taking the azimuthal angle ψ' at random with uniform probability.

3. Carrier-carrier interaction

We have seen in Sec. II.G.1 that several attempts have been made to include carrier-carrier interaction in Monte Carlo simulations, and that one approach consists of taking *e-e* collisions as one of the possible scattering mechanisms. In any case, the difficulty arises from the lack of knowledge of the distribution function $f(\mathbf{k})$ that enters into the formulation of the scattering itself.

When *e-e* interaction is taken as one of the scattering mechanisms, a knowledge of $f(\mathbf{k})$ is necessary in order to evaluate (i) the expression to be given to the screening factor of the interaction potential and (ii) the probability that the simulated electron collides with another electron of given wave vector $\mathbf{k}_1$.

If the screening factor is taken as equal to its equilibrium value and $\mathbf{k}_1$ is somehow known (cf. Sec. II.G.1), then the scattering problem between two identical charged particles can be solved in the center-of-mass frame of reference, in the same way as for the case of ionized impurities. The resulting total scattering probability per unit time is (Matulionis *et al.*, 1975)

$$P_{e\text{-}e}(\mathbf{k},\mathbf{k}_1)=\frac{2^{1/2}\pi n e^4}{\kappa^2\epsilon_\beta^2 m^{1/2}}\frac{\epsilon_r^{1/2}}{1+\epsilon_r/\epsilon}, \tag{3.115}$$

where

$$\epsilon_r=\frac{\hbar^2 k_r^2}{2m}, \tag{3.116}$$

$$\mathbf{k}_r=\mathbf{k}_1-\mathbf{k}. \tag{3.117}$$

The final state is determined in a way which is similar to that of the ionized impurity case. If $\mathbf{k}_r'=\mathbf{k}_1-\mathbf{k}'$, then the magnitude of $\mathbf{k}_r'$ is equal to that of $\mathbf{k}_r$; the angle χ between $\mathbf{k}_r$ and $\mathbf{k}_r'$ chosen by means of a random number r is such that

$$\cos\chi_r=1-\frac{2(1-r)}{1+r\epsilon_r/\epsilon_\beta}. \tag{3.118}$$

The azimuthal angle of $\mathbf{k}_r'$ in the plane normal to $\mathbf{k}_r$ is a random number between 0 and 2π. The final state of the simulated electron is then

$$\mathbf{k}'=\tfrac{1}{2}(\mathbf{k}+\mathbf{k}_1-\mathbf{k}_r'). \tag{3.119}$$

4. Relative importance of the different scattering mechanisms

In practical problems, it is often useful to have some *a priori* knowledge of the type of mechanisms which may be important in given conditions of temperature and field, in order to set up the correct simulation model for the special phenomenon under investigation. Without entering into details, a general picture can be obtained from the following considerations.

(i) Phonon scattering is more effective at higher temperatures and higher carrier energies; when the carrier energy is above its mean equilibrium value, emission prevails over absorption. While acoustic phonons can exchange arbitrary small quantities of energy, optical and intervalley phonons have a characteristic energy equivalent to a few hundred Kelvin.

(ii) Ionized impurity scattering becomes less effective as the carrier energy increases; it dissipates momentum but not energy.

(iii) Carrier-carrier scattering does not dissipate energy nor momentum, but it influences the shape of the distribution function, tending to make it Maxwellian.

Therefore, at low temperatures ($\lesssim$100 K) and low fields the following generalizations can be made. Impurities are most probably important, unless the material is particularly pure. Acoustic phonons are certainly important, and their energy dissipation must be accurately taken into account. Optical phonons are generally not essential. Intervalley phonons must be considered if repopulation problems are to be investigated. This last point may be rather critical since, due to the characteristic energy of the intervalley phonons, intervalley transitions may be very rare. They will depend strongly upon the tail of the energy distribution function of the carriers, so that

carrier-carrier interaction may also become relevant to anisotropy problems.

At low temperatures and high fields, due to the higher electron energies, all kinds of phonon spontaneous emission become predominant (zero-point limit, $N_q \ll 1$); acoustic scattering may to some extent be approximated by an elastic process, and the relative importance of impurities becomes negligible.

At high temperatures the situation is similar to that of low temperatures and high fields, except for the fact that phonon absorption and stimulated emission also play significant roles.

In a later section (Sec. IV.B.8) we shall see how it is possible to obtain from the Monte Carlo simulation information about the role of each scattering mechanism in dissipating the momentum and energy imparted to the carrier gas by the field under steady-state conditions.

IV. APPLICATIONS TO COVALENT SEMICONDUCTORS—RESULTS

Taking advantage of the fact that Monte Carlo simulation enables us to obtain an exact solution of the Boltzmann equation, we can investigate any microscopic model in full detail as regards the effect of the particular band structure and scattering mechanisms on transport properties. Accordingly, we shall devote the first part of this section to an analysis of the three main transport quantities, i.e., mean energy, drift velocity, and longitudinal diffusion coefficient, as a function of field strength, for a simple-model semiconductor. The aim of such a model is to provide general background knowledge from which the correlation between the simple model and macroscopic transport parameters can be clearly understood. In this way, we shall also see how the failure of a simple theory to interpret experiments can be overcome by appropriate modifications of the model.

A. The simple model

The simple covalent-semiconductor model consists of a single spherical and parabolic band with effective mass m, and accounts for acoustic and nonpolar optical scattering as described in the deformation-potential approach by single scattering coupling constants $\mathscr{E}_1^0$ and d_0, respectively. Values characteristic of heavy holes in Ge (see Table IV in Appendix C) are assumed. This choice is motivated by the fact that transport properties of this material have been investigated widely from an experimental point of view and, in first approach, the simple model used here is well suited to a realistic microscopic interpretation.

For the quantities of interest, the mean energy is calculated, using Eq. (2.14) of Sec. II.B.6.*b*,

$$\langle \epsilon \rangle = \frac{1}{N} \sum_i \epsilon_{bi} \ , \tag{4.1}$$

ϵ_{bi} being the carrier energy just before scattering and N the number of all free flights. By applying Eq. (2.10) of Sec. II.B.6.*a*, we obtain the drift velocity from

$$V_d = \frac{1}{eET} \sum (\epsilon_f - \epsilon_i) \ , \tag{4.2}$$

where the sum is evaluated over all carrier free flights [this estimator, owing to its simple form, independent of the special shape of the band and of the assumed form of self-scattering, may be preferred to that given in Eq. (2.14)].

The longitudinal diffusion coefficient is calculated from the second central moment [see Eq. (2.27)], as reported in Sec. II.D.1.

The results are reported as a function of field strength for the two temperatures of 8 and 300 K in Fig. 22. As

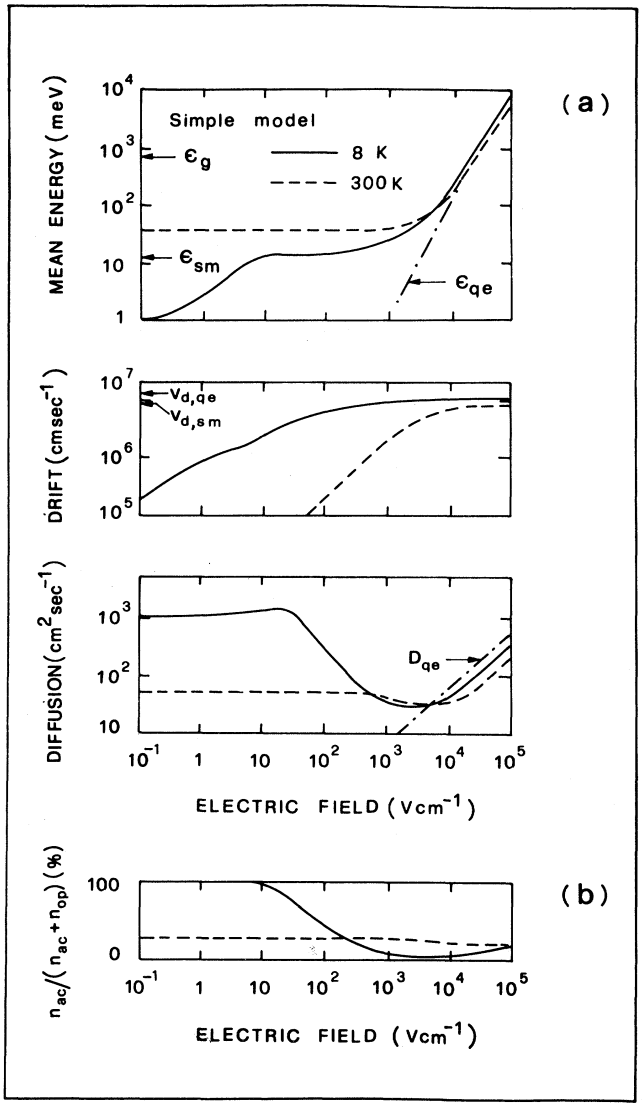

FIG. 22. (a) Mean energy, drift velocity, and longitudinal diffusion coefficient as functions of electric field strength for the simple-model semiconductor at the given temperatures. The values of different quantities under the streaming motion (sm) and the quasielastic approximations (qe) are indicated for the sake of comparison. ϵ_g is the value of the energy gap. (b) Ratio between acoustic-scattering events n_{ac} and total scattering events $(n_{ac}+n_{op})$ as a function of electric field strength for the simple-model semiconductor at the given temperatures.

usual, for discussion purposes the electric field range can be divided into three regions, namely, the linear-response region (i.e., $E \to 0$), an intermediate region where heating effects of carriers become evident, and the highest-field region (i.e., $E \to \infty$; the comparison between carrier mean energy and the value of the energy gap of the material sets a physically plausible upper limit on E). To better analyze the behavior of different quantities in terms of single microscopic processes, we shall first discuss the low-temperature (8-K) case.

In the linear-response region E (<0.2 V/cm in the figure) the following relations hold:

$$\langle \epsilon \rangle = \tfrac{3}{2} K_B t_0 \ , \tag{4.3}$$

$$v_d = \mu E \ , \tag{4.4}$$

$$D = \frac{\mu K_B T_0}{e} \ . \tag{4.5}$$

The above equations, which are usually referred to as equipartition of energy, Ohm's law, and the Einstein diffusion relation, respectively, are well reproduced by Monte Carlo results at the lowest field strengths [see Fig. 22(a)].

The intermediate region starts at about 1 V/cm, and up to about 10 V/cm the acoustic scattering mechanism is the only active one [see Fig. 22(b)]. Owing to the quasielastic nature of this mechansim the mean energy is found to increase and the diffusion coefficient to increase slightly above its thermal equilibrium value. Furthermore, since the scattering efficiency of acoustic modes increases with electron energy (see Sec. III.D.1.*d*), the drift velocity is found to behave in a sublinear way.

In the region of field strengths between 10 and 10^3 V/cm, the optical scattering mechanism builds up until it predominates over acoustic scattering [see Fig. 22(a)]. The strong optical emission process prevents further strong heating, so that the mean energy attains an approximately constant value, the drift velocity tends to saturate, and the diffusion coefficient decreases. These features follow what is predicted by the streaming motion approximation, which at this temperature well applies to the field range and for which simple theoretical considerations lead to the relations

$$\langle \epsilon \rangle = \tfrac{1}{3} K_B \theta_{\rm op} \ , \tag{4.6}$$

$$v_d = \left[\frac{K_B \theta_{\rm op}}{2m} \right]^{1/2} \ , \tag{4.7}$$

$$D_l = 0 \ . \tag{4.8}$$

The limiting values given by Eqs. (4.6) and (4.7) are reported with Monte Carlo results in Fig. 22(a) for the sake of comparison.

In the region of field strengths above 10^3 V/cm, the optical scattering mechanism keeps its predominant role, but is no longer able to fully dissipate the energy gained by the carriers from the field. As a consequence the carrier mean energy is found to increase more and more steeply with field toward a limiting quadratic dependence; furthermore, the drift velocity achieves a new saturation level higher than the previous one, and the diffusion coefficient increases again towards a limiting linear dependence. These features are predicted by an analytical solution of the Boltzmann equation with the small anisotropy and quasielastic approximations (Levinson, 1965; Price, 1970). This solution, which well applies to the highest-field region ($E \geq 10^4$ V/cm in the figure), considers only optical-phonon emission processes and leads to the following relations:

$$\langle \epsilon \rangle = \tfrac{3}{2} (K_B \theta_{\rm op}) \frac{E^2}{E_c^2} \ , \tag{4.9}$$

$$v_d = \left[\frac{2^3 K_B \theta_{\rm op}}{3\pi m} \right]^{1/2} \ , \tag{4.10}$$

$$D_l = v_d l_{\rm op} \frac{E}{E_c} \ . \tag{4.11}$$

Here E_c is a critical field given by

$$E_c = \frac{3^{3/2} m^2 d_0^2}{2^2 \pi e \hbar^2 a_0^2 \rho} \tag{4.12}$$

which, under $E/E_c > 1$, well justifies the above asymptotic solution; $l_{\rm op}$ is the mean free path due to optical-phonon scattering given by

$$l_{\rm op} = \frac{3^{1/2} K_B \theta_{\rm op}}{e E_c} \ . \tag{4.13}$$

The asymptotic prediction of Eqs. (4.9)–(4.11), which within statistical uncertainty are found to agree with Monte Carlo calculations, are reported in Fig. 22(a).

In the high-temperature case ($T_0 = 300$ K), owing to the increased efficiency of the scattering mechanisms in dissipating to the lattice the energy gained by the field, the region of field strengths for which the linear-response region holds is extended ($E < 10^3$ V/cm in the figure). Owing to the increased importance of acoustic-phonon scattering and the optical absorption process, the streaming-motion region disappears, and at the highest-field region ($E > 10^4$ V/cm) the results are no longer in close agreement with those of Eqs. (4.9)–(4.11).

B. Real-model applications

The simple model represents too crude a simplification to offer any deep microscopic physical insights or to permit a quantitative comparison between theory and experiments. Consequently, in the following we present a survey of the more significant results which, in our opinion, have been obtained for elemental semiconductors of group four when full details of the band structure and scattering mechanisms are taken into account.

1. Drift velocity

Methods for calculating the drift velocity have been reported in Sec. II.B.6. Usually this quantity is investigated for the material of interest at given temperatures as a

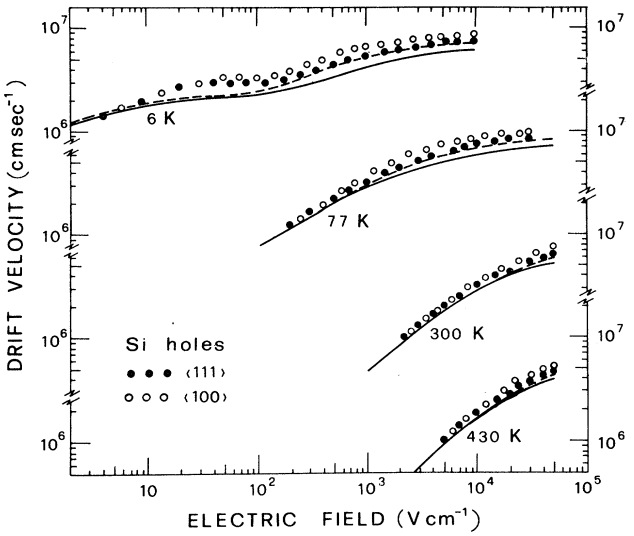

FIG. 23. Drift velocity as a function of electric field strength for holes in Si at the given temperatures. Points refer to experiments and curves to theoretical Monte Carlo calculations (Reggiani, 1980).

function of electric field strength applied along different crystallographic directions.

Figure 23 shows a set of results for the case of holes in Si (Ottaviani *et al.*, 1975; Reggiani, 1980). Here the anisotropy of the drift velocity with field orientation, which occurs at high field strength, reflects the warped shape of the equienergetic surfaces of heavy holes. Furthermore, at 6 K a peculiar effect of a near-saturation region at intermediate fields ($50 < E < 200$ V/cm) is interpreted as a nonparabolic effect of the band (Canali *et al.*, 1973).

Figure 24 shows a set of results for the case of electrons in Ge (Jacoboni *et al.*, 1981a). In this case the drift velocity exhibits anisotropic effects due to the many-valley structure of the conduction band. Furthermore, the presence of higher minima, lying a few hundred meV above the conduction-band minimum, makes possible scattering to higher minima. Thus, in order to be realistic, the microscopic model should include four equivalent absolute minima located at L points, one upper minimum located at the Γ point, and six further minima higher than the Γ one, located along Δ. The presence of these upper minima, together with nonparabolicity, is found to be the

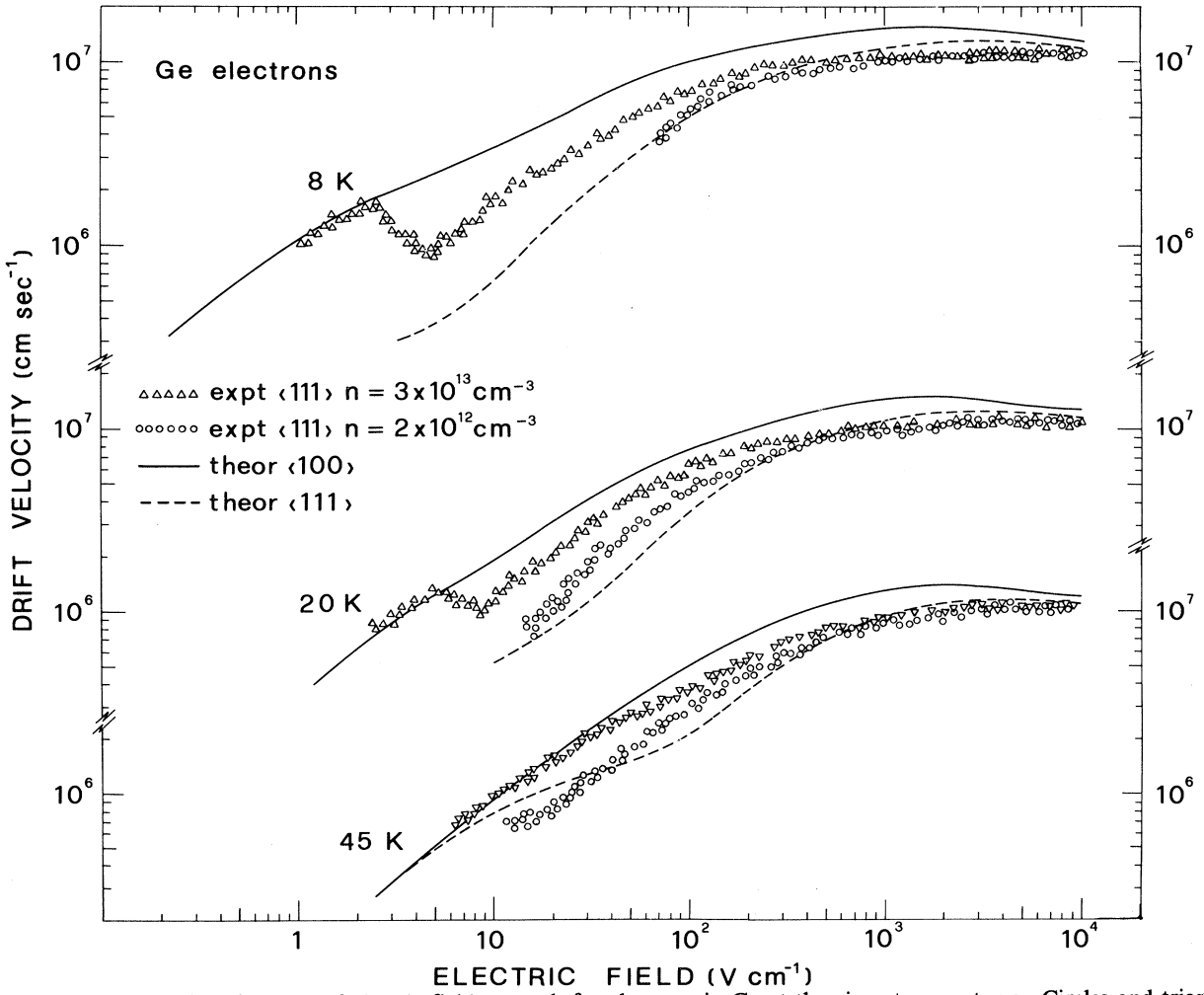

FIG. 24. Drift velocity as a function of electric field strength for electrons in Ge at the given temperatures. Circles and triangles refer to experiments performed at the two concentrations of electrons reported. Curves refer to theoretical Monte Carlo calculations (Jacoboni *et al.*, 1981a).

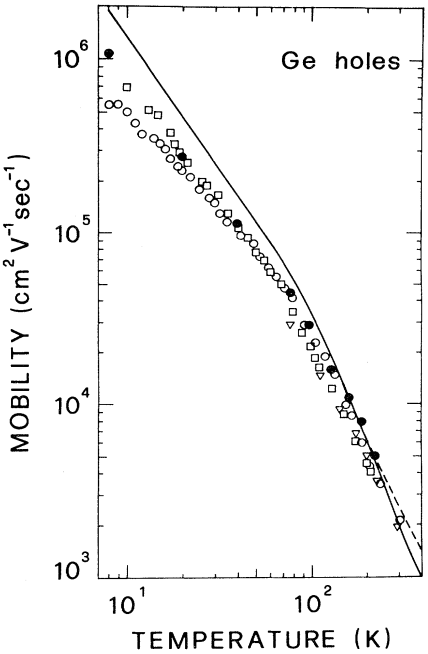

FIG. 25. Mobility of holes in Ge as a function of temperature. Different points refer to experiments: dashed curve, Monte Carlo theoretical results in the parabolic case; solid curve, Monte Carlo results when nonparabolic effects are taken into account (Reggiani *et al.*, 1977).

source of a negative differential mobility region which occurs at the highest field strengths for the case of low temperature ($T_0 < 77$ K). It is worth noting that experiments give evidence of a dependence of the drift velocity along the ⟨111⟩ direction upon electron concentration, that is, upon electron-electron scattering, which has not yet been fully interpreted (Jacoboni, 1976).

2. Ohmic mobility

In order to find the Ohmic mobility at a given temperature by Monte Carlo simulation, one can calculate the ratio v_d/E for a set of field values low enough to verify the independence of this ratio from field strength (the concomitant tendency to the equilibrium value of the mean energy provides a good check). Figure 25 shows the results of such a calculation for the case of holes in Ge (Reggiani *et al.*, 1977). It must be noted that inclusion of nonparabolicity effects in the theoretical model slightly lowers the mobility values at higher temperatures with respect to the parabolic case (dashed curve in Fig. 25).

However, as indicated in Sec. II.E, a more appropriate procedure consists of evaluating the diffusion coefficient at zero field; then the mobility is obtained from the Einstein relation [see Eq. (4.5)]. Figure 26 shows results obtained for the case of electrons in Si (Canali *et al.*, 1975). Here the dashed-dotted curve refers to the case for which impurity scattering with a concentration of 10^{13} cm^{-3} is included.

The diffusion coefficient method can be applied by means of a direct simulation of the integrated velocity autocorrelation function in the absence of a field (Gherardi *et al.*, 1975). This quantity is related to the electron mobility by

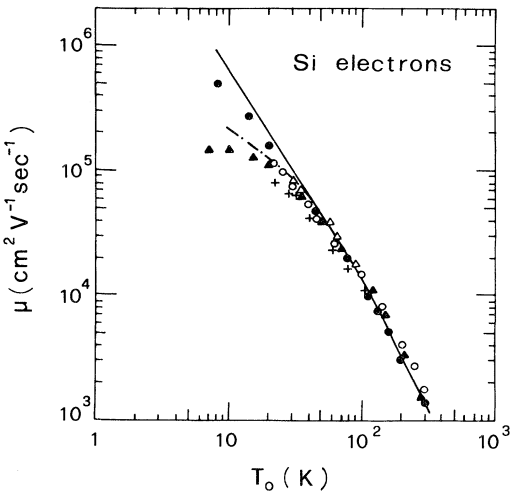

FIG. 26. Mobility of electrons in Si as a function of temperature. Different points refer to experiments: solid curve, theoretical results when lattice scattering only is considered; dot-dashed curve, theoretical results with lattice scattering plus ionized impurity scattering with $n_I = 10^{13}$ cm^{-3} (Canali *et al.*, 1975).

$$\mu = \frac{e}{K_B T_0} \int_0^\infty C(\tau) d\tau \ . \tag{4.14}$$

Figures 27 and 28 show the results of such a calculation for the case of electrons in Si when only acoustic scattering is carried out in an exact approach. Figure 27 shows the mobility obtained at different temperatures as a func-

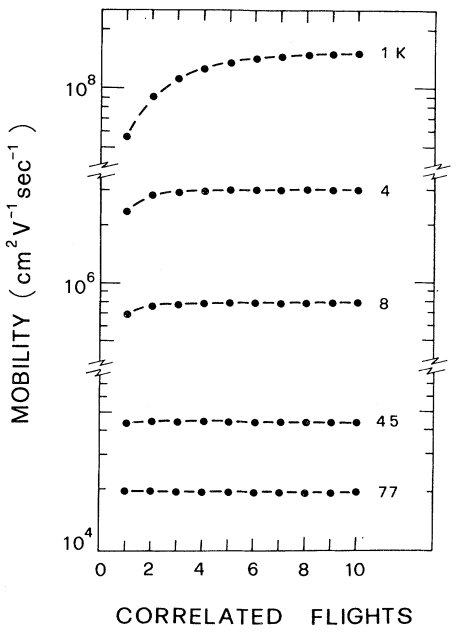

FIG. 27. Mobility of electrons in Si as a function of correlated flights at the indicated temperatures (Gherardi *et al.*, 1975).

tion of the number of correlated flights. It can be seen that the assumption of totally randomizing scattering, which corresponds to a flat curve in Fig. 27, is justified for temperatures around and above 45 K. Furthermore, as a result of avoiding the usual elastic and energy equipartition approximations, below about 45 K the mobility is found to increase more rapidly over the well-known result $\mu \propto T_0^{3/2}$ (see Fig. 28).

3. Diffusion

The method for calculating the diffusion coefficient has been discussed in Sec. II.D. It is worth noting that the Monte Carlo technique first provided an exact calculation of diffusion. As in the case of drift velocity, at given temperatures this quantity is investigated as a function of electric field strength for different crystallographic directions.

Figure 29 shows a set of results for the case of holes in Si (Navi *et al.*, 1979; Reggiani, 1980). Here the anisotropy of the longitudinal diffusion coefficient again reflects the warped shape of the equienergetic surfaces of heavy holes. Furthermore, the tendency to saturate at the highest field strengths is ascribed to nonparabolicity effects of the heavy-hole band.

Figure 30 shows a set of results for the case of electrons in Si (Brunetti *et al.*, 1981). Here the anisotropy of the longitudinal diffusion coefficient with respect to the orientation of the field in the crystal is related to an additional intervalley diffusion which arises owing to the fact that, when the field is oriented along a ⟨100⟩ direction, electrons exhibit different mean velocities in different valleys. In addition, the microscopic simulation enables us to compare the magnitudes of the transverse and longitudinal diffusion coefficients [$D_t/D_l \geq 1$ in this case, contrary to results obtained by analytical calculations (Persky and Bartelink, 1970), which is to be explained in terms of the energy dependence of the scattering probability]. In Fig. 31 the electron mean energy (continuous line) and the

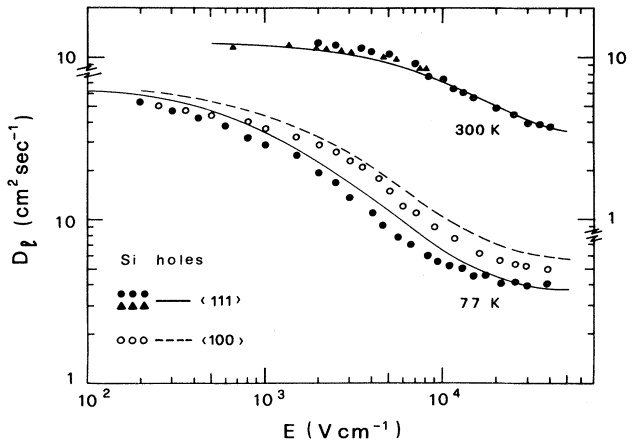

FIG. 29. Longitudinal diffusion coefficient of holes in Si as a function of electric field strength at the given temperatures. Points refer to experiments and curves to theoretical Monte Carlo calculations (Reggiani, 1980).

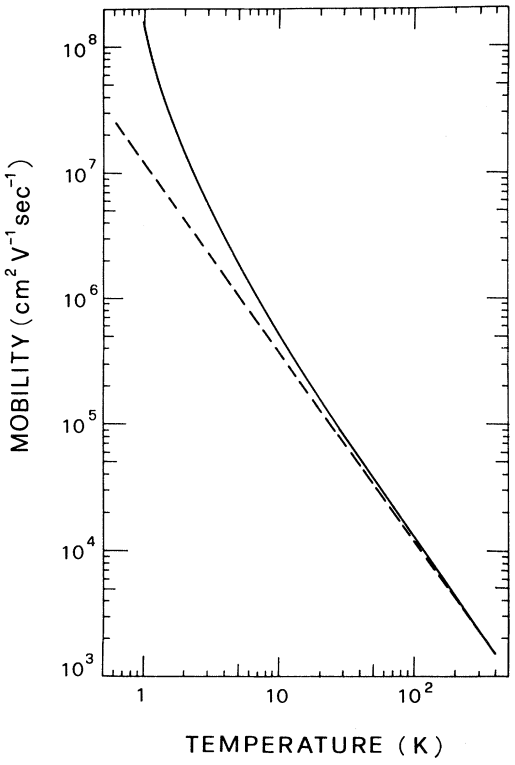

FIG. 28. Mobility of electrons in Si as a function of temperature, obtained with the simulated velocity autocorrelation function (solid curve), compared with the traditional result $\mu \propto T_0^{3/2}$ (dashed curve) (Gherardi *et al.*, 1975).

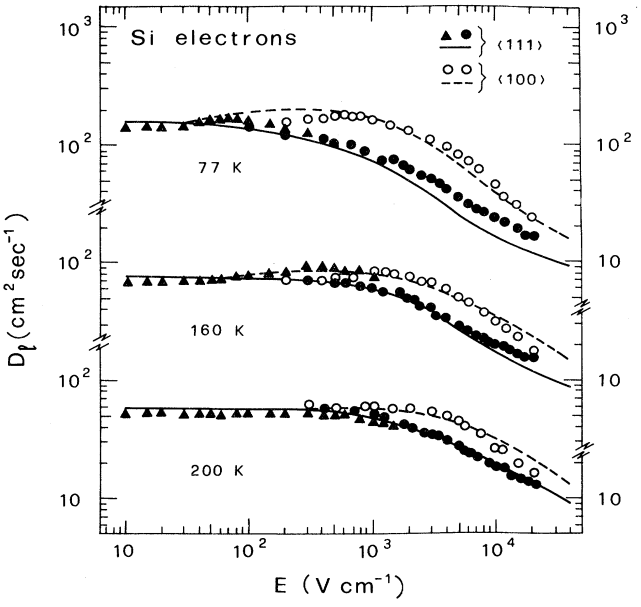

FIG. 30. Longitudinal diffusion coefficient of electrons in Si as a function of electric field strength at the given temperatures. Points refer to experiments and curves to theoretical Monte Carlo calculations (Brunetti *et al.*, 1981).

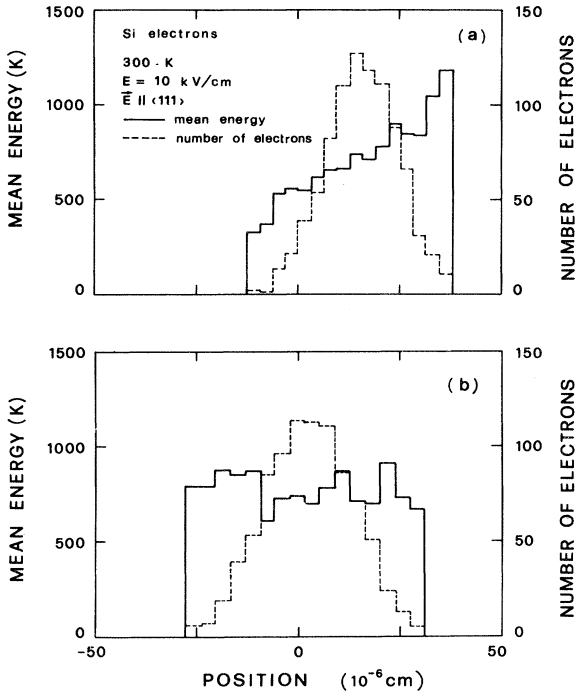

FIG. 31. Mean energy (solid curve and left scale) and number of electrons (dashed curve and right scale) as a function of position for the case of electrons in Si: (a) longitudinal direction; (b) transverse direction. The simulation time is 2.2×10^{-12} sec for an initial spatial distribution of the Dirac type (Brunetti *et al.*, 1981).

number of electrons (dashed line) are shown as a function of electron position in the cloud along [see Fig. 31(a)] and perpendicular to [see Fig. 31(b)] the field, oriented along a ⟨111⟩ direction. Along a direction orthogonal to the field the mean energy is, apart from random fluctuations, independent of position. In contrast, along the direction of the field, electrons in the front of the cloud have gained more energy from the field and thus have a mean energy higher than electrons in the rear. Since the scattering probability increases with energy, it will be higher for the front electrons (and the mobility lower) than for rear electrons, and consequently the cloud will expand less than in the homogeneous transverse case.

4. Mean energy

A method of calculating the mean energy is given by Eq. (4.1) or by the adaptation of Eq. (2.10) to the case of energy. Figure 32 shows the results for the case of electrons in Ge (Jacoboni *et al.*, 1981a). At 8 K the mean energy exhibits an initial rise due to the dominant contribution of the acoustic scattering mechanism, then a nearly constant region shows up at intermediate field strengths owing to the buildup of intervalley phonon emission, as expected from the simple model. At the highest field strengths the mean energy does not exhibit the E^2 asymptotic tendency, as found in the simple model, as an effect of nonparabolicity of the band and because the scattering to upper valleys gives rise to additional dissipation mechanisms which combine to moderate the heating of the electron gas (Fawcett and Paige, 1971). It is worth noting that at field strengths as high as 10^4 V/cm the mean energy keeps values lower than the energy gap (0.66 eV at 300 K).

From these curves, by analyzing the departure from thermal equilibrium, one can evaluate the region of field strengths at which hot-electron effects are expected to begin at a given temperature; as a general trend, it is found that this region starts at higher fields for higher temperatures. The knowledge of the mean energy as a function of field can be of special value when a rough estimate of breakdown fields of bulk devices is desired.

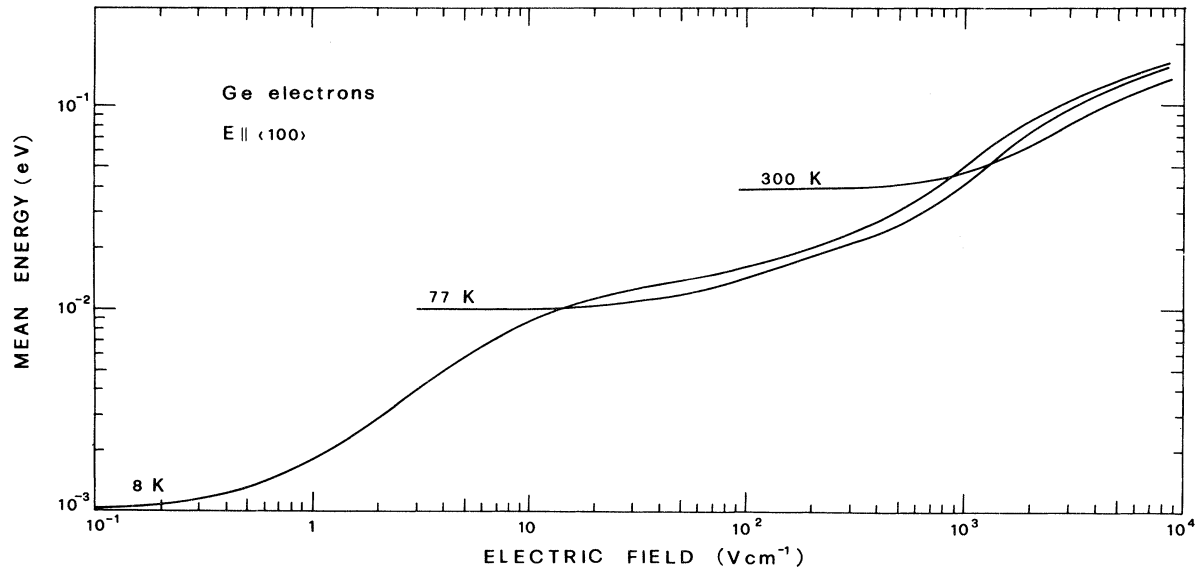

FIG. 32. Mean energy of electrons in the lower valleys of Ge as a function of electric field strength at the given temperatures.

5. Distribution function

The method for calculating the distribution function has been reported in Sec. II.B.6.*b*.

Figure 33 shows the results for the case of holes in Ge (Reggiani *et al.*, 1977). Here the anisotropy with field direction of the energy distribution function reflects the warped shape of the equienergetic surfaces of heavy holes. Furthermore, the strong optical-phonon emission gives rise to a depopulation of the high-energy region in favor of the low-energy region.

Figure 34 shows the distribution in the lower valleys (*L* minima) of electrons in Ge (Jacoboni *et al.*, 1981a). At intermediate fields the distribution exhibits kinks at the energy of intervalley and optical phonons and at the energy of the bottom of the upper valleys, while at the highest field strengths only the latter remains.

In compound semiconductors, owing to their characteristic band structures and scattering mechanisms, the energy distribution function was found to assume a peculiar form with strong inversion (Fawcett and Rees, 1969; Borsari and Jacoboni, 1972). The anisotropy of the distribution function in **k** space has also been studied in detail. In particular, a significant contribution of the third term was found in a spherical harmonic expansion of the distribution (Fawcett and Rees, 1967). These particular shapes of the distribution function showed, at the beginning of the Monte Carlo development, the usefulness of exact numerical techniques, since no analytical approximation had ever suggested such "irregular" distributions.

6. Repopulation

When the band model includes more bands and/or more minima, from the record of the time spent by the simulated carrier in each band and/or minimum, Monte Carlo calculations can deduce their populations.

Figure 35 shows the results for the field dependence of

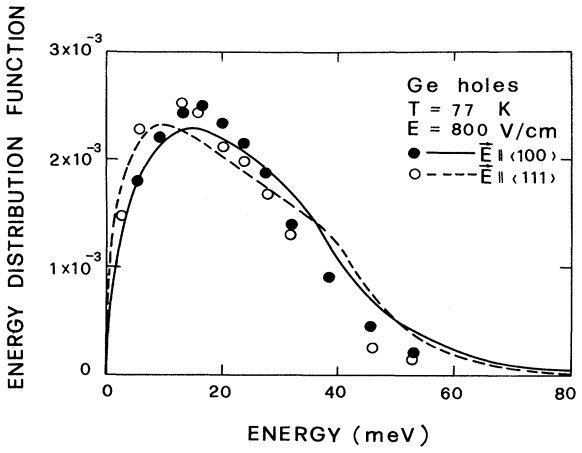

FIG. 33. Energy distribution function of holes in Ge. Points refer to experiment and curves to theoretical Monte Carlo calculations (Reggiani *et al.*, 1977).

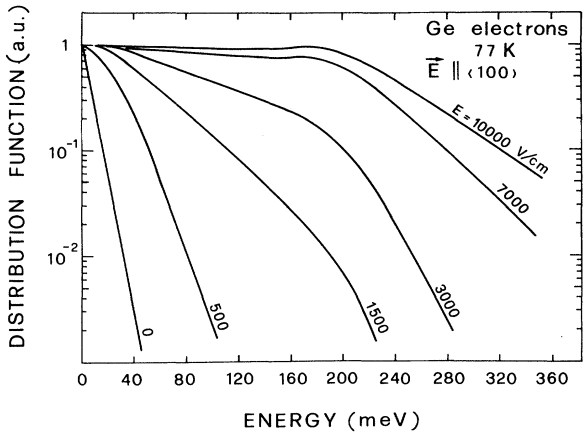

FIG. 34. Energy distribution function of electrons in the lower valleys of Ge for different values of the electric field strength (Jacoboni *et al.*, 1981a).

the ratio between light- and heavy-hole concentration normalized to its equilibrium value for the case of holes in diamond (Reggiani *et al.*, 1981b). The decrease from unity, at increasing field strengths (depopulation effect) is due to the fact that heating of light holes is more efficient than that of heavy holes. Thus scattering by optical-phonon emission from light to heavy bands becomes more active than the reverse process. At the highest fields, when the mean energy of both types of carriers is well above the optical-phonon energy, the increased efficiency of interband scattering tends to equalize the mean energies, so that the population depends only on the relative density of states as at equilibrium.

Figure 36 shows the fraction of electrons in the different valleys in Ge as a function of the electric field applied along a ⟨111⟩ direction at different temperatures (Jacoboni *et al.*, 1981a). It can be seen that the population of the hot valleys ⟨$\bar{1}$11⟩ exhibits a wavy behavior, with a first minimum (which is about zero at 8 K) followed by a maximum (which is about its equilibrium value 0.75) and then a final decreasing tendency related to upper-valley ⟨100⟩ populations. The opposite behavior is exhibited by the populations of cold valleys ⟨111⟩. This is another example of the fact that intervalley scattering is

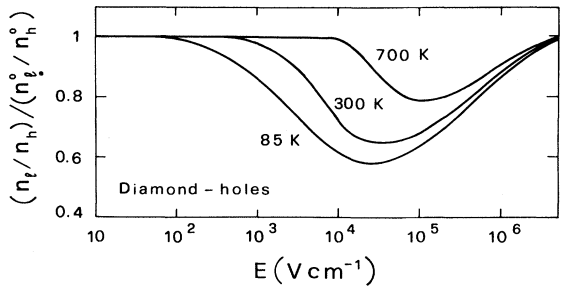

FIG. 35. Ratio of population between light and heavy bands normalized to its equilibrium value n_l^0/n_h^0 for the case of holes in diamond as a function of electric field strength (Reggiani *et al.*, 1981).

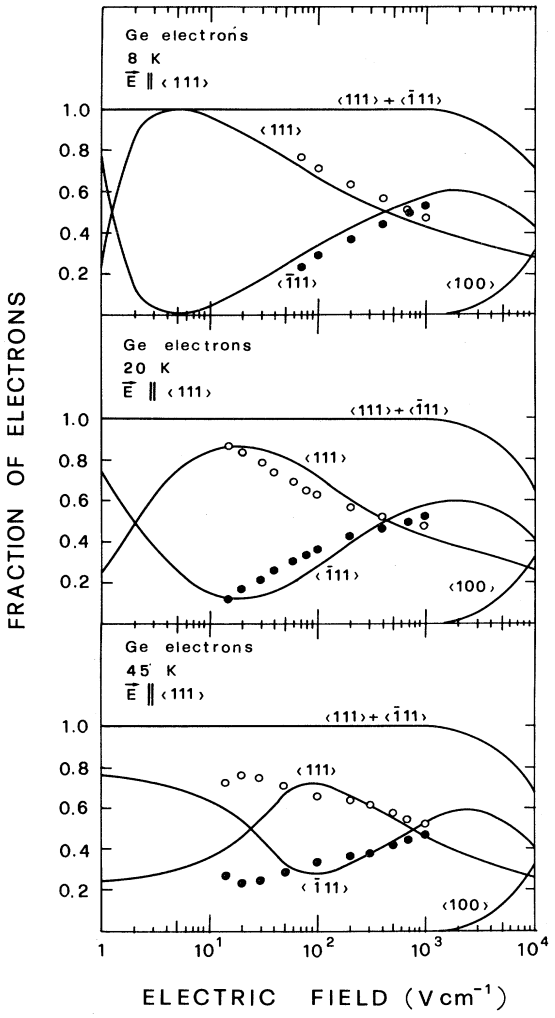

FIG. 36. Population of the different valleys as a function of electric field strength for the case of electrons in Ge at the given temperatures. Points indicate experimental results, curves theoretical Monte Carlo calculations (Jacoboni *et al.*, 1981a).

more probable for electrons in hot valleys, thus bringing about repopulation. The total effect is reduced as the temperature increases, since in this case the difference in energy between hot and cold valleys is reduced.

7. Energy relaxation time

The energy relaxation time, which should describe in a phenomenological way the tendency of the isotropic part of the distribution function to decay toward its equilibrium value, is defined by (see the textbook of Seeger, 1973)

$$\tau_\epsilon = \frac{\langle \epsilon \rangle - \langle \epsilon_0 \rangle}{v_d e E} , \tag{4.15}$$

where $\langle \epsilon_0 \rangle$ is the thermal-equilibrium mean energy of the carriers, and $\langle \epsilon \rangle$ is the mean energy in the presence of a field. By substituting for $\langle \epsilon \rangle$ and v_d the values obtained

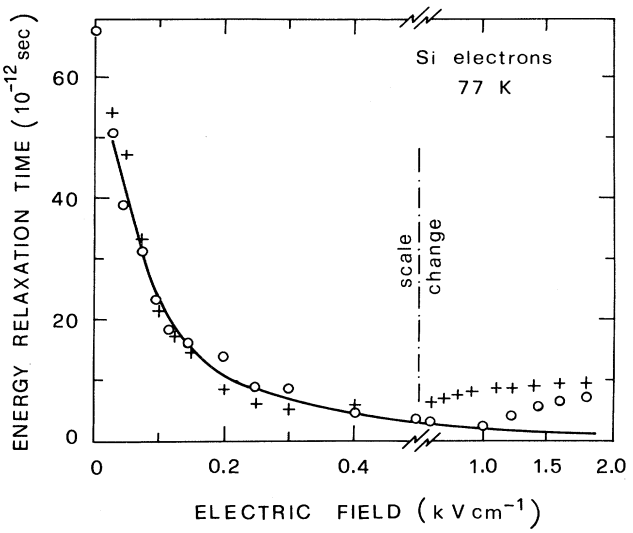

FIG. 37. Energy relaxation time of electrons in Si as a function of electric field strength. Points refer to experiments, curves to theoretical Monte Carlo calculations (Jacoboni, 1976).

from the Monte Carlo simulation, we obtain a theoretical evaluation of τ_ϵ.

Monte Carlo results for electrons in Si (Jacoboni, 1976) are shown in Fig. 37, which reports the results of τ_ϵ as a function of electric field strength, and in Fig. 38, which reports the results of τ_ϵ as a function of temperature. The decrease of τ_ϵ with an increase in either E or T_0 has the same physical origin: when electron energies are increased, intervalley phonons become more effective in dissipating energy.

8. Efficiency of scattering mechanisms

The efficiency of a scattering mechanism is measured by its energy and momentum dissipation rate. By collect-

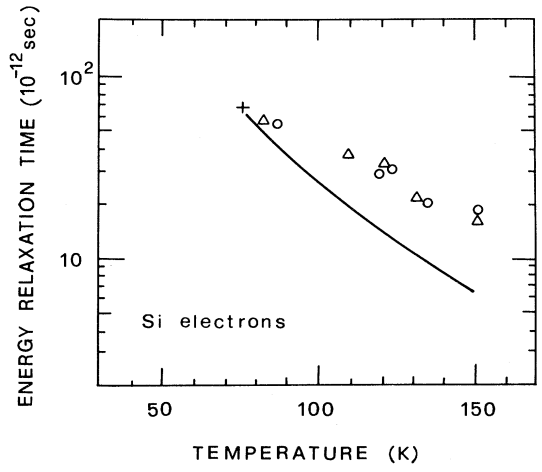

FIG. 38. Low-field energy relaxation time of electrons in Si as a function of temperature. Points refer to experiments, the curve to theoretical Monte Carlo calculations (Jacoboni, 1976).

ing for each type of scattering the amount of energy and momentum dissipated at the scattering events, one can evaluate these efficiencies in the Monte Carlo simulation.

Figure 39 shows the energy (a) and momentum (b) dissipation rates for all scattering mechanisms considered in the lower valleys for electrons in Ge (Jacoboni *et al.*, 1981a). At the temperature considered, acoustic scattering is dominant at low fields for momentum dissipation, but negligible for energy dissipation, which is ensured by optical and equivalent intervalley scattering. At the highest fields, nonequivalent intervalley scattering is the most important means for dissipating both energy and momentum. Let us note that the results reported here already include a reduction in efficiency due to valley depopulation at high fields, since the dissipation rates have been evaluated by dividing the dissipated quantity of interest by the total simulation time.

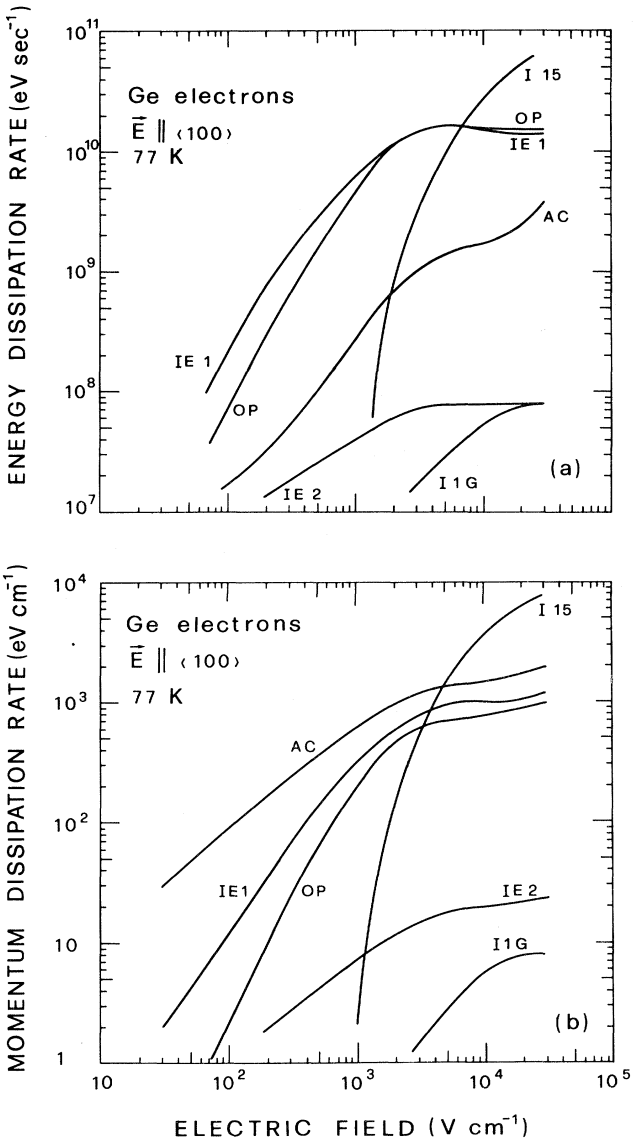

FIG. 39. Energy (a) and momentum (b) dissipation rates for the case of electrons in Ge due to the various scattering mechanisms in the lower valleys as functions of electric field strength: AC, acoustic; OP, optical; IE, intervalley between equivalent minima; *I*, intervalley between nonequivalent minima (Jacoboni *et al.*, 1981a).

9. White noise

Monte Carlo calculations of the noise spectrum of the velocity fluctuations S_v, as obtained by Fourier transforming the velocity autocorrelation function [see Eq. (2.41)], are shown in Fig. 40 for the case of electrons in Si (Brunetti, 1982). At low frequency the well-known white spectrum is exhibited; the transverse component is found to be larger than the longitudinal one, in accord with a $D_t > D_l$ [see Eq. (2.42)]. At the highest frequencies, structures appear in the longitudinal case which can be correlated with the characteristic intervalley scattering time, while the transverse case exhibits only simple Lorentzian decay.

An interesting comparison of Monte Carlo results with noise experiments can be carried out under the following conditions. When a two-terminal device exhibits a positive value of the real small-signal impedance Re($\mathscr{Z}$), and carrier-carrier scattering is neglected, the equivalent noise temperature associated with velocity fluctuations (white-noise temperature) T_n is given by (Shockley, 1966; Van Vliet *et al.*, 1975; Nougier *et al.*, 1981)

$$T_n(E)=\frac{e^2}{K_B \mathrm{Re}[\mathscr{Z}(E)]} \times \int_V n(\mathbf{r})\nabla_r \mathscr{Z}(\mathbf{r},E) D(E) \nabla_r \mathscr{Z}(\mathbf{r},E) d\mathbf{r} , \tag{4.16}$$

where $\nabla_r \mathscr{Z}(\mathbf{r},E)$ is the impedance field and the integration is performed over the volume of the device *V*.

Provided the geometry and doping of the device are

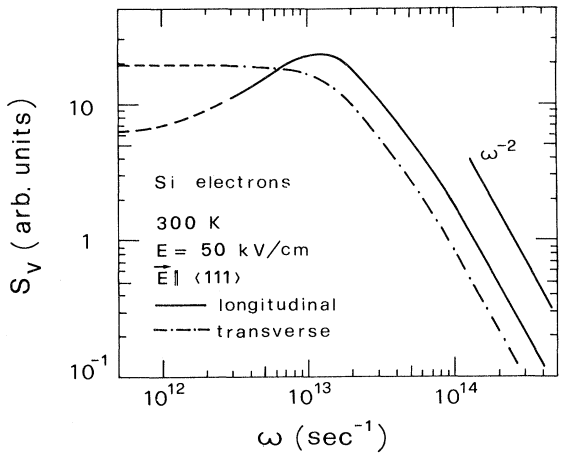

FIG. 40. Noise spectrum of the velocity fluctuations as a function of angular frequency for the case of electrons in Si: solid curve, longitudinal component; dot-dashed curve, transverse component; dashed curves at lowest frequencies are extrapolations to the zero-frequency values of S_v. The Lorentzian decay as ω^{-2} is shown for the sake of comparison.

known, the Monte Carlo calculation of $v_d(E)$ and $D(E)$, together with the use of the Poisson equation, makes possible a microscopic calculation of T_n (Zijlstra, 1978). It is worthwhile noting that under homogeneous field conditions Eq. (4.16) reduces to (Price, 1965)

$$T_n = \frac{eD}{K_B \mu'} , \tag{4.17}$$

where μ' is the differential mobility. Equation (4.17) can be interpreted as a generalized Einstein relation.

Figure 41 shows the comparison between theory and available experiments on the noise temperature of electrons in Si for homogeneous conditions (Reggiani *et al.*, 1981d). It is apparent that theory agrees better with experiments obtained at high frequency and with high-resistivity samples, thus providing useful information on the relative importance of other sources of noise, such as generation-recombination. Figure 42 shows the comparison between theory and experiment for the case of holes in Si for nonhomogeneous conditions (Reggiani, 1980).

As a common feature, these results show a monotonic increase above thermal-equilibrium values of the noise temperature, a fact that agrees with the so-called "noise temperature conjecture" (Schlup, 1976) stating that, in a nonequilibrium transport state of a semiconductor with a uniform electric field, the noise temperature is higher than its equilibrium value. Let us note that this monotonic increase can be qualitatively interpreted in terms of Eq. (4.17) as a dominant effect of impedance over diffusion in the behavior of the noise temperature versus field; in fact, on increasing field strengths, one finds that a possible decrease in diffusion proves to be more than compensated for by the increase in impedance.

10. Velocity autocorrelation function

One of the most recent and interesting achievements of the Monte Carlo method has been the calculation of the autocorrelation function of carrier velocity fluctuations $C(t)$, which is obtained as described in Sec. II.D.2. The

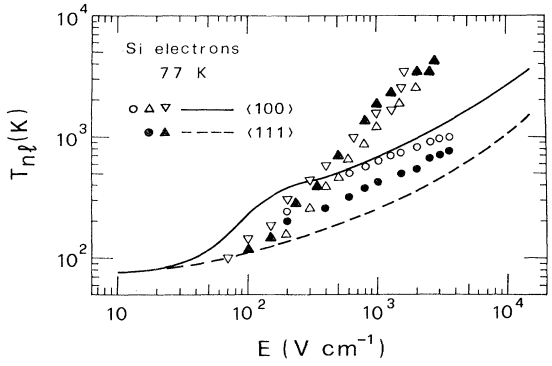

FIG. 41. Longitudinal noise temperature of electrons in Si: ● and ○, experiments performed at 10 GHz on 30 Ω cm samples; ▲, Δ, and ∇, experiments performed at 0.95 GHz on 15 Ω cm samples. Curves refer to Monte Carlo calculations (Reggiani *et al.*, 1981d).

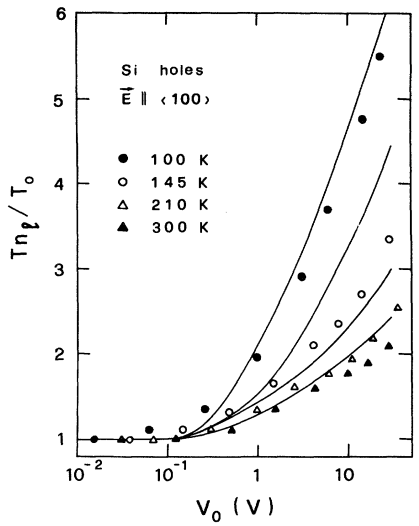

FIG. 42. Normalized longitudinal noise temperature of holes in Si as a function of applied voltage in devices under nonhomogeneous field conditions. Points refer to expeiments, curves report theoretical calculations (Reggiani, 1980).

study of this quantity for different electric field strengths and different directions makes possible a microscopic description of diffusion and white-noise quantities. Under linear-response conditions, in the relaxation-time approximation, $C(t)$ decreases to zero in an exponential way characterized by a constant decay time τ_C. However, when the nonlinear response condition is considered and the microscopic model becomes more complicated, this is, in general, no longer the case. Figure 43 shows the normalized autocorrelation function of velocity fluctuations $\Phi(t)$ for the case of electrons in Si (Brunetti, 1982). It is apparent that, because of the increased efficiency of

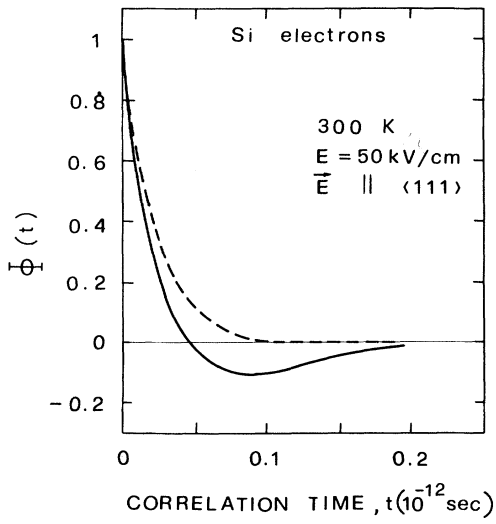

FIG. 43. Normalized autocorrelation function of velocity fluctuations as a function of time for the case of electrons in Si: solid curve, longitudinal component; dashed curve, transverse component.

scattering, for the high-field case $\Phi(t)$ decreases to zero faster, the transverse component being larger than the longitudinal one, in agreement with a $D_t > D_l$.

Figure 44 shows a set of curves for the longitudinal $\Phi(t)$ when the field is along the ⟨100⟩ and ⟨111⟩ directions. The peculiar negative behavior exhibited by $\Phi(t)$ in this figure is correlated with long flights in **k** space, characterized by initial negative velocity fluctuations which carriers can undergo after an intervalley scattering.

11. Alternating electric fields

The application of the Monte Carlo technique to the case of periodic fields has been reported in Sec. II.C.3.

Figure 45 shows the real and imaginary parts of the differential mobility as a function of frequency for the case of electrons in Si, when the static electric field is 10 and 50 kV/cm, respectively (Zimmermann *et al.*, 1978). The real part of the mobility at the lower frequency coincides with the differential mobility at the bias point; then, with increasing frequency, it peaks and finally tends to zero. This is a general feature of the frequency dependence of all transport phenomena when a strong scattering process with a threshold energy determines an oscillatory behavior of charge carriers. Recalling that the optical absorption coefficient of free charge carriers is proportional to the small signal conductivity, this peak represents a resonant absorption at the corresponding frequency. The imaginary part of the mobility, which is known to give the free-carrier contribution to the dielectric constant, has the frequency dependence predicted by Kramers-Kronig relations (Zimmermann *et al.*, 1978).

12. Magnetic fields

The method of introducing a magnetic field in Monte Carlo calculations has been reported in Sec. II.F. Quite

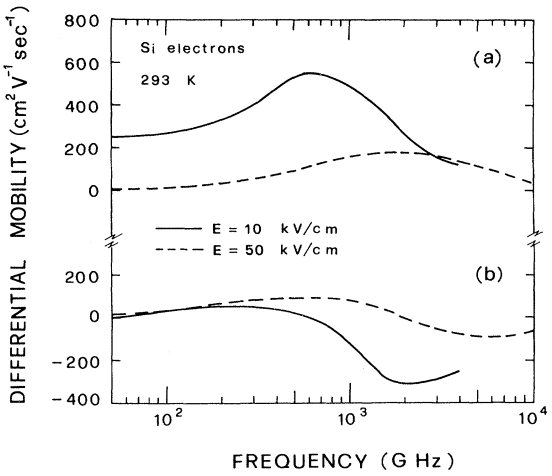

FIG. 45. Real (a) and imaginary (b) part of the differential mobility of electrons in Si as a function of frequency at the field strengths reported (Zimmermann, 1978).

interesting results have been obtained under streaming-motion conditions (Maeda and Kurosawa, 1972; Andronov *et al.*, 1980; Kurosawa, 1980). For a simple-model semiconductor, the simultaneous presence of a streaming motion and of a circular motion with a frequency $\omega_c = eB/(mc)$ gives rise to an accumulation region in **k** space, which assumes a spindle shape (see Fig. 46). This effect is easily understood by considering the different behavior of a carrier depending on its initial conditions of motion immediately after optical-phonon emission. If the carrier is outside the accumulation region, it is short lived, since it will be accelerated up to energies larger than $\hbar\omega_{op}$ within a short time (of the order of ω_c^{-1}). If the carrier is inside the accumulation region it is long lived, since the circular motion continues for a long time. As a consequence, the energy distribution function shows a population inversion reflecting the strong accumulation in

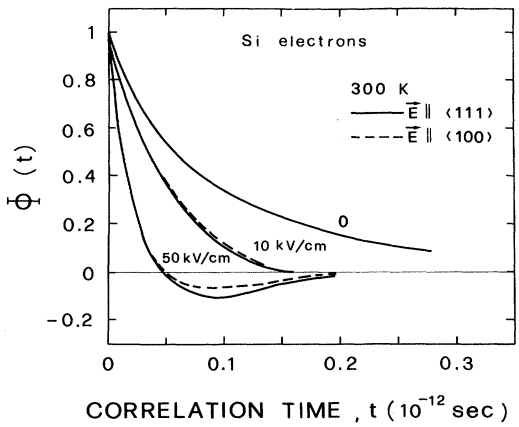

FIG. 44. Normalized autocorrelation function of longitudinal velocity fluctuations as a function of time for the case of electrons in Si: solid curves, electric field along the ⟨111⟩ axis; dashed curves, electric field along the ⟨100⟩ axis.

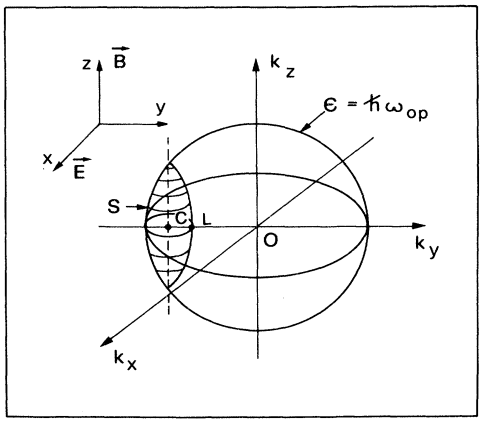

FIG. 46. Carrier motion in **k** space under an electric field **E** and a magnetic field **B** perpendicular to **E**. Spindle region is labeled *S*; the dashed line represents the axis of the spindle region and crosses the center point at $C\,[0, -mcE/(\hbar B), 0]$. $\hbar\omega_{op}$ is the energy of the optical phonon (Maeda and Kurosawa, 1972).

the spindle region (see Fig. 47). These predictions have been experimentally confirmed for the case of holes in Ge by Komiyama and Spies (1981).

13. Transients

The method of calculating time-dependent phenomena (under transient conditions) has been described in Sec. II.C.1. Figure 48 shows Monte Carlo calculations for the case of electrons in Si with given initial conditions of motion (Reggiani *et al.*, 1981a). The main features of the results are the tendency of the drift velocity and diffusivity to exceed their value at long times for a brief period of time (overshoot effects).

Figure 49 shows results for the case of holes in Si (Reggiani *et al.*, 1981b). Here the transient behavior of the drift velocity and mean energy is investigated at different initial energies. As can be seen in Fig. 49(a), the overshoot is maximum for the coldest initial distribution, while it disappears for the hottest case. This phenomenon reflects the energy dependence of the momentum relaxation time, as discussed in Sec. II.B.2 (see Fig. 2). In other words, when carriers start with a low energy, they begin to accelerate before dissipating energy, and, provided the field strength is high enough, they have the possibility on average of reaching velocity values higher than the stationary ones. If the carriers start with high energies, they simultaneously start accelerating and dissipating energy through phonon emission; this fact leads to a smooth increase with time of the drift velocity, so that overshoot effects are not present.

As regards the transient energy [see Fig. 49(b)] no overshoot is observed.

C. Devices

The Monte Carlo method is finding fruitful applications in the area of modeling real devices (see for example Constant and Boittiaux, 1981). As explained in the Introduction, this topic is not within the scope of this review;

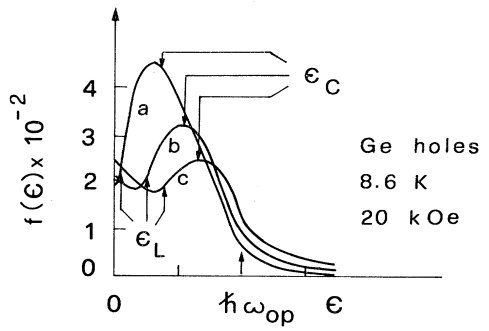

FIG. 47. Energy distribution function of holes in Ge for the geometry of fields in Fig. 46: (a) electric field strength of 2.5 kV/cm; (b) electric field strength of 3 kV/cm; (c) electric field strength of 3.25 kV/cm. Energies ϵ_L and ϵ_C correspond to points L and C in Fig. 46, and $\hbar\omega_{op}$ is the optical-phonon energy (Maeda and Kurosawa, 1972).

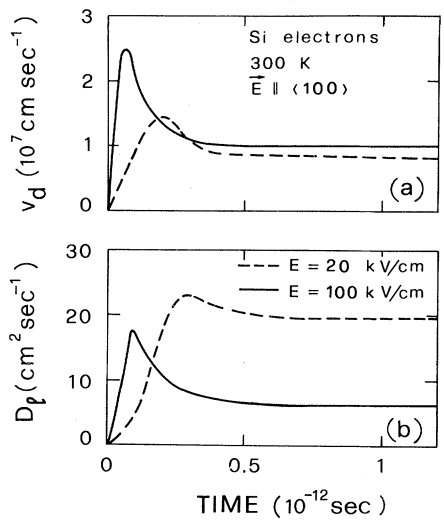

FIG. 48. Drift velocity (a) and longitudinal diffusion coefficient (b) as functions of time for the case of electrons in Si. The initial conditions of motion are taken with all carriers starting from the same point ($x=0$) at fixed energy equal to $(\frac{3}{2})K_BT_0$ with **k** orthogonal to **E**.

however, owing to its practical importance, in this section we shall briefly outline the main objectives of such a use and summarize some interesting applications that have appeared in the literature.

When the dimensions of devices become very small

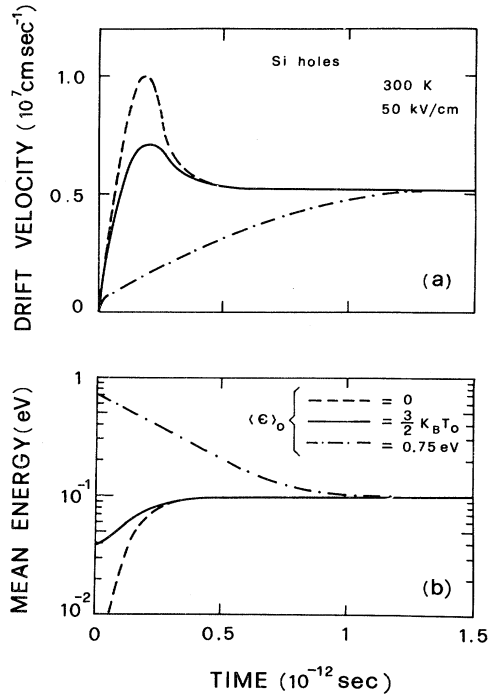

FIG. 49. Drift velocity (a) and mean energy (b) as functions of time for the case of holes in Si. Different curves refer to the reported different values of the initial mean energy with velocity randomly distributed (Reggiani *et al.*, 1981).

(submicron devices) and the frequencies of the applied fields very high (over 10 GHz), classical phenomenological transport equations are no longer adequate to describe charge current, and a direct solution of the kinetic equation has to be undertaken (Rees, 1973). Under the above conditions, the Monte Carlo method becomes a powerful tool for modeling devices. The major remaining problem is to describe in a self-consistent way the spatial dependence of the field inside the crystal.

Interesting applications of Monte Carlo to device modeling have already appeared in the literature. Domain formation in Gunn devices has been analyzed by Lebwohl and Price (1971b). The Gunn effect in ferromagnetic semiconductors has been studied by Aers *et al.* (1976). The transport of carriers across the base of a Si, narrow-base, bipolar transistor has been investigated by Baccarani *et al.* (1977). The high-field drift velocity of carriers in the *p*- and *n*-channel inversion layers of Si has been reported by Basu (1977) and Zimmermann *et al.* (1980). Unipolar components for both diffusion noise properties and static characteristics have been investigated by Zimmermann and Constant (1980). The simulation of real-space electron transfer in GaAs-AlGaAs heterostructures has been carried out by Glisson *et al.* (1980).

V. CONCLUSIONS

In the last decade Monte Carlo, by making possible the use of sophisticated microscopic models for both band structure and scattering mechanisms of any material, has proved to be an extremely powerful method for the study of transport phenomena in semiconductors.

In particular, this method has provided a detailed physical interpretation of the response of a semiconductor to arbitrary fields. Mobility and diffusivity have been the main objects of investigation, but many other particular features of the transport process have been elucidated in Monte Carlo simulations, such as, for example, space, velocity, and energy distributions, valley repopulations, efficiencies of scattering mechanisms, fluctuations, and so on. In this respect the method has become a sort of simulated experimental technique with very strong insight potentiality, through which experimentalists belonging to different areas have found a unifying theoretical method for understanding the physics that underlies their results. Some features of the Monte Carlo technique have been taken to a high level of refinement, such as, for example, the use of the entire conduction band instead of the effective-mass approximation (Shichijo and Hess, 1981). On the other hand, one problem that still requires a definitive clarification is the best way for the generalization of the model to include electron-electron interaction.

The feasibility of the Monte Carlo method is such that almost all the areas where it could be applied have been investigated in a relatively short time, so that it is now reasonable to think of its extension to new areas which are becoming ripe for deeper investigation. The transport properties of new physical systems—for example, quasi-one-dimensional structures, intercalation compounds, and amorphous materials—will be profitably studied by means of the Monte Carlo technique as soon as their basic physical properties are well enough understood for the construction of realistic and reliable models to be used in the simulation. A similar consideration holds for device design where, however, a further difficulty arises from the need to know the field distribution inside the device itself. In this case a self-consistent calculation must be performed. When submicron structures are involved, direct simulation seems to be the only feasible approach to device analysis.

A major field that, presumably, will benefit significantly by application of the Monte Carlo technique is quantum transport (Barker and Ferry, 1979). It is not yet clear how close we are to proceeding to this important step; it is, however, exciting to consider the possibility that numerical simulation of the quantum transport equation may reveal further hidden analogies between quantum and classical transport which may justify the success of the Boltzmann equation in such wide areas of application, even when rigorous calculations seem to call for a more correct quantum approach.

To conclude, we should like to suggest that the great popularity and wide use of Monte Carlo simulation for the solution of transport problems in semiconductors indicates that the time has come for the construction of some sort of official library of programs or, at least, for the definition of standards on its features.

ACKNOWLEDGMENTS

The authors would like to express their gratitude to Dr. Rossella Brunetti for her essential contribution in the accomplishment of this work. The Centro di Calcolo Elettronico of the Modena University is also thanked for computational support.

APPENDIX A: GENERATION OF RANDOM NUMBERS

All simulative techniques for stochastic processes make use of random numbers in order to simulate events which occur with given probability distributions. Here we shall describe how random numbers are generated in general. We shall see that random numbers with any probability distribution can be obtained starting from a sequence of random numbers evenly distributed between 0 and 1. These numbers are designated in the present paper by the letter r.

1. Generation of evenly distributed random numbers

The history of the methods devised by Monte Carlo workers to generate sequences of random numbers r may be of interest in itself. However, for reasons of space, we refer the interested reader to the specific literature (Hammersley and Handscomb, 1964; Buslenko *et al.*, 1966).

Here we only mention that library functions which generate appropriate sequences of numbers r are available today in large electronic computers. The method of generation most commonly used is the multiplicative congruential method: the ith element r_i of the sequence is given by the previous element r_{i-1} by a relation such as

$$r_i = pr_{i-1} (\mathrm{mod} q) \tag{A1}$$

where p and q are appropriate constants. The first element of the sequence (seed) must be given by the user. The numbers r_i of the sequence in Eq. (A1) are obtained with a precise mathematical algorithm, and therefore they are not at all random; in fact, given the seed of the sequence, all its numbers are perfectly predictable. However, for "good" choices of the constants p and q, the sequences of r_i behave as random in the sense that they passed a large number of statistical tests of randomness. Numbers r of such a type are called pseudorandom numbers. They have the advantage over truly random numbers of being generated in a fast way without having to resort to special physical devices and of being reproducible, when desired, especially for program debugging.

2. Generation of random numbers with given distributions

Random numbers x with given probability distribution $f(x)$ in an interval (a,b) can be obtained starting from numbers r evenly distributed in the interval (0,1) with different techniques (Hammersley and Handscomb, 1964; Buslenko *et al.*, 1966). We shall describe here the three simplest techniques, which are usually used in Monte Carlo transport calculations.

a. Direct technique

If the function $f(x)$ is normalized to one in the interval of definition (a,b), let us call $F(x)$ the integral function of f. Then, given a number r, we correspondingly choose x_r such that

$$r = F(x_r) = \int_a^{x_r} f(x)dx \ . \tag{A2}$$

The probability $P(x)dx$ that x_r obtained in this way lies within an interval dx around x is equal to the corresponding dF, since r has a flat distribution. Thus (see Fig. 50)

$$P(x)dx = dF = f(x)dx \ , \tag{A3}$$

as desired. If $f(x)$ is not normalized, then Eq. (A2) must be replaced by

$$r = \int_a^{x_r} f(x)dx \Big/ \int_a^b f(x)dx \tag{A4}$$

with a constant $f(x)$, this technique provides the obvious formula for the generation of a random number evenly distributed between a and b:

$$x_r = a + (b-a)r \ . \tag{A5}$$

Often, in real cases, the above simple direct technique cannot be used because it is not possible either to evaluate analytically the integral in Eq. (A2) or to solve with respect to x_r the equation which results from Eq. (A2). In these cases one of the following techniques can be used.

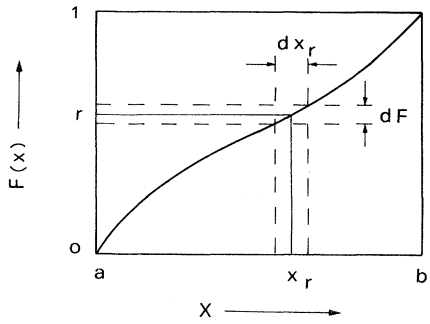

FIG. 50. Geometrical representation of the generation of a stochastic variable x with given probability function $f(x)=dF(x)/dx$ by means of random numbers r between 0 and 1.

b. Rejection technique

Let C be a positive number such that

$$C \geq f(x) \tag{A6}$$

in the whole interval (a,b), and let r_1 and r_1' be two random numbers obtained with a flat distribution in (0,1). Then

$$x_1 = a + (b-a)r_1 \quad \text{and} \quad f_1 = r_1' C \tag{A7}$$

are two random numbers obtained with flat distributions in (a,b) and $(0,C)$, respectively. If

$$f_1 \leq f(x_1) \tag{A8}$$

then x_1 is retained as choice of x, otherwise x_1 is rejected, and a new pair r_2, r_2' is generated; the process is repeated until Eq. (A8) is satisfied. Since for each pair r_i, r_i' a point with coordinates (x_i, f_i) is obtained from the uniform distribution in the rectangle $abCC$ of Fig. 51, the probability that x_i within an interval dx around x will be

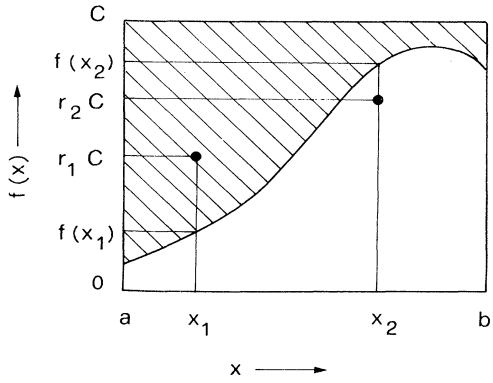

FIG. 51. Geometrical representation of the rejection technique (see text). The comparison between the area under $f(x)$ and the shaded region gives evidence of the efficiency of the technique.

accepted is proportional to the probability that x_i lies within this interval, proportional to dx, times the probability of accepting x_i, proportional to $f(x_i)$, as desired.

The above technique is always applicable, with any bounded $f(x)$ in a finite interval (a,b). However, when $f(x)$ is strongly peaked, many pairs of numbers might be generated before a successful trial, with a resulting large expense for computer time. The technique described below may overcome this difficulty by combining the two previous techniques.

c. Combined technique

Let x_1 be a random number generated with the direct technique according to a distribution $g(x)$. If, furthermore, K is a constant such that

$$Kg(x) \geq f(x) \tag{A9}$$

in the whole range (a,b) of interest, a new random number r_1 is generated in (0,1), and x_1 is accepted as the value of the random variable x if

$$r_1 Kg(x_1) < f(x_1) . \tag{A10}$$

In fact, in this way the probability of having an accepted x_1 within an interval dx around x is proportional to the probability that x_1 lies within this interval, proportional to $g(x)dx$, times the probability of accepting x_1, proportional to the ratio $f(x)/Kg(x)$. The final probability is therefore proportional to $f(x)dx$, as desired. A geometrical interpretation of the combined technique is shown in Fig. 52: the selection of x_1 is equivalent to the generation of a point with flat distribution below the curve $Kg(x)$, while the condition of acceptance requires that the point lie in the area below the curve $f(x)$. If the curve $Kg(x)$ is not too far from $f(x)$, few attempts will be necessary per successful trial.

The rejection technique described in the previous section is a particular case of the combined technique, for $g=$const. The combined technique, however, can also be applied to unbounded functions or to functions defined in unbounded intervals.

As we said above, other techniques can be used for special cases. As an example we may mention the use of the sum of a certain number of random numbers r to generate x according to a normal distribution (Eadie *et al.*, 1971). For such a distribution the combined technique can also be used (Price, 1979).

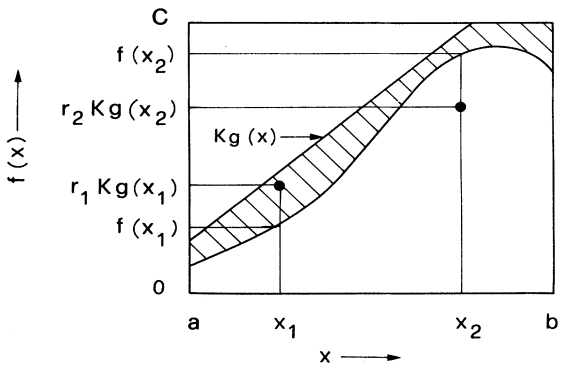

FIG. 52. Geometrical representation of the combined technique (see text). The comparison between the area under $f(x)$ and the shaded region gives evidence of the efficiency of the technique.

d. Discrete case

When an event must be chosen from among a given number of different possibilities or, in other words, when the variable x must be chosen from a discrete set, the direct technique can be used with $f(x)$ given by the sum of δ functions. Figure 53 illustrates this case: if P_i is the probability of occurrence of the ith event x_i, then a random number

$$y = rP , \tag{A11}$$

where

$$P = \sum P_i \tag{A12}$$

is generated and compared successively with

$$P_1 ,$$
$$P_1 + P_2 ,$$
$$P_1 + P_2 + P_3 ,$$
$$\cdots .$$

The jth event is chosen if j is such that the first of the above partial sums which is larger than y is $P_1 + P_2 + \cdots + P_j$. Figure 53 shows immediately that the probability of choosing the jth event is proportional to P_j, as desired.

APPENDIX B: NONPARABOLICITY PARAMETER FOR SI-LIKE CONDUCTION BAND

Following Hensel and Hasegawa (1964), we can write the energy-wave-vector relationship for the Si conduction

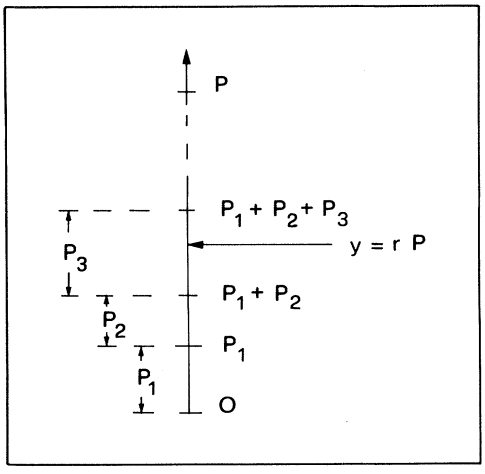

FIG. 53. Stochastic determination of an event in the discrete case. P_i with $i=1,2,3,\ldots$ gives the probability of occurrence of the ith event (see text).

TABLE IV. Bulk constants.

	Diamond[a]	Silicon	Germanium	Units
a_0	3.57	5.43[c]	5.66[c]	Å
ρ	3.51	2.33[b]	5.32[b]	g/cm^3
u_l	18.21×10^5	9.0×10^5 [b]	5.4×10^5 [b]	cm/sec
u_t	12.30×10^5	5.3×10^5 [b]	3.2×10^5 [b]	cm/sec
χ	5.7	11.7[b]	16[b]	
θ_{op}	1938	735[b]	430[b]	K
$\epsilon_g(T=300$ K)	5.49	1.107[c]	0.67[c]	eV

[a]Reggiani *et al.*, 1981c.
[b]Jacoboni and Reggiani, 1979.
[c]Agrain and Balkanski, 1961.

band near $\mathbf{k}=(k_0,0,0)$ k_0 being measured from the X_1 band-edge point, in terms of a longitudinal and a transverse component, as

$$\epsilon_l=\frac{\hbar^2}{2m_l}k_l^2\,, \tag{B1}$$

$$\epsilon_t=\frac{\hbar^2}{2m_t}k_t^2-\frac{N^2k_y^2k_z^2}{\Delta\epsilon_0}\,, \tag{B2}$$

with $k_t^2=k_y^2+k_z^2$,

$$N=\frac{\hbar^2}{m_0}\left[\frac{m_0}{m_t}-1\right] \tag{B3}$$

and

$$\Delta\epsilon\simeq\frac{2\hbar^2k_0^2}{m_l}=(\epsilon_{\Delta'_{2c}}-\epsilon_{\Delta_{1c}})\,. \tag{B4}$$

The quartic term in Eq. (B2) becomes negligible at the minimum of the conduction band, where a parabolic energy-wave-vector relationship is recovered, but introduces significant nonparabolic effects in the transverse direction as the electron wave vector moves from the minimum. In the following we shall present a simple calculation which enables us to estimate the nonparabolic parameter from the above relations.

By averaging ϵ_t of Eq. (B2) over the plane $k_l=0$ we obtain

$$\bar{\epsilon}_t=\frac{\hbar^2}{2m_t}k^2\left[1-\frac{N^2m_t}{4\hbar^2\Delta\epsilon_0}k^2\right]\,, \tag{B5}$$

which, making use of Eqs. (B3) and (B4), can be written as

$$\bar{\epsilon}_t=\frac{\hbar^2}{2m_t}k^2\left[1-\alpha\frac{\hbar^2k^2}{2m_t}\right] \tag{B6}$$

with

$$\alpha=\frac{1}{2\Delta\epsilon_0}\left[1-\frac{m_t}{m_0}\right]^2\,. \tag{B7}$$

Equation (B6) under $\alpha\epsilon_t\ll1$ conditions can be well approximated with the usual expression

$$\frac{\hbar^2k^2}{2m_t}=\bar{\epsilon}_t(1+\alpha\bar{\epsilon}_t)\,. \tag{B8}$$

Equation (B8), as reported in Sec. III.A.2, is the usual way of introducing nonparabolicity in practical calculations so that α, as given in Eq. (B7), can be taken as a plausible definition of the nonparabolic parameter for a Si-like conduction band. By substituting the values for Si in Eqs. (B4) and (B7) we find $\alpha=0.7$ eV^{-1} in reasonable agreement with the experimental value of 0.5 eV^{-1}. (See Table V of Appendix C, where nonparabolicity is taken as the same in all directions.)

APPENDIX C: PARAMETERS FOR DIAMOND, SILICON, AND GERMANIUM

In this appendix we report the bulk constants (see Table IV) together with the most recent values of the band pa-

TABLE V. Band parameters of holes (Reggiani, 1980).

	Diamond	Silicon	Germanium	Units
$\lvert A\rvert$	3.61	4.22	13.38	
$\lvert B\rvert$	0.18	0.78	8.48	
$\lvert C\rvert$	3.76	4.80	13.14	
ϵ_{so}	0.006	0.044	0.295	eV
$m_h(\epsilon/\epsilon_{so}\ll1)$	0.53	0.53	0.346	m_0
$m_h(\epsilon/\epsilon_{so}\gg1)$	1.08	1.26	0.73	m_0
$m_l(\epsilon/\epsilon_{so}\ll1)$	0.19	0.155	0.042	m_0
$m_l(\epsilon/\epsilon_{so}\gg1)$	0.36	0.36	0.25	m_0
$\mathscr{E}_1^0$	5.5	5.0	4.6	eV
d_0	61.2	26.6	40.3	eV

TABLE VI. Band parameters of electrons (Reggiani, 1980; Brunetti *et al.*, 1981).

	Diamond	Silicon	Germanium	Units
ϵ_Δ			0.18	eV
ϵ_L	7.22	0.74		eV
ϵ_Γ	6.22	2.95	0.14	eV
$m_{l\Delta}$	1.4	0.98	1.35	m_0
$m_{t\Delta}$	0.36	0.19	0.29	m_0
m_{lL}			1.59	m_0
m_{tL}			0.08	m_0
m_Γ			0.04	m_0
$\mathscr{E}_{1\Gamma}$			5.0	eV
$\mathscr{E}_{1L}$			11.0	eV
$\mathscr{E}_{1\Delta}$	8.7	9.0	9.0	eV
$(D_tK)_L$			5.5	10^8 eV/cm
$\text{Inter}_{\Delta\Delta}$				
θ_{g1}		140 (TA)		K
$(D_tK)_{g1}$		0.5		10^8 eV/cm
θ_{g2}		215 (LA)	100 (LA)	K
$(D_tK)_{g2}$		0.8	0.79	10^8 eV/cm
θ_{g3}	1900 (LO)	720 (LO)	430 (LO)	K
$(D_tK)_{g3}$	8.0	11.0	9.5	10^8 eV/cm
θ_{f1}		220 (TA)		K
$(D_tK)_{f1}$		0.3		10^8 eV/cm
θ_{f2}	1560 (LA)	550 (LA)		K
$(D_tK)_{f2}$	8.0	2.0		10^8 eV/cm
θ_{f3}	1720 (TO)	685 (TO)		K
$(D_tK)_{f3}$	8.0	2.0		10^8 eV/cm
Inter_{LL}				
θ_{LL1}			320 (LA, LO)	K
$(D_tK)_{LL1}$			3.0	10^8 eV/cm
θ_{LL2}			120 (TA)	K
$(D_tK)_{LL2}$			0.2	10^8 eV/cm
$\text{Inter}_{L\Delta}$				
$\theta_{L\Delta}$			320 (LA)	K
$(D_tK)_{L\Delta}$			4.1	10^8 eV/cm
$\text{Inter}_{L\Gamma}$				
$\theta_{L\Gamma}$			320 (LA)	K
$(D_tK)_{L\Gamma}$			2.0	10^8 eV/cm
$\text{Inter}_{\Delta\Gamma}$				
$\theta_{\Delta\Gamma}$			320 (LA)	K
$(D_tK)_{\Delta\Gamma}$			10.0	10^8 eV/cm
α_Δ		0.5		eV^{-1}
α_Γ			0.3	eV^{-1}

rameters which describe realistic microscopic models of diamond, silicon, and germanium (see Tables V and VI).

APPENDIX D: NUMERICAL EVALUATION OF INTEGRALS OF INTEREST

In this appendix we present an analytical approximation of the integrals that involve the Bose-Einstein distribution function $N_q(x)=[\exp(x)-1]^{-1}$ (see Sec. III) in terms of the dimensionless variable x.

To a good approximation N_q can be taken as

$$N_q(x)=\begin{cases}\dfrac{1}{x}-\dfrac{1}{2}+\displaystyle\sum_{m=1}^{\infty}B_{2m}x^{2m-1}/(2m)!, & x\le\bar{x}\\ \exp(-x), & x>\bar{x}\end{cases} \tag{D1}$$

where B_{2m} are the Bernoulli numbers, and $\bar{x} < 2\pi$ in order to ensure the validity of the series expansion (Gradshteyn and Ryzhik, 1966). The best value of $\bar{x}$ slightly depends upon the number of terms considered in the power series, and can be taken as about 3.5.

For the case of electrons (see Sec. III.D.1.*a*), by considering in Eq. (D1) terms up to the ninth power, for the integrals in Eq. (3.59) we obtain

$$F_1(x)=\begin{cases}\dfrac{x^2}{2}-\dfrac{x^3}{6}+\dfrac{x^4}{48}-\dfrac{x^6}{4320}+\dfrac{x^8}{241\,920}-\dfrac{x^{10}}{12\,096\,000}+\dfrac{x^{12}}{622\,702\,080}, & x\le\bar{x}_a\\ \dfrac{\bar{x}_a^2}{2}-\dfrac{\bar{x}_a^3}{6}+\dfrac{\bar{x}_a^4}{48}-\dfrac{\bar{x}_a^6}{4320}+\dfrac{\bar{x}_a^8}{241\,920}-\dfrac{\bar{x}_a^{10}}{12\,096\,000}+\dfrac{\bar{x}_a^{12}}{622\,702\,080} & \\ \qquad+\exp(-\bar{x}_a)(\bar{x}_a^2+2\bar{x}_a+2)-\exp(-x)(x^2+2x+2), & x>\bar{x}_a\end{cases} \tag{D2}$$

$$G_1(x)=\begin{cases}\dfrac{x^2}{2}+\dfrac{x^3}{6}+\dfrac{x^6}{4320}+\dfrac{x^8}{241\,920}-\dfrac{x^{10}}{12\,096\,000}+\dfrac{x^{12}}{622\,702\,080}, & x\le\bar{x}_e\\ \dfrac{\bar{x}_e^2}{2}+\dfrac{\bar{x}_e^3}{6}+\dfrac{\bar{x}_e^4}{48}-\dfrac{\bar{x}_e^6}{4320}+\dfrac{\bar{x}_e^8}{241\,920}-\dfrac{\bar{x}_e^{10}}{12\,096\,000}++\dfrac{\bar{x}_e^{12}}{622\,702\,080} & \\ \qquad+\exp(-\bar{x}_e)(\bar{x}_e^2+2\bar{x}_e+2)-\dfrac{\bar{x}_e^3}{3}-\exp(-x)(x^2+2x+2)+\dfrac{x^3}{3}, & x>\bar{x}_e\end{cases} \tag{D3}$$

where $F_1(x)$ refers to absorption ($\bar{x}_a=3.5$), and $G_1(x)$ refers to emission ($\bar{x}_e=4$), respectively.

As regards the integrals entering Eq. (3.68), we find by analogous calculations

$$F_2(x)=\begin{cases}\dfrac{x^3}{3}-\dfrac{x^4}{8}+\dfrac{x^5}{60}-\dfrac{x^7}{5040}+\dfrac{x^9}{272\,160}-\dfrac{x^{11}}{143\,305\,600}+\dfrac{x^{13}}{622\,702\,080}, & x\le\bar{x}_a\\ \dfrac{\bar{x}_a^3}{3}-\dfrac{\bar{x}_a^4}{8}+\dfrac{\bar{x}_a^5}{60}-\dfrac{\bar{x}_a^7}{5040}+\dfrac{\bar{x}_a^9}{272\,160}-\dfrac{\bar{x}_a^{11}}{143\,305\,600}+\dfrac{\bar{x}_a^{13}}{622\,702\,080} & \\ \qquad+\exp(-\bar{x}_a)(\bar{x}_a^3+3\bar{x}_a^2+6\bar{x}_a+6)-\exp(-x)(x^3+3x^2+6x+6), & x>\bar{x}_a\end{cases} \tag{D4}$$

$$G_2(x)=\begin{cases}\dfrac{x^3}{3}+\dfrac{x^4}{8}+\dfrac{x^5}{60}-\dfrac{x^7}{5040}+\dfrac{x^9}{272\,160}-\dfrac{x^{11}}{143\,305\,600}+\dfrac{x^{13}}{622\,702\,080}, & x\le\bar{x}_e\\ \dfrac{\bar{x}_e^3}{3}+\dfrac{\bar{x}_e^4}{8}+\dfrac{\bar{x}_e^5}{60}-\dfrac{\bar{x}_e^7}{5040}+\dfrac{\bar{x}_e^9}{272\,160}-\dfrac{\bar{x}_e^{11}}{143\,305\,600}+\dfrac{\bar{x}_e^{13}}{622\,702\,080} & \\ \qquad+\exp(-\bar{x}_e)(\bar{x}_e^3+3\bar{x}_e^2+6\bar{x}_e+6)-\dfrac{\bar{x}_e^4}{4}-\exp(-x)(x^3+3x^2+6x+6)+\dfrac{x^4}{4}, & x>\bar{x}_e\,.\end{cases} \tag{D5}$$

For the case of holes (see Sec. III.D.1.*d*), by considering only the first terms of the series in Eq. (D1), we can give, for the integrals in Eqs. (3.79)–(3.82), the expressions (Reggiani *et al.*, 1977):

$$F_3(x)=\begin{cases}2x^2\left[1-\dfrac{34}{105}\sqrt{2}x+\dfrac{x^2}{12}\right], & x\le\dfrac{3}{\sqrt{2}}\\ \dfrac{1017}{280}+\left[68-\dfrac{2358}{x^2}+\dfrac{41\,931}{x^4}\right]\exp(-3)-8\exp(-\sqrt{2}x)\left[x^2+4\sqrt{2}x+28+\dfrac{72\sqrt{2}}{x}+\dfrac{252}{x^2}\right. & \\ \qquad\left.+\dfrac{270\sqrt{2}}{x^3}+\dfrac{270}{x^4}\right], & x>\dfrac{3}{\sqrt{2}}\end{cases} \tag{D6}$$

$$F_4(x)=\begin{cases} x^3\left[\dfrac{136\sqrt{2}}{105}-x+\dfrac{44\sqrt{2}x^2}{315}\right], & x\le\dfrac{3}{\sqrt{2}} \\ \dfrac{801}{140}+\exp(-3)\left[312-\dfrac{13\,248}{x^2}+\dfrac{300\,078}{x^4}\right]-\exp(\sqrt{2}x)\left[8\sqrt{2}x^3+72x^2+288\sqrt{2}x\right. & \\ \qquad\left.+1824+\dfrac{4320\sqrt{2}}{x}+\dfrac{14\,400}{x^2}+\dfrac{15\,120\sqrt{2}}{x^3}+\dfrac{15\,120}{x^4}\right], & x>\dfrac{3}{\sqrt{2}} \end{cases} \tag{D7}$$

$$G_3(x)=\begin{cases} 2x^2\left[1+\dfrac{34\sqrt{2}}{105}x+\dfrac{x^2}{12}\right], & x\le\dfrac{3}{\sqrt{2}} \\ \dfrac{5913}{280}+\dfrac{136\sqrt{2}}{105}x^3-9\left[4-\dfrac{162}{5x^2}+\dfrac{729}{7x^4}\right], & x>\dfrac{3}{\sqrt{2}} \end{cases} \tag{D8}$$

$$G_4(x)=\begin{cases} x^3\left[\dfrac{136\sqrt{2}}{105}+x+\dfrac{44\sqrt{2}}{315}x^2\right], & x\le\dfrac{3}{\sqrt{2}} \\ \dfrac{6371}{140}+2x^4-81+\dfrac{729}{x^2}-\dfrac{19\,683}{8x^4}, & x>\dfrac{3}{\sqrt{2}}\ . \end{cases} \tag{D9}$$

REFERENCES

Adawi, I., 1959, Phys. Rev. **115**, 1152.

Adawi, I., 1960, Phys. Rev. **120**, 118.

Aers, G., A. D. Boardman, and E. D. Isaac, 1976, Phys. Status Solidi A **36**, 357.

Agrain, P., and M. Balkanski, 1961, *Selected Constants Relative to Semiconductors* (Pergamon, Oxford).

Alberigi-Quaranta, A., V. Borsari, C. Jacoboni, and G. Zanarini, 1973, Appl. Phys. Lett. **22**, 103.

Alberigi-Quaranta, A., C. Jacoboni, and G. Ottaviani, 1971, Riv. Nuovo Cimento **1**, 445.

Andronov, A. A., V. A. Valov, V. A. Kozlov, and L. S. Mazov, 1980, Solid State Commun. **36**, 603.

Asche, M., B. L. Boichenko, V. M. Bondar, and O. G. Sarbei, 1971, Phys. Status Solidi B **44**, 173.

Asche, M., and O. G. Sarbei, 1969, Phys. Status Solidi B **33**, 9.

Asche, M., and O. G. Sarbei, 1981, Phys. Status Solidi B **103**, 11.

Baccarani, G., C. Jacoboni, and A. M. Mazzone, 1977, Solid State Electron. **20**, 5.

Bacchelli, L., and C. Jacoboni, 1972, Solid State Commun. **10**, 71.

Barker, J. R., and D. K. Ferry, 1979, Phys. Rev. Lett. **42**, 1779.

Basu, P. K., 1977, J. Appl. Phys. **48**, 350.

Bauer, G., 1974, in *Solid-State Physics,* Vol. 74 of *Springer Tracts in Modern Physics,* edited by G. Höhler (Springer, Berlin).

Bir, G. L., and G. E. Pikus, 1961, Fiz. Tverd. Tela Leningrad **2**, 2287 [Sov. Phys.—Solid State **2**, 2039 (1961)].

Bir, G. L., and G. E. Pikus, 1974, *Symmetry and Strain-Induced Effects in Semiconductors,* translated by P. Shelnitz, translation edited by D. Louvish (Wiley, New York).

Boardman, A. D., W. Fawcett, and G. Ruch, 1971, Phys. Status Solidi A **4**, 133.

Borsari, V., and C. Jacoboni, 1972, Phys. Status Solidi B **54**, 649.

Bosi, S., and C. Jacoboni, 1976, J. Phys. C **9**, 315.

Bosi, S., C. Jacoboni, and L. Reggiani, 1979, J. Phys. C **12**, 1525.

Brooks, H., and C. Herring, 1951, Phys. Rev. **83**, 879.

Brunetti, R., 1982, unpublished.

Brunetti, R., C. Jacoboni, F. Nava, L. Reggiani, G. Bosman, and R. J. J. Zijlstra, 1981, J. Appl. Phys. **52**, 6713.

Budd H., 1966, in *Proceedings of the International Conference on the Physics of Semiconductors, Kyoto,* J. Phys. Soc. Japan Suppl. **21**, 420.

Budd, H., 1967, Phys. Rev. **158**, 798.

Buslenko, N. P., D. I. Golenko, Yu. A. Shreider, I. M. Sobol, and V. G. Sragovich, 1966, *The Monte Carlo Method: The Method of Statistical Trials,* edited by Yu. A. Shreider, translated from Russian by G. J. Tee (Pergamon, London), International Series of Monograph in Pure and Applied Mathematics, Vol. 87.

Canali, C., M. Costato, G. Ottaviani, and L. Reggiani, 1973, Phys. Rev. Lett. **31**, 536.

Canali, C., C. Jacoboni, F. Nava, G. Ottaviani, and A. Alberigi-Quaranta, 1975, Phys. Rev. B **12**, 2265.

Chambers, R. G., 1952, Proc. Phys. Soc. London Sect. A **65**, 458.

Chattopadhyay, D., 1974, J. Appl. Phys. **45**, 4931.

Chattopadhyay, D., and H. J. Queisser, 1981, Rev. Mod. Phys. **53**, 745.

Cohen, M. H., M. J. Harrison, and W. Harrison, 1960, Phys. Rev. **117**, 937.

Constant, E., and B. Boittiaux, 1981, in *Proceedings of the 3rd International Conference on Hot Carriers in Semiconductors,* J. Phys. (Paris) Colloq. **42**, C7-73.

Conwell, E.M., 1967, *High Field Transport in Semiconductors,* Solid State Phys., Suppl. 9 (Academic, New York).

Conwell, E.M., and M. O. Vassel, 1968, Phys. Rev. **166**, 797.

Conwell, E. M., and V. F. Weisskopf, 1950, Phys. Rev. **77**, 388.

Costato, M., G. Gagliani, C. Jacoboni, and L. Reggiani, 1974, J. Phys. Chem. Solids. **35**, 1605.

Costato, M., and L. Reggiani, 1970, Nuovo Cimento Lett. **4**, 1179.

Costato, M., and L. Reggiani, 1973, Phys. Status Solidi B **58**, 47 and 471.
Curby, R. C., and D. K. Ferry, 1973, Phys. Status Solidi A **15**, 319.
Davydov, B., 1936, Phys. Z. Sowjetunion **9**, 443.
Davydov, B., 1937, Phys. Z. Sowjetunion **12**, 269.
Dean, P. J., E. C. Lightowlers, and D. R. Wight, 1965, Phys. Rev. **140**, 352A.
Dresselhaus, G., A. F. Kip, and C. Kittel, 1955, Phys. Rev. **98**, 368.
Eadie, W. T., D. Drijard, F. E. James, M. Roos, and B. Sadoulet, 1971, *Statistical Methods in Experimental Physics* (North-Holland, Amsterdam).
Eaves, L., R. A. Hoult, R. A. Stradling, R. J. Tidey, J. C. Portal, and S. Askenazy, 1975, J. Phys. C **8**, 1034.
Fauquembergue, R., J. Zimmermann, A. Kaszynski, E. Constant, and G. Microondes, 1980, J. Appl. Phys. **51**, 1065.
Fawcett, W., 1973, in *Electrons in Crystalline Solids,* edited by A. Salam (IAEA, Vienna), p. 531.
Fawcett, W., D. A. Boardman, and S. Swain, 1970, J. Phys. Chem. Solids **31**, 1963.
Fawcett, W., C. Hilsum, and H. D. Rees, 1969, Solid State Commun. **7**, 1257.
Fawcett, W., and E. G. S. Paige, 1971, J. Phys. C **4**, 1801.
Fawcett, W., and H. D. Rees, 1969, Phys. Lett. **11**, 731.
Ferry, D. K., 1976, Phys. Rev. B **14**, 1605.
Ferry, D. K., 1980, Phys. Lett. A **78**, 379.
Ferry, D. K., and J. R. Barker, 1981, J. Appl. Phys. **52**, 818.
Fröhlich, H., 1947, Proc. R. Soc. London Ser. A **188**, 521 and 532.
Fröhlich H., and B. Paranjape, 1956, Proc. Phys. Soc. London Sect. B **69**, 21.
Gagliani, G., and L. Reggiani, 1975, Nuovo Cimento B **30**, 207.
Gantsevich, S. V., V. L. Gurevich, and R. Katilius, 1974, Phys. Condens. Matter **18**, 165.
Gantsevich, S. V., V. L. Gurevich, and R. Katilius, 1979, Riv. Nuovo Cimento **2**, 1.
Gherardi, L., A. Pellacani, and C. Jacoboni, 1975, Lett. Nuovo Cimento **14**, 225.
Glisson, T. H., J. R. Hauser, M. A. Littlejohn, K. Hess, B. G. Streetman, and H. Shichijo, 1980, J. Appl. Phys. **51**, 5445.
Gradshteĭn, I. S., and I. M. Ryzhik, 1965, *Table of Integrals, Series and Products,* 4th ed., translated from Russian by Scripta Technica, Inc., translation edited by A. Jeffrey (Academic, New York).
Gunn, J. B., 1963, Solid State Commun. **1**, 88.
Hammar, C., 1971, Phys. Rev. B **4**, 417.
Hammar, C., 1972, Phys. Status Solidi A **11**, 495.
Hammar, C., 1973, J. Phys. C **6**, 70.
Hammarsley, J. M., and D. C. Handscomb, 1964, *Monte Carlo Methods,* edited by M. S. Bartlett (Methuen/Chapman and Hall, London).
Harrison, W. A., 1956, Phys. Rev. **104**, 1281.
Hauser, J. R., M. A. Littlejohn, and T. H. Glisson, 1976, Appl. Phys. Lett. **28**, 458.
Hensel, J. C., and H. Hasegawa, 1964, in *Proceedings of the 7th International Conference on the Physics of Semiconductors,* edited by M. Hulin (Dunod, Paris), p. 105.
Herman, F., 1952, Phys. Rev. **88**, 1210.
Herring, C., and E. Vogt, 1956, Phys. Rev. **101**, 944.
Hill, G., P. N. Robson, and W. Fawcett, 1979, J. Appl. Phys. **50**, 356.
Humphreys, R. G., 1981, J. Phys. C **14**, 2935.
Ivey, J. L., and R. L. Mieher, 1972, Phys. Rev. Lett. **29**, 176.
Jacoboni, C., 1974, Phys. Status Solidi B **65**, 61.
Jacoboni, C., 1976, in *Proceedings of the 13th International Conference on the Physics of Semiconductors,* edited by G. Fumi (Marves, Roma), p. 1195.
Jacoboni, C., G. Gagliani, L. Reggiani, and O. Turci, 1978, Solid State Electron. **21**, 315.
Jacoboni, C., R. Minder, and G. Majni, 1975, J. Phys. Chem. Solids **36**, 1129.
Jacoboni, C., F. Nava, C. Canali, and G. Ottaviani, 1981a, Phys. Rev. B **24**, 1014.
Jacoboni, C., and L. Reggiani, 1979, Ad. Phys. **28**, 493.
Jacoboni, C., L. Reggiani, and R. Brunetti, 1981b, in *Proceedings of the 3rd International Conference on Hot Carriers in Semiconductors,* J. Phys. (Paris) Colloq. **42**, C7-123.
Kane, E. O., 1956, J. Phys. Chem. Solids **1**, 82.
Kittel, C., 1963, *Quantum Theory of Solids* (Wiley, New York).
Kocevar, P., 1980, in *Physics of Nonlinear Transport in Semiconductors,* edited by D. K. Ferry, J. R. Barker, and C. Jacoboni (Plenum, New York), p. 401.
Komiyama, S., and R. Spies, 1981, Phys. Rev. B **23**, 6839.
Kurosawa, T., 1966, in *Proceedings of the International Conference on the Physics of Semiconductors, Kyoto,* J. Phys. Soc. Jpn. Suppl. **21**, 424.
Kurosawa, T., 1980, in *Proceedings of the 15th International Conference on the Physics of Semiconductors, Kyoto,* J. Phys. Soc. Jpn. Suppl. A **49**, 345.
Landau, L., and A. Kompanejez, 1934, Phys. Z. Sowjetunion **6**, 163.
Lax, M., and J. L. Birman, 1972, Phys. Status Solidi B **49**, K153.
Lawaetz, P., 1967, Doctoral dissertation, University of Lyngby.
Lawaetz, P., 1969, Phys. Rev. **183**, 730.
Lebwohl, P. A., 1973, J. Appl. Phys. **44**, 1744.
Lebwohl, P. A., and P. J. Price, 1971a, Solid State Commun. **9** 1221.
Lebwohl, P. A., and P. J. Price, 1971b, Appl. Phys. Lett. **19**, 530.
Levinson, I. B., 1965, Fiz. Tverd. Tela Leningrad **6**, 2113 [Sov. Phys.—Solid State **6**, 1665 (1965)].
Maeda, H., and T. Kurosawa, 1972, in *Proceedings of the Eleventh International Conference on the Physics of Semiconductors, Warsaw* (Elsevier, New York), p. 602.
Marchuk, G. I., G. A. Mikhailov, M. A. Nazaraliev, R. A. Darbinjan, B. A. Kargin, and B. S. Elepov, 1980, *"The Monte Carlo Methods in Atmospheric Optics,"* Vol. 12 of Springer Series in Optical Sciences (Springer, Berlin).
Matulionis, A., J. Požela, and A. Reklaitis, 1975, Solid State Commun. **16**, 1133.
Meyer, H. A., 1956, Ed., *Symposium on Monte Carlo Methods* (Wiley, New York).
Nash, J. G., and J. W. Holm-Kennedy, 1974, Appl. Phys. Lett. **24**, 139.
Nava, F., C. Canali, C. Jacoboni, and L. Reggiani, 1980, Solid State Commun. **33**, 475.
Nava, F., C. Canali, L. Reggiani, D. Gasquet, J. C. Vaissière, and J. P. Nougier, 1979, J. Appl. Phys. **50**, 922.
Nougier, J. P., and M. Rolland, 1973, Phys. Rev. B **8**, 5728.
Nougier, J. P., J. C. Vaissière, D. Gasquet, and A. Motadid, 1981, J. Appl. Phys. **52**, 5683.
Ottaviani, G., L. Reggiani, C. Canali, F. Nava, and A. Alberigi-Quaranta, 1975, Phys. Rev. B **12**, 3318.
Paige, E. G. S., 1964, *The Electrical Conductivity of Germanium,* edited by A. F. Gibson and R. E. Burgess (Heywood, London).
Persky, G., and D. J. Bartelink, 1970, Phys. Rev. B **1**, 1614.
Philips, A., Jr., and P. J. Price, 1977, Appl. Phys. Lett. **30**, 528.

Pötz, W., and P. Vogl, 1981, Phys. Rev. B **24**, 2025.
Price, P. J., 1965, in *Fluctuation Phenomena in Solids,* edited by R. E. Burgess (Academic, New York), p. 355.
Price, P. J., 1968, in *Proceedings of the 9th International Conference on the Physics of Semiconductors,* edited by S. M. Ryvkin (Nauka, Leningrad), p. 753.
Price, P. J., 1970, IBM J. Res. Dev. **14**, 12.
Price, P. J., 1973, IBM J. Res. Dev. **17**, 39.
Price, P. J., 1979, *Semiconductors and Semimetals* (Academic, New York), p. 249.
Price, P. J., and R. L. Hartman, 1964, J. Phys. Chem. Solids **25**, 219.
Rees, H. D., 1968, Phys. Lett. A **26**, 416.
Rees, H. D., 1969, J. Phys. Chem. Solids **30**, 643.
Rees, H. D., 1973, J. Phys. C **6**, 262.
Reggiani, L., 1978, Phys. Rev. B **17**, 2800.
Reggiani, L., 1980, in *Proceedings of the 15th International Conference on the Physics of Semiconductors, Kyoto,* J. Phys. Soc. Jpn. Suppl. A **49**, 317.
Reggiani, L., S. Bosi, C. Canali, F. Nava, and S. F. Kozlov, 1981a, Phys. Rev. B **23**, 3050.
Reggiani, L., R. Brunetti, and C. Jacoboni, 1981d, in *International Symposium on Noise in Physical Systems,* edited by P. H. E. Meijer, R. D. Mountain, and R. J. Soulen (NBS Special Publications 614, Washington), p. 414.
Reggiani, L., R. Brunetti, and C. Jacoboni, 1981b, in *Proceedings of the 3rd International Conference on Hot Carriers in Semiconductors,* J. Phys. (Paris) Colloq. **42**, C7-111.
Reggiani, L., and C. Calandra, 1973, Phys. Lett. A **43**, 339.
Reggiani, L., C. Canali, F. Nava, and G. Ottaviani, 1977, Phys. Rev. B **16**, 2781.
Reggiani, L., J. C. Vaissière, J. P. Nougier, and D. Gasquet, 1981c, in *Proceedings of the 3rd International Conference on Hot Carriers in Semiconductors,* J. Phys. (Paris) Colloq. **42**, C7-357.
Reif, F., 1965, *Fundamentals of Statistical and Thermal Physics* (McGraw-Hill, New York).
Reik, H. G., and H. Risken, 1962, Phys. Rev. **126**, 1737.
Ruch, J. G., 1972, IEEE Trans. Electron. Devices **ED-19**, 652.
Ruch, J. G., and W. Fawcett, 1970, J. Appl. Phys. **41**, 384.
Schlup, W. A., 1971, Phys. Kondens. Mater. **13**, 307.
Schlup, W. A., 1976, in *Proceedings of the 13th International Conference on the Physics of Semiconductors,* edited by G. Fumi (Marves, Rome), p. 1210.
Seeger, K., 1973, *Semiconductor Physics* (Springer, Vienna).
Shichijo, H., and K. Hess, 1981, Phys. Rev. B **23**, 4197.
Shichijo, H., K. Hess, and G. E. Stillman, 1981, Appl. Phys. Lett. **38**, 89.
Shockley, W., 1951, Bell Syst. Tech. J. **30**, 990.
Shockley, W., J. A. Copeland, and R. P. James, 1966, in *Quantum Theory of Atoms, Molecules and the Solid State,* edited by P.-O. Lowdin (Academic, New York), p. 537.
Stratton, R., 1958a, J. Electron. **5**, 157.
Stratton, R., 1958b, Proc. R. Soc. London Ser. A **246**, 406.
Streitwolf, H. W., 1970, Phys. Status Solidi B **37**, K47.
Tauber, G. E., 1959, J. Franklin Inst. **268**, 175.
Tiersten, M., 1961, IBM J. Res. Dev. **5**, 122.
Tiersten, M., 1964, J. Phys. Chem. Solids **25**, 1151.
van Vliet, K. M., A. Friedman, R. J. J. Zijlstra, A. Gisolf, and A. van der Ziel, 1975, J. Appl. Phys. **46**, 1804 (Part I); **46**, 1814 (Part II).
Vassel, M. O., 1970, J. Math. Phys. **11**, 408.
Vinter, B., 1973, doctoral dissertation, University of Lyngby.
Vogl, P., 1976, Phys. Rev. **13**, 694.
Wiley, J. D., 1971, Phys. Rev. B **4**, 2485.
Yamashita, J., and K. Inoue, 1959, J. Phys. Chem. Solids **12**, 1.
Yamashita, J., and M. Watanabe, 1954, Prog. Theor. Phys. **12**, 443.
Zijlstra, R. J. J., 1978, in *Noise in Physical Systems: Proceedings of the 5th International Conference on Noise,* edited by D. Wolf (Springer, Heidelberg), p. 90.
Ziman, J. M., 1960, *Electrons and Phonons* (Oxford University, Oxford, England).
Ziman, J. M., 1972, *Principles of the Theory of Solids* (Cambridge University, Cambridge, England).
Zimmermann, J., and E. Constant, 1980, Solid State Electron. **23**, 915.
Zimmermann, J., R. Fauquembergue, M. Charef, and E. Constant, 1980, Electron. Lett. **16**, 664.
Zimmermann, J., Y. Leroy, and E Constant, 1978, J. Appl. Phys. **49**, 3378.
Zunger, A., and A. J. Freeman, 1977, Phys. Rev. B **15**, 5049.